Università degli Studi di Salerno

Dipartimento di Chimica e Biologia

Dottorato di Ricerca in Chimica – XII Ciclo

Tesi Dottorale 2013/2014

"Synthesis, Structure and Properties of Cyclopeptoids and Cyclopeptides"

Studente PhD:
Brunello Nardone

Tutore:
Prof.ssa Irene Izzo
Co-tutori:
Dott.ssa Consiglia Tedesco,
Prof. Fernando Albericio
(IRB, Barcelona)

Coordinatore:
Prof. Gaetano Guerra

a Ortensia e Iris

List of abbreviations

ACN: acetonitrile

DCM: dichloromethane

DIC: *N,N'*-diisopropylcarbodimide

DIPEA: ethyldiisopropilamine

DMF: *N,N'*-dimethylformamide

Fmoc: 9-fluorenylmethoxycarbonyl

HATU: *O*-(7-azabenzotriazol-1-yl)-*N*,*N*,*N*',*N*'-tetramethyluronium hexafluorophosphate

HFIP: hexafluoroisopropanol

TIS: triisopropylsilane

RP-HPLC: reversed-phase high-performance liquid chromatography

1 INTRODUCTION

1.1 Cyclopeptides **1**

1.1.1 Importance of cyclopeptides 1

1.1.2 Biologically active cyclopeptides 2

1.1.3 Complexation and transport of metal ions 9

1.1.4 Nanostructures 14

1.2 Peptoids **16**

1.2.1 Introduction 16

1.2.2 Synthesis 19

1.2.3 Conformationally constrained peptoid oligomers 21

1.2.4 Cyclopeptoids 28

1.2.5 Complexation and transport of metal ions 33

1.2.6 Biologically active peptoids 37

1.2.7 Catalytic properties 41

1.2.8 Nanostructures 42

1.3 The research project **44**

2 PROLINE-RICH CYCLOPEPTOIDS

2.1 The role of proline in peptoid conformation **49**

2.2 Aims of the work **53**

2.3 *N*-methoxyethyl cyclopeptoids containing proline **54**

2.3.1 Synthesis 54

2.3.2 Decomplexation procedure of the triprolinate cyclopeptoid 58

2.3.3 Structural analysis 59

2.3.4 Structural analysis of the triprolinate cyclopeptoid 62
2.3.5 Structural analysis of N-methoxyethyl cyclohexapeptoid 65

2.4 *N*-methoxyethyl cyclopeptoid containing pseudo-proline residues 69

2.5 Conclusions 74

2.6 Experimental section 76

3 AMPHIPHILIC CYCLOPEPTOIDS

3.1 Introduction 98

3.2 Aims of the work 101

3.3 Synthesis 102

3.4 Structural analysis of the alternate protected cyclopeptoid 105

3.5 Crystallization trials for 73 108

3.6 Crystallization trials for 45 108

3.7 Crystallization trials for 46 109

3.8 Conclusions 109

3.9 Experimental section 110

4 CYCLOPEPTOIDS AS PHASE TRANSFER CATALYSTS

4.1 Introduction **120**

4.2 Aims of the work **128**

4.3 Cyclopeptoids as PT catalysts in a benchmark S_N2 reaction **132**

4.3.1 Design and synthesis of the new catalysts 132

4.3.2 Determination of association constants by Cram's method 134

4.3.3 Evaluation of ionophoric activities with the HPTS assay 136

4.3.4 Catalytic activities and comparison with commercial phase transfer catalysts 139

4.4 Cyclopeptoids in the role of asymmetric PT catalyst **143**

4.4.1 Design and synthesis of the first generation catalysts 143

4.4.2 Catalytic activities in the enantioselective epoxidation 147

4.4.3 Catalytic activities in the enantioselective alkylation 149

4.4.4 Catalytic activities in the enantioselective alkylation: second generation catalysts 151

4.5 Conclusions **156**

4.6 Experimental section **157**

5 SYNTHETIC STRATEGIES FOR KALATA B1 CYCLOTIDE

5.1 Introduction 187

5.2 Fmoc/t-Bu solid-phase synthesis of kalata B1: General strategy 188

5.3 Aims of the work 195

5.4 Comparation of the methodologies a-d 198

5.5 Cyclization via NCL of kalata B1-Nbz(Me) 203

5.6 Folding of kalata B1 204

5.7 Conclusions 206

5.8 Experimental section 206

1 INTRODUCTION

1.1 Cyclopeptides

1.1.1 Importance of cyclopeptides

Cyclopeptides are a class of molecules which assume a great importance in the role of host defense molecules in many natural organisms (*e.g.* plants, marine species).[1]
Notably, men have used cyclopeptides as leading molecules in the therapeutic field due to the fact that they have significantly contributed to combat widespread and common diseases. For istance, vancomycin (**1**) and cyclosporin A (**2**) are classic therapeutic cyclopeptides (figure 1.1). The greater therapeutic importance of cyclopeptides with respect to linear peptides can be explained making reference to their higher resistance to *in vivo* enzymatic degradation, enhanced bioactivity, higher conformational stability which confers a more effective receptor-binding ability to target proteins in cells and tissues.[2]

In general, cyclopeptides are very versatile and promising molecules which are characterized by wide-ranging

[1] D. J. Craik, N. L. Daly, I. Saska, M. Trabi, K. Rosengren *J. Bacteriol.*, **2003**, *185*, 4011-4021.
[2] M. Katsara, T. Tselios, S. Deraos, G. Deraos, M. T. Matsoukas, E. Lazoura, J. Matsoukas, V. Apostolopoulos *Current Medicinal Chemistry*, **2006**, *13*, 2221-2232.

applications in the field of biomedicine and in nanotechnology.

With respect to the biomedical applications, cyclopeptides are currently used in the clinic as antibacterials, analgesics, ionophores, chemioterapics.[3] In addition, studies in connection with the use of these compounds as immunotherapeutic vaccines for diabetes and autoimmune diseases, therapeutic agents for skin disorders, modulators of protein-protein interactions, and molecular scaffolds for the grafting of small bioactive peptides are *in itinere*.[2,4]

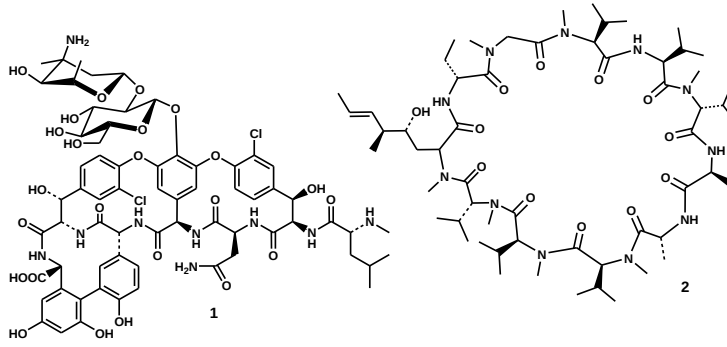

Figure 1.1: Structure of vancomycin (**1**) and cyclosporin A (**2**).

1.1.2 Biologically active cyclopeptides

Taking into account the above considerations there is a significant number of cyclopeptides presenting different biological activities and some of them find use in

[3] H. K. Kruger, F. Albericio *Future Med. Chem.*, **2012**, *4*, 1527-1531.

[4] S. Namyoshi, H. A. Benson *Biopolymers*, **2010**, *94*, 673-680; D. J. Craik, S. Simonsen, N. L. Daly *Current Opinion in Drug Discovery & Development*, **2002**, *5*, 251-260.

pharmaceutical industry. Some intriguing examples are reported below.

Azumamides A- E, five cyclotetrapeptides isolated by Fusetani *et al.* from the marine sponge *Mycale izuensis*, exhibit potent inhibitory activity against histone deacetylase (HDAC) enzymes.[5]

Histone deacetylases (HDACs) are a family of metalloenzymes regulating transcriptional processes, apoptosis, cell-cycle progression, and angiogenesis.[6]

The modulation of histone modifying enzymes is recognized as a crucial factor for the epigenetic control of oncogene transcription and the activation of tumor repressors.[7] These synergic effects can induce growth arrest of cancer cells rendering HDAC inhibitors promising candidates for the development of specific, noncytotoxic antitumor compounds.

HDAC inhibitors are divided in six distinct groups of zinc chelators.[8] Amongst them, azumamides belong to the small family of hydrophobic cyclotetrapeptides. Structurally, they include four nonribosomal amino acid residues, three of which are α-amino acids of the D series (D-Phe, D-Tyr, D-Ala, D-Val), while the fourth one is a unique β-amino acid, assigned as (*Z*)-(2*S*,3*R*)-3-amino-2-methyl-5-nonenedioic acid

[5] Y. Nakao, S. Yoshida, S. Matsunaga, N. Shindoh, Y. Terada, K. Nagai, J. K. Yamashita, A. Ganesan, R. W. M. van Soest, N. Fusetani *Angew. Chem. Int. Ed.*, **2006**, *45*, 7553-7557.

[6] F. Guo, C. Sigua, J. Tao, P. Bali, P. Gorge, Y. Li, S. Wittmann, L. Moscinski, P. Atadja, K. Bhalla *Cancer Res.*, **2004**, *64*, 2580-2589.

[7] M. Biel, V. Washolowski, A. Giannis, *Angew. Chem. Int. Ed*., **2005,** *44*, 3186 – 3216.

[8] T. A. Miller, D. J. Witter, S. J. Belvedere *Med. Chem.*, **2003**, *46*, 5097-5116.

9-amide (Amnaa) in azumamides A (**3**), B (**4**), and D (**6**), and as (*Z*)-(2*S*,3*R*)-3-amino-2-methyl-5-nonendioic acid (Amnda) in azumamides C (**5**) and E (**7**) (figure 1.2).[5]

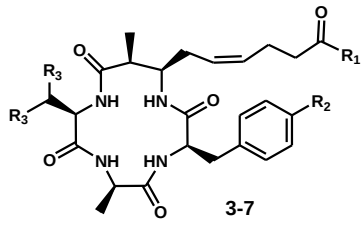

	R_1	R_2	R_3
A (**3**)	NH_2	H	CH_3
B (**4**)	NH_2	OH	CH_3
C (**5**)	OH	OH	CH_3
D (**6**)	NH_2	H	H
E(**7**)	OH	H	CH_3

Figure 1.2: Structures of azumamides A-E.

The total synthesis of azumamides A and E was successful performed by De Riccardis *et al.* in 2006, allowing to establish undoubtedly the stereochemical configurations of the azumamides.[9]

Recently, the bicyclic depsipeptide romidepsin, a natural HDAC inhibitor obtained from *Chromobacterium violaceum* bacterium and isolated from a Japanese soil sample, was approved for the treatment of cutaneous T-cell lymphoma.[10] It contains one proteinogenic (L-Val) and three non-proteinogenic aminoacids (D-Val, D-Cys, *Z*-dehydrobutyrine) in combination with a hydroxy-heptenoic

[9] I. Izzo, N. Maulucci, G. Bifulco, F. De Riccardis *Angew. Chem. Int. Ed.*, **2006**, *45*, 7557-7560.
[10] V. Baeriswyl, C. Heinis *Chem. Med. Chem.*, **2013**, *8*, 377-384.

acid moiety bearing the second thiol group (figure 1.3). The mechanism of action of romidepsin consists in the initial reduction of its disulfide bond by glutathione in the cell so that a zinc binding thiol is produced. Finally, the thiol interacts with a zinc ion in the active site of class I and II histone deacetylases, inhibiting their activity.[10]

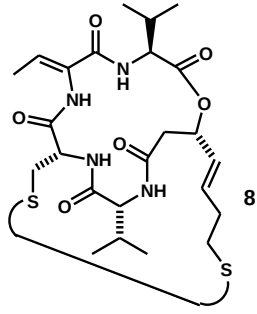

Figure 1.3: Structure of romidepsin.

An interesting class of cyclopeptides with biological activities are head-to-side chain cyclodepsipeptides. These peptides are characterized by a special structural arrangement in which the cyclization is realized through an ester bond between the *C*-terminus and a β-hydroxyl group.

In 2013 Albericio *et. al.* reported the first total synthesis of pipecolidepsin A (figure 1.4), an head-to-side chain cyclodepsipeptide isolated from the marine sponge *Homophymia lamellose*, which exhibits good cytotoxic properties *in vitro* against specific lung, colon and breast

human tumour cell lines.[11] This compound contains many unnatural amminoacids and the most intriguing residue is the bulky γ-branched β-hydroxy-α-aminoacid D-*allo*-(2*R*,3*R*,4*R*)-2-amino-3-hydroxy-4,5-dimethylhexanoic acid (AHDMHA). The β-hydroxyl group of AHDMHA residue allows the formation of an ester bond with the the *C*-terminus, producing a macrolactone.

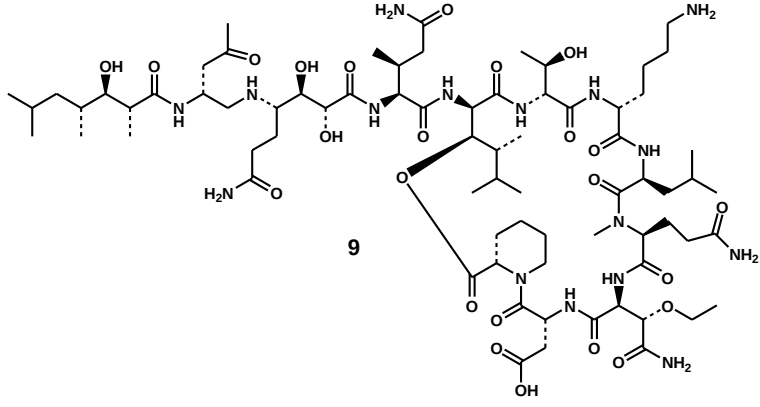

Figure 1.4: Structure of pipecolidepsin A.

Another intriguing class of biologically active cyclopeptides are cyclotides, a novel class of polycyclic peptides of vegetal origin which have drawn a great interest due to their potential application in drug design.

Cyclotides are small (~30 amino acids), disulfide-rich peptides that were originally discovered in plants of the

[11] M. Pelay-Gimeno, Y. Garcia-Ramos, M. J. Martin, J. Sprengler, J. M. Molina-Guijarro, S. Munt, A. M. Francesch, C. Cuevas, J. Tulla-Puche, F. Albericio *Nature Comm.*, **2013**, DOI: 10.1038/ncomms3352.

Rubiaceae (coffee) and *Violaceae* (violet) families.[12] The archetype cyclotide, kalata B1, is just one member of a very large family. The feature that combines all cyclotides is their head-to-tail cyclic backbone and three conserved disulfide bonds that form a special knotted motif, formally defined as 'cyclic cystine knot' (CCK). In particular, the CCK topology is characterized by the presence of an embedded ring, formed by two disulfide bridges and their connecting backbone segments, which is threaded by a third disulfide bond. Figure 1.5 shows the structure of kalata B1 (**10**), highlighting the CCK motif. The backbone segments between successive cysteine residues are named loops (numbered 1-6), and generally the loop sequences are amenable to substitution.

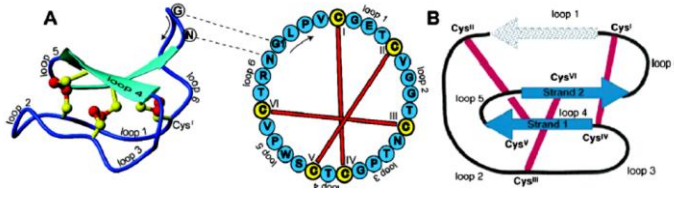

10

Figure 1.5: Structure of kalata B1 (**10**). Panel A shows the NMR structure and panel B illustrates a schematic representation of the topology of the cyclic cystine knot (CCK) motif characteristic of cyclotides. The framework also incorporates a triple-stranded β-sheet, indicated by the arrows.

Cyclotides in turn fall into three subfamilies, known as Möbius, bracelet and trypsin inhibitor subfamilies (figure 1.6). Anyway, a common feature of cyclotides from all three

[12] D. J. Craik, N. L. Daly, T. Bond, C. Waine *J. Mol. Biol.*, **1999**, *294*, 1327-1336.

subfamilies is their excellent stability. For example, a cyclotide solution can be boiled without the peptide being denatured. This stability is ascribed to the CCK core.

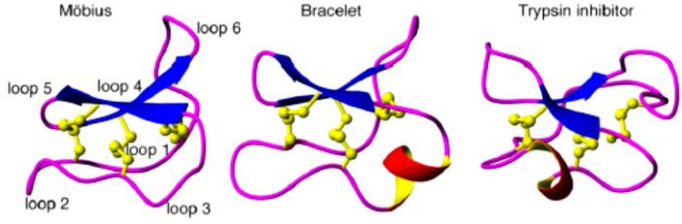

Figure 1.6: Subfamilies of cyclotides. The Möbius and bracelet subfamilies are defined on the basis of the presence (Möbius) or absence (bracelet) of a conceptual twist in the circular backbone deriving from a *cis*-peptide bond, preceding a Pro residue in loop 5. The trypsin inhibitor subfamily was named as so after that was discovered a trypsin inhibiting activity for the cyclotide MCoTI-II, member of the subfamily.[13]

Cyclotides exhibit a wide range of biological activities, including antiviral, antifungal and antibacterial activities. However, most interest in cyclotides has derived from their usability in drug design as robust molecular scaffolds.

Recently, it was proposed the strategy of grafting small bioactive peptide epitopes into turns in the CCK framework in order to stabilize them.[14] In this way it is possible to overcome the problem of the poor bioavailability of peptides, which limits their development as oral therapeutics.

[13] N. L. Daly, D. J. Craik *J. Biomol. Chem.,* **2001**, *276*, 22875-22882.
[14] D. J. Craik, J. S. Mylne, N. L. Daly *Cell. Mol. Life Sci.,* **2010**, *67*, 9-16.

There are many recent examples of grafting in cylotides reported from Craik and other groups.[15] These include applications in the field of cancer, cardiovascular disease, wound healing, infectious disease and inflammatory pain. An intrigous grafting study involved the insertion of a tetrapeptide sequence from the hormone α-MSH into kalata B1.[16] The resultant mutant peptide was characterized by a melanocortin-4 agonist activity, and therefore it might represent an effective model molecule for the development of anti-obesity drugs.

1.1.3 Complexation and transport of metal ions

A common feature of cyclopeptides, often related to their biological activity, is the ability of complexing ions.
Molecular recognition is of fundamental importance in biochemistry and chemistry, and antibiotic ionophores are small biological molecules that recognize ions and transport them across cell membranes.[17] A classic cyclopeptide capable of forming transmembrane ion channels is valynomicin, an antibiotic obtained from the cells of several *Streptomyces* strains, which acts as a highly selective potassium ionophore.[18,19] In particular, it has long been studied for its

[15] D. J. Craik *J. Pept. Sci.*, **2013**, *19*, 393-407.
[16] R. Eliasen, N. L. Daly, B. S. Wulff, T. L. Andresen, K. W. Conde-Frieboes, D. J. Craik *J. Biomol. Chem.*, **2012**, *287*, 40493-40501.
[17] M. Dobler *Ionophores and Their Structures;* John Wiley and Sons: New York, 1981.
[18] T. R. Forester, W. Smith, J.H.R. Clarke *J. Chem. Soc. Faraday Trans*., **1997**, *93*, 613-619.
[19] T. J. Marrone, K. N. Jr. Merz *J. Am. Chem. Soc.*, **1995**, *117*, 779–791.

selectivity to K^+ against Na^+. For example, valinomycin binds K^+ more strongly than Na^+ by ~5 kcal/mol in methanol.[20] This high selectivity is intriguing because the molecule is known to be conformationally flexible in methanol. On the contrary, synthetic ionophores tipically achieve selectivity through rigidity ensuring that the ion fits perfectly into the central cavity. Moreover, in the case of valinomycin, the selectivity is strangely espoused to conformation flexibility.

Structurally, valinomycin is an hydrophobic cyclodepsipeptide consisting of 12 alternating monomers of amino acid and hydroxy acid residues (figure 1.7). It has the formula (D-Val-L-lactic acid- L-Val-D-hydroxyvaleric acid)$_3$.

It is interesting to report that the excellent ionophoric properties of valynomicin were more recently exploited through the design of a chemical microsensor of K^+ for biomedical and clinical applications. This microsensor is a CHEMFET device, namely it was builded by a photolitographic deposition on the gate area of ISFET (ion-selective field effect transistor) chips of a biocompatible polymeric membrane (acrylated urethane) which included a ionophore sensor element (2.2% valynomicin).[21]

[20] R. M. Izatt, J. S. Bradshaw, S. A. Nielson, J. D. Lamb, J. J. Christensen, D. Sen, *Chem. Rev,*. **1985**, *85*, 271-339.

[21] J. Munoz, C. Jimenez, A. Bratov, J. Bartroli, S. Alegret, C. Dominguez *Biosensors & Bioelectronics*, **1997**, *12*, 577-585.

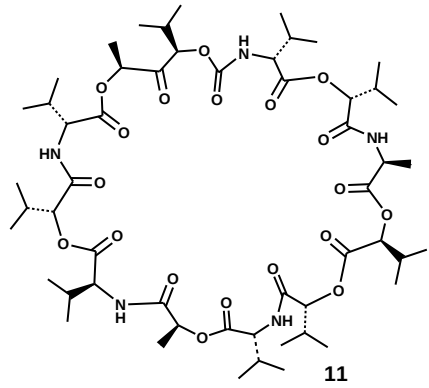

11

Figure 1.7: Structure of valynomicin.

Another example of cyclopeptides with ionophoric properties is the family of enniatins. Enniatins are cyclohexadepsipeptides made of alternated residues of three L-*N*-methyl aminoacids, typically valine, leucine, isoleucine, and three hydroxy acids, usually D-α-hydroxyisovaleric acid. These molecules are mainly isolated from *Fusarium* species of fungi, and are characterized by a large range of biological activities, such as antimicrobial, anticancer and enzyme inhibitor properties.[22]

The antimicrobial activity stems from the ability of enniatins to complex and transport alkali metals (K^+, Na^+, Ca^{++}) through biological membranes.[22] They penetrate into the cell membrane forming cation selective channels.

In figure 1.8 it is reported the X-ray structure of an enniatin B potassium 1:1 complex (**12**). In the central cavity of enniatin

[22] A. A. Sy-Corderom, C. J. Pearce, N. H. Oberlies *J. Antibio.*, **2012**, *65*, 541-549.

B is placed the metal ion, which is coordinated to six amide carbonyls *via* ion-dipole interactions.[23]

An analogous equimolar complex is formed between enniatin B and sodium.[23]

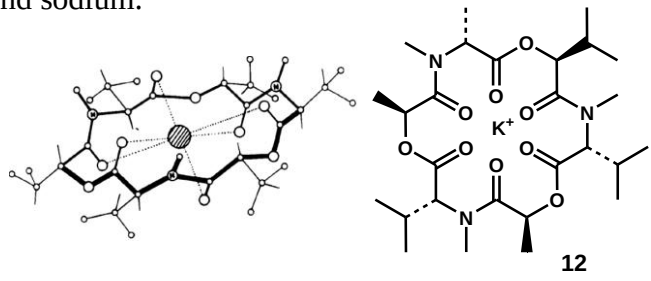

Figure 1.8: X-ray structure of enniatin B potassium1:1 complex (*left)* and chemical structure of the same compound (*right*).

In the same way as valynomicin and enniatins, other natural cyclopeptides were recognized as suitable molecules for metal complexation and transport, for example some azole-based cyclopeptides of marine origin, secreted as secondary metabolites from ascidians (‘sea squirts’) of the genus *Lissoclinum*.[24] These organisms are a prolific source of rare cyclic peptides with both D- and L-amino acids, many modified in the form of thiazole, oxazole, thiazoline or oxazoline ring (the heterocycle comes between the terminal carbonyl of the acidic function and the α-carbon). There is currently a vast literature which demonstrates that these

[23] M. Dobler, J. D. Dunitz, J. Krajewski *J. Mol. Biol.*, **1969**, *42*, 603-606; Y. A. Ovchinnikov, V. T. Ivanov, A. V. Evstratov, I. I. Mikhaleva, V. F. Bystrov, S. L. Portnova, T. A. Balashova, E. N. Meshcheryakova, V. M. Tulchinsky *Int. J. Peptide Protein Res.*, **1974**, *6*, 465–498.

[24] A. Bertram, G. Pattenden *Nat. Prod. Rep.*, **2007**, *24*, 18-30.

marine metabolites, specifically, are characterized by an high attitude to chelate metal ions.

A significative example is represented by the compound ascidiacyclamide isolated from the sea squirt *Lissoclinum patella*.[24] In 1994 Gahan *et al.* characterized a bis-copper(II) complex of ascidiacyclamide *via* X-ray crystallography.[24] This complex (**13**, figure 1.9) contains two copper ions each one coordinated to two nitrogens from thiazole and oxazoline unit, a deprotonated amine and a water molecule. In addition, is present a carbonate anion in a bridge position between the two copper ions.

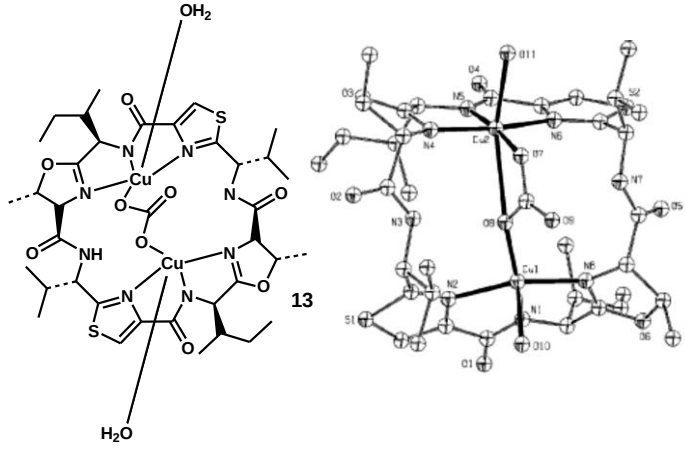

Figure 1.9: Bis-copper(II) complex of ascidiacyclamide (left) and ORTEP representation of the crystal structure (right)**.**

1.1.4 Nanostructures

Cyclic peptides are of interest also in nanotechnology, and in this regard Ghadiri and co-workers discovered in 1993 that noncovalently bonded nanotubes are formed by the stacking of cyclopeptides *via* hydrogen bonds.[25] Specifically, in order to form the nanotubes was prepared the octapeptide *cyclo*-[(L-Gln-D-Ala-L-Glu-D-Ala)$_2$-], (**14**). The presence of glutamic acid in deprotonated form in basic aqueous solution prevents the uncontrolled stacking of the subunits through coulombic repulsion. Controlled acidification generates microcrystalline aggregates that were extensively characterized by electron diffraction, electron microscopy and FT-IR spectroscopy.

These analyses firmly demonstrated that the structure was constituted from the cyclic units stacked through antiparallel β-sheet hydrogen bonding. By this way were formed hollow tubes with internal diameter of 7.5 Å and distances between ring-shaped units of 4.73 Å (figure 1.10).

In order to better understand nanotube structure, Ghadiri's group also prepared nanotubes using different uncharged D,L-α-octapeptides.[26]

[25] M.R. Ghadiri, J.R. Granja, R.A. Milligan, D.E. McRee, N. Khazanovich *Nature*, **1993**, *366*, 324-327.

[26] J. Hartgerink, J. R. Granja, R. A. Milligan, M. R. Ghadiri *J. Am. Chem. Soc.*, **1996**, *118*, 43-50.

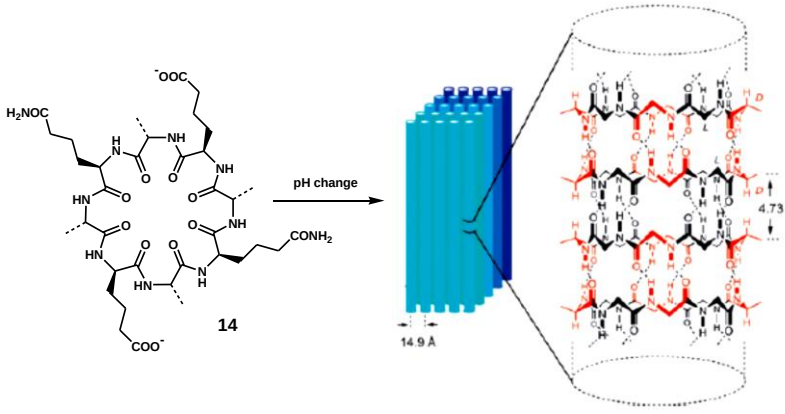

Figure 1.10: Proton-controlled self-assembly process for the preparation of microcrystalline aggregates of nanotubes composed of *cyclo*-[(L-Gln-D-Ala-L-Glu-D-Ala)$_2$-] (**14**).

The nanotubes above described present some advantages with respect to the covalently bonded nanostructures (zeolites, graphite etc.) due to the fact that are very modulable: the diameter of the nanotube can be controlled by varying the number of amino acid residues in each ring and, secondly, the properties of the outer surface of the nanotube can easily be modified by varying the amino acid side chains. Indeed, the tunability of these materials has allowed their use in fields such as biosensing, pharmacology, catalysis and electronics.[27]

A recent application of the cyclopeptide nanotubes (CPs) has been the preparation of peptide-polymer nanotubular hybrids using CPs in the role of templates (figure

[27] R. J. Brea, C. Reiriz, J. R. Granja *Chem. Soc. Rev*. **2010**, *39*, 1448-1456.

1.11).[28] The synthetic strategy consisted in the self-assembly of CPs with polymerization initiator groups on distint side chains (**15**, figure 1.11) to form a peptide nanotube that possessed the initiator groups only on the outer surface. A furher polymerization reaction coated the peptide core with a covalently bound polymer shell.

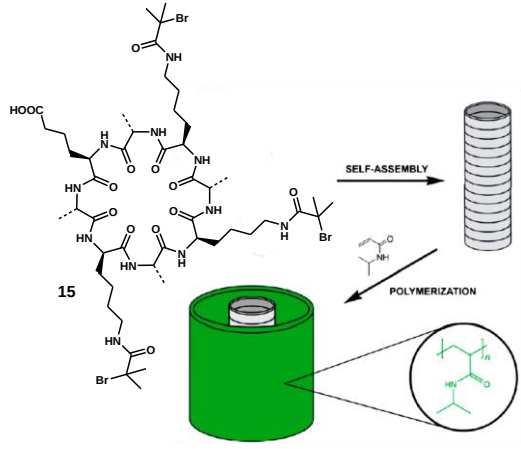

Figure 1.11: Preparation of peptide-polymer nanotubular hybrids.

1.2 Peptoids

1.2.1 Introduction

Peptoids are oligomers of *N*-substituted glycine and were devoleped by Bartlett and co-workers in the early

[28] J. Couet, J. D. J. S. Samuel, A. Kopyshev, S. Santer, M. Biesalski, *Angew. Chem. Int. Ed.*, **2005**, *44*, 3297-3301.

1990's.[29] Structurally, the placement of the monomer side chains on the amide nitrogen (as opposed to the α-carbon in α-peptides, figure 1.12) confers achirality to the peptoid backbone, and contemporary the presence of tertiary amide bonds (rapidly isomerizing between *cis* and *trans* conformation) and the absence of hydrogen donors lead to a flexible structure, hydrogen bond deficient. As a consequence, the design of a well-defined secondary structures in peptoids, which is very important for peptoid-target protein interactions and for the general understanding of structure-function relationships, is a complex outcome, achievable making use of specific amide side chains or through macrocyclization strategies.

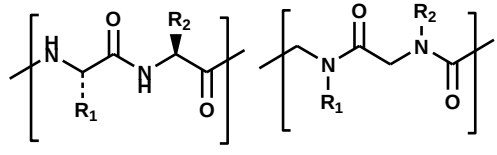

Peptide **16** Peptoid **17**

Figure 1.12: General structure of peptides and peptoids.

Anyway, these peptido-mimetic compounds present many advantages with respect to peptides such as an higher resistance to enzymatic proteases (enhanced oral

[29] R.J. Simon, R.S. Kania, R.N. Zuckermann, V.D. Huebner, D.A. Jewell, S. Banville, S.L. Wang, S. Rosenberg, C.K. Marlowe, P. A. Bartlett *Proc. Natl. Acad. Sci.* U.S.A., **1992**, *89*, 9367-9371.

bioavailability and half-life in the body), an increased cellular permeability due to the more hydrophobic backbone, absence of immunogenic properties. In addition, they can be synthesized using a straightforward, modular synthesis that allows the incorporation of a plethora of amide side chains. Indeed, peptoids have being developed as mimics of biologically active peptides, as replacements of small molecule drugs, as versatile biomolecular tools in order to study complex biomolecular interactions, and have becoming attractive candidates in nanotechnology, catalysis, and for therapeutic and diagnostic applications.[30,31]

Ultimately, peptoids represent a very challenging research field as indicated by the graphic in figure 1.13, which shows the numerous articles and patents on peptoids from 1992 to 2010.[32]

[30] M. T. Dohm, R. Kapoor, A. E. Barron *Current Pharmaceutical Design*, **2011**, *17*, 2732-2747.
[31] S. A. Fowler, H. E. Blackwell *Org. Biomol. Chem.*, **2009**, *7*, 1508-1524.
[32] A. S. Culf, R. J. Ouellette *Molecules*, **2010**, *15*, 5282-5335.

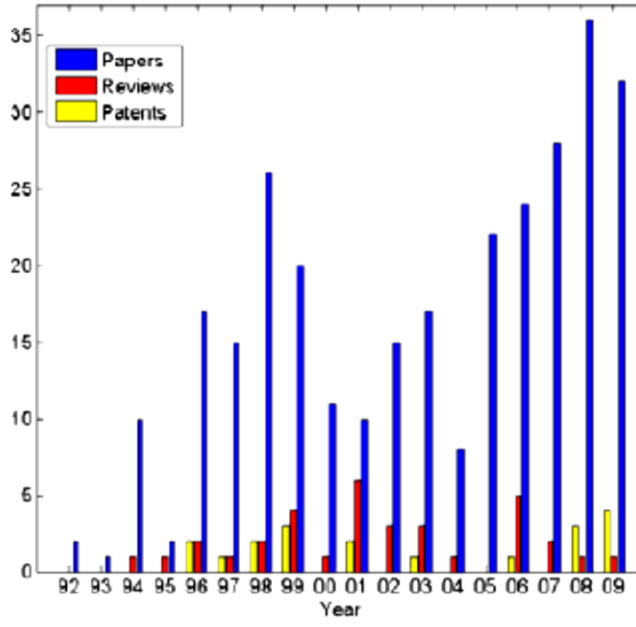

Figure 1.13: Primary research articles, reviews and patents on peptoids published from 1992 to 2010.

1.2.2 Synthesis

Peptoids are normally synthesized making use of the solid-phase monomer or submonomer approach.

Monomer method was developed by Merrifield[33] in relation to peptide synthesis (scheme 1.1). Typically, in the monomer synthesis of peptides the most common α-amino-protecting groups are Fmoc and Boc groups used in the Fmoc/*tert*-butyl (*t*Bu) and Boc/benzyl (Bn) strategies, respectively.

[33] R. B. Merrifield, *J. Am. Chem. Soc*, **1964**, *86*, 2149–2154.

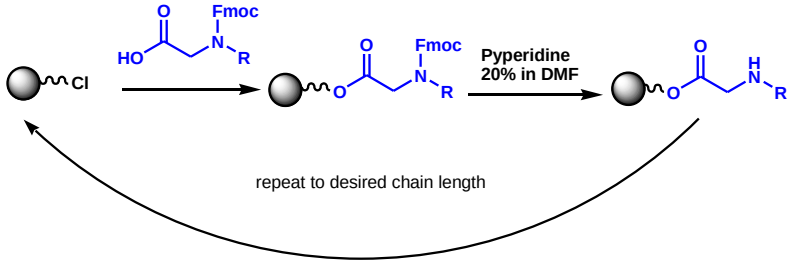

Scheme 1.1: Monomer synthesis of peptoids.

Peptoids can be synthesized by coupling *N*-substituted glycines using standard α-peptide synthesis methods. Nevertheless, the mean drawback of using the monomer approach in the case of peptoids consists in the synthetic effort required to prepare a suitable set of chemically diverse monomers.[4] In addition, the secondary *N*-terminal amine in peptoid oligomers is more bulky than primary amine of an amino acid, leading to slower coupling reactions.

The favourite synthetic method for peptoids is the submonomer approach, developed by Zuckermann *et al.* (scheme 1.2).[34]

[34] R. N. Zuckermann, J. M. Kerr, B. H. Kent, W. H. Moos, *J. Am. Chem. Soc.*, **1992**, *114*, 10646-10647.

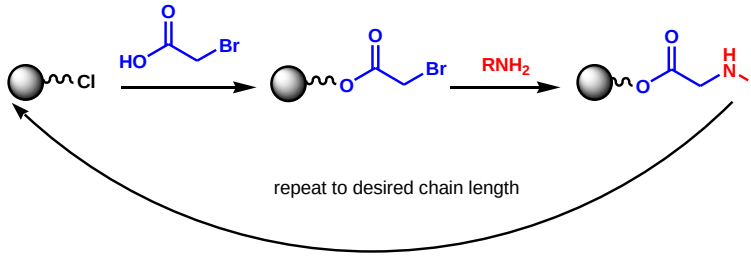

Scheme 1.2: Submonomer synthesis of peptoids.

This method is called as so because each cycle of monomer addition is divided in
two steps, an acylation step with bromoacetic acid and a nucleophilic displacement step with a primary amine.
In general, it is the reference method for peptoid synthesis because it is very straightforward and efficient. Futhermore, there is no need to use protecting groups in elongating the main chain and the availability of a large number of primary amines permits the simple preparation of a vast peptoid library.

1.2.3 Conformationally constrained peptoid oligomers

The question of generating stable secondary structures in peptoids is very challenging because, as aforementioned, the peptoid backbone exhibits an intrinsic flexibility due to the absence of hydrogen bond donors and to the *cis-trans* isomerization of tertiary amide bonds. This causes a substantial conformational heterogeneity of the peptoid backbone.

However, researchers have developed strategies to stabilize helical, loop and turn motifs in peptoids by incorporating amide side chains that reduce conformational fluxionality. Specifically, several side chains have been individuated which effectively control the *cis-trans* geometry of the backbone amide bonds, and induce the formation of stable secondary structures.[35]

The peptoid helix and threaded loop constitute the first peptoid secondary structural topology to be discovered, and are formed in presence of α-chiral amide side chains such as *N*(*S*)-(1-phenylethyl)glycine (*N*spe), *N*(*S*)-(*sec*-butyl)glycine (*N*ssb), *N*(*S*)-(1-cyclohexylethyl)glycine (*N*sch), *N*-(*S*)-(1-naphthylethyl)glycine (*N*snpe) (figure 1.14).

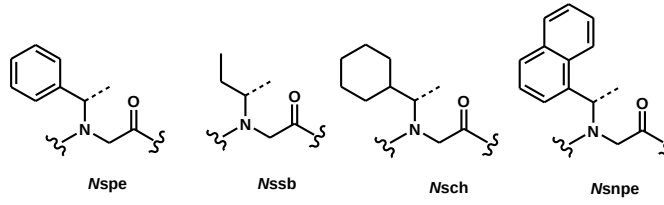

Figure 1.14: Common bulky aliphatic and aromatic α-chiral monomers used to induce helical conformations in peptoids.

These bulky residues produce steric repulsion between side chains, and in addition establish hydrophobic and n→ Π* interactions. In this way, it is favoured a polyproline type I helical conformation, totally composed of *cis* amide bonds (figure 1.15). The helical structures of different homo-

[35] J. Sun, R. N. Zuckermann ACS NANO, **2013**, *7*, 4715-4732.

oligopeptoids containing α-chiral amide side chains were analyzed by circular dicroism, 2D NMR, molecular modeling studies, and X-ray crystallography.[36] Clearly, the handedness of the helix is determined by the handedness of the α-chiral side chains.

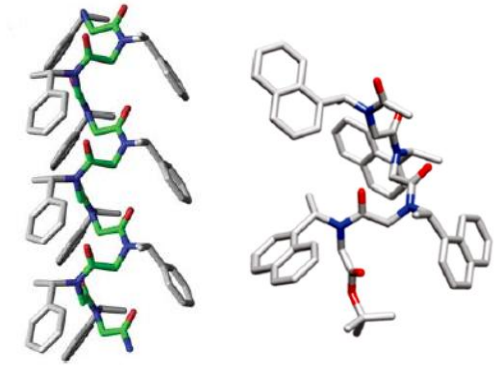

Figure 1.15: The peptoid helix, shown here as the structure of $(N\text{spe})_{10}$ (*left*). Structure generated by molecular mechanics from the calculated structure of $(N\text{spe})_8$. X-ray crystal structure of Ac-$(N\text{snpe})_4$-COO*t*Bu (*right*), which shows the so called "naphtoid" helix. Atom designations: red = oxygen; blue = nitrogen; gray = carbon.

Interestingly, the highest stabilization of *cis* backbone conformation was reached using *N*snpe side chains ($K_{cis/trans}$ = 9.7), due to the fact that n→ Π* interactions between the lone pair on the carbonyl oxygen of the backbone and the Π* orbital of an adjacent aromatic side chain were demonstrated to enforce *cis* geometry. Moreover, the "naphtoid" helix (

[36] C. W. Wu, K. Kirshenbaum, T. J. Sanborn, K. A. Dill, R. N. Zuckermann, A E. Barron *J. Am. Chem. Soc.*, **2003**, *125*, 13525-13530.

figure 1.15) represents the most robust polyproline type I helix to date.[37]

Barron and co-workers investigated the effect of peptoid sequence on helix stability, and in the end established that the minimum chain length to observe an helix is five residues with stability increasing with chain length up to 15 residues, and a minimum of 50% α-chiral side chains are required to form a stable helix.[38]

Accidentally, during the analysis of the peptoid helix, they also discovered a second peptoid structure, the threaded loop. This unusual structure is unique to peptoid nonamers with α-chiral side chains, and was first found in (*N*spe)$_9$ TFA salt (**18**, figure 1.16).[39] It is stabilized via multiple intramolecular hydrogen bonds between the protonated amino terminus and three backbone carbonyls as highlighted by 2D NMR study in CD_3CN (figure 1.16). Curiously, the loop conformation converts into the classic peptoid helix in presence of a solvent with hydrogen bond potential (*e.g.*. 50% methanol in acetonitrile), which is able to destroy the intramolecular hydrogen bonds.

[37] J. R. Stringer, J. A. Crapster, I. A. Guzei, H. E. Blackwell *J. Am. Chem. Soc.*, **2011**, *133*, 15559-15567.
[38] C. W. Wu, T. J. Sanborn, K. Huang, R. N. Zuckermann, A. E. Barron *J. Am. Chem. Soc.*, **2001**, *123*, 6778-6784.
[39] K. Huang, C. W. Wu, T. J. Sanborn, J. A. Patch, K. Kirshenbaum, R. N. Zuckermann, A. E. Barron *J. Am. Chem. Soc.*, **2006**, *128*, 1733-1738.

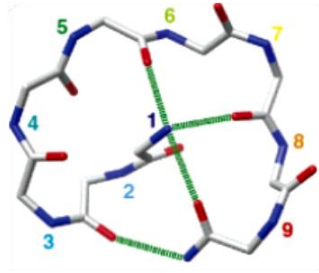

18

Figure 1.16: Solution structure of $(Nspe)_9$ TFA salt in CD_3CN containing the hydrogen bond interactions. Residues from the N- to the C-terminus in the peptoid chain are color-ramped from blue to red following the rainbow pattern. Atom designations: red = oxygen; blue = nitrogen; gray = carbon. Substituents were omitted for clarity.

Anyway, it was also intriguing to favour *trans*-amide bonds in the peptoid backbone. In particular, Kirshenbaum and co-workers demonstrated the stabilization of the *trans*-amide conformer with more than 90% by making use of *N*-aryl side chains.[40] Notably, in their work was predicted a polyproline type II helix for *N*-aryl peptoid oligomers.

In the wake of Kirshenbaum's discover, Blackwell's group demonstrated a special acyclic peptoid reverse-turn conformation with an all-*trans* amide backbone through the incorporation of *ortho*-hydroxy *N*-aryl side chains capable of hydrogen bonding in the backbone of a tripeptoid (**19**, figure 1.17).[41] Specifically, X-ray crystallography and 2D NMR indicate the presence of two intramolecular 8-membered-ring

[40] N. H. Shah, G. L. Butterfoss, K. Nguyen, B. Yoo, R. Bonneau, K. Kirshenbaum *J. Am. Chem. Soc.*, **2008**, *130*, 16622-16632.
[41] J. R. Stringer, J. A. Crapster, I. A. Guzei, H. E. Blackwell *J. Org. Chem.*, **2010**, *75*, 6068-6078.

hydrogen bonds in which are involved the side chain hydroxyl proton, two backbone carbonyls and a backbone amide proton (figure 1.17).

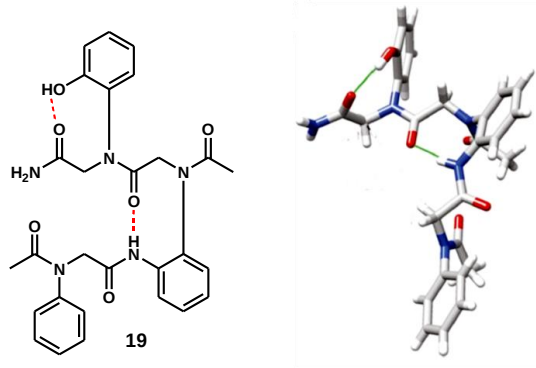

Figure 1.17: Chemical structure of tripeptoid **19** with 8-membered-ring hydrogen bonds depicted in red (*left*) and X-ray crystal structure of the same compound with hydrogen bonds indicated as solid green lines (*right*). Atom designations: red = oxygen; blue = nitrogen; gray = carbon.

Later, Blackwell and co-workers discovered a special sheet-like secondary structure making use of *N*-hydroxy side chains in a dipeptoid structure (figure 1.18).[42] In particular, in the crystal structure individual peptoid backbones are arranged in an antiparallel fashion and are linked through intermolecular hydrogen bonds.

[42] J. A. Crapster, J. R. Stringer, I. A. Guzei, H. E. Blackwell *Peptide Science*, **2011**, *96*, 604-616.

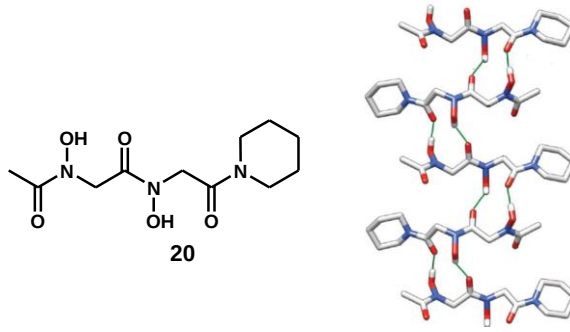

Figure 1.18: Chemical structure of dipeptoid **20** (*left*) and X-ray crystal structure of the same compound with hydrogen bonds indicated as solid green lines (*right*). Atom designations: red = oxygen; blue = nitrogen; gray = carbon.

More recently, the same Blackwell's group found that, alternating substituted *N*-aryl side chains and *N*snpe side chains in the backbone of an hexapeptoid, a ribbon-like structure hydrogen bond deficient (figure 1.19) is induced.[43] The peptoid ribbon can be described as a succession of turn units, in analogy with β-bend ribbon folds in α-peptides. Anyway, while in peptide ribbons all amide bonds are in the *trans* configuration, in the case of peptoid ribbon is present an alternating *cis*/*trans* geometry, due to the contemporary use of *trans*- and *cis*- inducing residues. In addition, the ribbon fold is largely stabilized by the steric demands of the bulky *N*snpe side chains.

[43] J. A. Crapster, I. A. Guzei, H. E. Blackwell *Angew. Chem. Int. Ed.*, **2013**, *52*, 1-7.

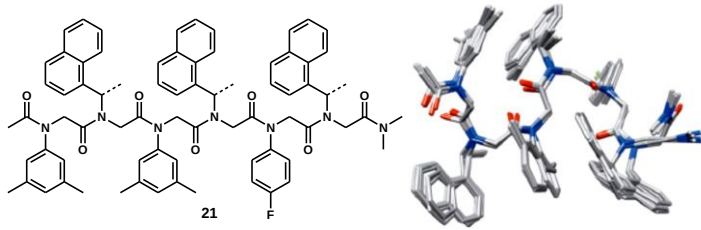

Figure 1.19: Chemical structure of hexapeptoid **21** (*left*) and an ensemble of 10 superimposed low-energy structures of **21** determined via 2D NMR in $CDCl_3$ (*right*). Atom designations: red = oxygen; blue = nitrogen; gray = carbon.

1.2.4 Cyclopeptoids

The flexible nature of peptoids may limit the development of peptoid-based protein ligands with high affinity and specificity. So a potentially promising way to overcome this limitation, in addition to the use of specific amide side chains in the peptoid backbone, is the effective and straightforward macrocylization of peptoids, which reduces conformational freedom, simply producing conformationally constrained structures.

Therefore, in the same manner as peptides, cyclization is of great importance also for peptoids and in this context cyclopeptoids represent an intriguing class of peptidomimetics.

Specifically, it is possible to synthesize cyclopeptoids through a direct head-to-tail cyclization reaction (*e.g.* scheme 1.3) or by ligation of opportunely functionalized side chains.

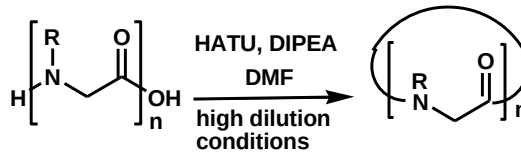

Scheme 1.3: Head-to-tail macrocyclization of peptoids.

The latter can be performed according to different approaches as following illustrated.

The first strategy used to form intramolecular covalent constraints between the side chains of a peptoid oligomer was the Cu^{I}-catalyzed azide/alkyne cycloaddition, a classic "click chemistry" reaction. For example, Kirshenbaum and co-workers made use of this reaction in order to successfully constrain helical peptoid conformations (figure 1.20) producing cyclic (*i*, *i*+3) oligomers.[44]

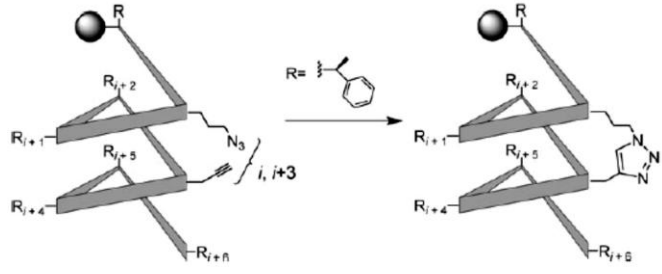

Figure 1.20: Positioning of azide and alkyne groups on an idealized polyproline type I helix. A helical template may pre-organize reactive functional groups at positions *i* and *i* +3 for optimum product formation.

[44]J. M. Holub, H. Jang, K. Kirshenbaum *Org. Lett.*, **2007**, *9*, 3275-3278.

Later, intramolecular lactam bridges were installed between peptoid side chains with the aim of enhancing conformational stability. This strategy was effectively tried in the case of helical peptoid structures.[45]

More recently, triazine-linked bicyclic peptoids were synthesized directly on the resin via a specific macrocyclization reaction (figure 1.21).[46]

The macrocyclization reaction was accomplished through a nucleophilic attack by the cysteine sulfhydryl group on a reactive chloride on the triazine ring, as shown for compound **22**.

Notably, bicyclic peptoids possess an enhanced conformational rigidity in comparation with monocyclic peptoids and, as a consequence, should be able to bind more tightly and specifically to target proteins.

[45] B. Vaz, L. Brunsveld *Org. Biomol. Chem.*, **2008**, *6*, 2988-2994.
[46] J. H. Lee, H. S. Kim, H. S. Lim *Org. Lett.*, **2011**, *13*, 5012-5015.

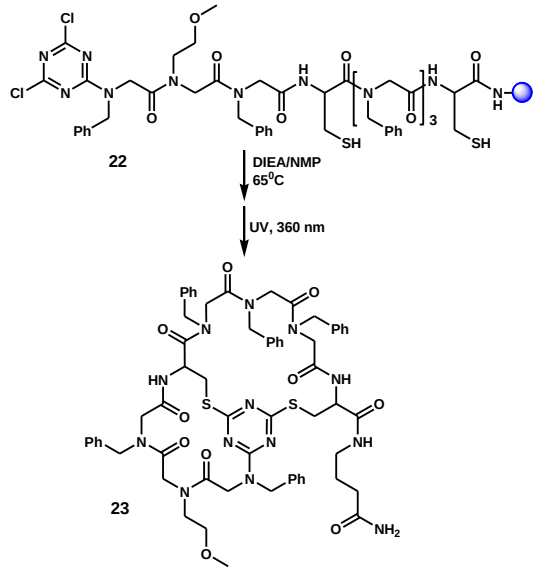

Figure 1.21: On-resin macrocyclization for a triazine-bridged bicyclic peptoid **22**.

Cyclopeptoids have permitted a structural investigation by X-ray crystallography a far more vast than in the case of peptoid oligomers.[47] This is clearly ascribable to the increase of the conformational order realized in macrocylic peptoids.

Interestingly, the first rigorous structural studies reported the X-ray crystallographic investigation on the cyclic oligopeptides of sarcosine (*N*-methyl glycine).[48] In addition, the first X-ray crystal structure of a cyclic peptoid hetero-

[47] B. Yoo, S. B. Y. Shin, M. L. Huang, K. Kirshenbaum *Chem. Eur. J.*, **2010**, *16*, 5528-5537.
[48] P. Groth *Acta Chem. Scand.*, **1976**, *30*, 838-840.

oligomer to date was obtained from a cyclohexapeptoid (**24**) by Kirshenbaum and co-workers (figure 1.22).[49]

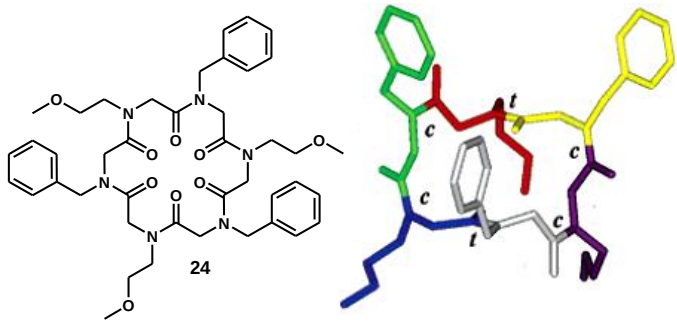

Figure 1.22: Chemical structure of cyclohexapeptoid **24** (*left*) containing alternated residues of benzylamine and methoxyethylamine. X-ray crystal structure of the same compound (*right*) showing segregation of polar and apolar side chains on opposite faces of the macrocycle and the peptide bond pattern of backbone. *Purple* - residue 1, *yellow* - residue 2, *red* - residue 3, *green* - residue 4, *blue* - residue 5, *gray* - residue 6, *c* - *cis*, *t* – *trans*.

The discussed structure turned out to be very interesting. Specifically, the crystal is triclinic and the backbone is characterized by a combination of four *cis* and two *trans* amide bonds according to a pattern *tcctcc*, with the *cis* amide bonds located at the corners of a roughly rectangular structure. More interestingly, the orientation of the side chains is such that is produced a partitioning of

[49] S. B. Y. Shin, B. Yoo, L. Y. Todaro, K. Kirshenbaum, *J. Am. Chem. Soc.*, **2007**, *129*, 3218-3225.

hydrophobic and polar side chains groups on either face of the macrocycle. This feature may be very useful for the prediction of the spatial arrangements of different side chain types in a cyclopeptoid alike to **24**.

Additionally, superposition of **24** with the idealized peptide β-turn type-I and type-III showed a RMSD (root mean square deviation of backbone C-α atoms) of 0.397 Å and 0.301 Å respectively, as a demonstration of the analogy between cyclopeptoid structures and peptide structures (figure 1.23).

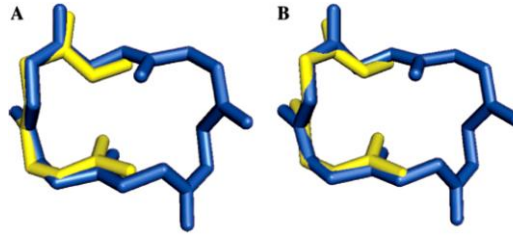

Figure 1.23: Superposition of the backbone atoms in cyclic peptoid hexamer **24** (blue) with canonical: (A) type I β-turn (yellow); (B) type III β-turn (yellow).

1.2.5 Complexation and transport of metal ions

Similarly to peptides, also peptoids can selectively complex and transport metal ions. In 2008 De Riccardis and co-workers synthesized two *N*-benzyloxyethyl cyclopeptoids (**25, 26**) (figure 1.24) which are characterized by a good

affinity towards alkali metals (table 1.1).[50] Specifically, the complex association constant host-ion (K_a) were determined by picrate extraction technique in $H_2O/CHCl_3$, as described by Cram and co-workers,[51] and highlighted a good degree of selectivity towards Na^+ for **25.** In addition, the bigger macrocycle **26** resulted to be selective to Cs^+.

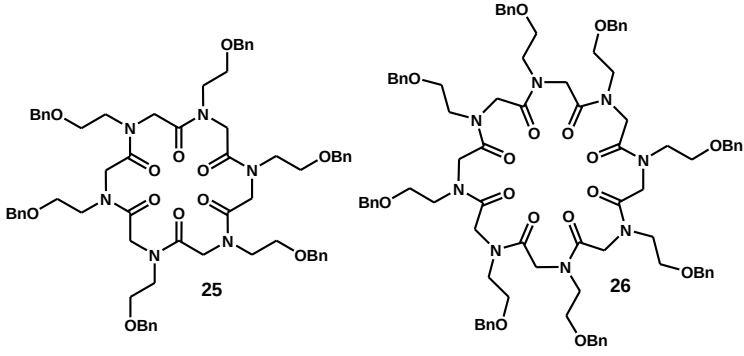

Figure 1.24: *N*-benzyloxyethyl cyclohexapeptoids synthesized from De Riccardis *et al.*

[50] N. Maulucci, I. Izzo, G. Bifulco, A. Aliberti, C. De Cola, D. Comegna, C. Gaeta, A. Napolitano, C. Pizza, C. Tedesco, D. Flot, F. De Riccardis *Chem. Commun.*, **2008**, 3927-3929; C. De Cola, S. Licen, D. Comegna, E. Cafaro, G. Bifulco, I. Izzo, P. Tecilla, F. De Riccardis *Org. Biomol. Chem.*, **2009,** *7*, 2851-2854.

[51] K. E. Koenig, G. M. Lein, P. Stuckler, T. Kaneda, D. J. Cram *J. Am. Chem. Soc.*, **1979**, *101*, 3553.

Table 1.1: Parametres for association between hosts and picrate salts in $CHCl_3$ at 25 °C.

Complexing agent	M^+	R_{CHCl_3} [a)]	$K_a \times 10^{-6}$ [M^{-1}]	$-\Delta G^0$ (kcal/mol)
25	Na^+	0.35	3.3	8.9
26	Cs^+	0.29	1.5	8.4

[a)] [Guest]/[Host] in $CHCl_3$ layer at equilibrium obtained by direct measurement, or calculated by difference from measurement made on aqueous phase.

The NMR spectrum of cycle **25** was very complicated due to the contemporary presence of more than one conformer in slow exchange on the NMR time scale. The conformational disorder in solution was seen as a propitious auspice for the complexation studies. Indeed, the stepwise addition of sodium picrate to **25** induced the formation of a new chemical species (the sodium complex), whose concentration increased with the gradual addition of the guest (figure 1.25 b and c). Finally, with an excess of guest, a simplified NMR spectrum was obtained, reflecting the formation of a 6-fold symmetric species (figure 1.25 c).

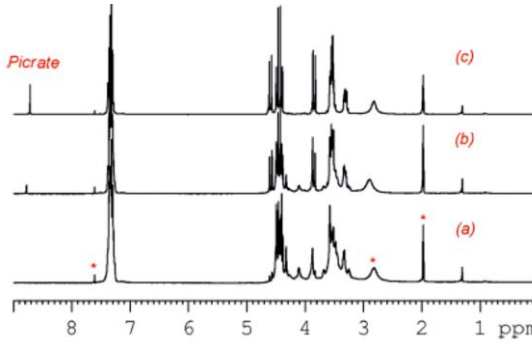

Figure 1.25: ^{1}H NMR spectra of free **25** (a) (CD_3CN–$CDCl_3$ 9:1 solution, 25 °C, [**25**] = 4.0 mM, 400 MHz) and in the presence of 0.5 eq. (b) or 1.5 eq. (c) of sodium picrate. Residual solvent peaks are labelled with *.

The first structure of a cyclopeptoid metal complex to be solved was obtained for a zwitterionic complex of **25** with strontium picrate (**25**$_2$.[Sr(picr)$_2$]$_3$).

Interestingly, the crystal was monoclinic and the backbone was characterized by a unique all-*trans* peptoid bond pattern, with the carbonyl groups alternatively pointing toward the strontium cations so that the *N*-linked side chains are made to adopt a pseudo-equatorial arrangement (figure 1.26). In addition, picrate anion behaves as a bidentate ligand interacting with the cation so that three picrates bind two external Sr cations. The presence of picrate in the complex allows to define it a zwitterionic species.

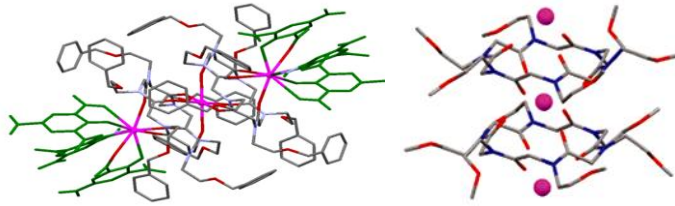

Figure 1.26: X-ray crystal structure of **25**$_2$.[Sr(picr)$_2$]$_3$. Atom designations (*right figure*): red = oxygen; blue = nitrogen; gray = carbon, magenta = strontium. In the left figure picrate anions are depicted in green, strontium ions in magenta and cyclopeptoid molecules in gray.

Later, the compounds **25, 26** were subjected to ion transport studies with the HPTS assay, demonstrating a size dependent selectivity for the first group alkali metals with transport preferences respectively for Na^+ and Cs^+, according to a carrier based mechanism.[50]

These results clearly indicate that cyclopeptoids represent novel motifs for the design of ionophoric antibiotics similarly to the peptide valynomicin.

1.2.6 Biologically active peptoids

Peptoids, exactly as peptides, can show some specific biological activities. In particular, amphiphilic cyclopeptoids have drawn interest in the role of antibacterial agents due to the fact that they contain both hydrophobic side chains, which make them soluble in bacterial membranes increasing the cell membrane permeability, and positive charged side chains interacting electrostatically with negative groups of bacterial porins.

In 2010 the antifungal and antibacterial properties of some new cationic hexacyclopeptoids correlating their efficacy with the linear cationic and cyclic neutral counterparts were evaluated by De Riccardis and co-workers. Specifically, the compounds contained a variable number of *N*-benzyloxyethyl/*N*-benzyl residues and protonated *N*-lysine residues.[52] This investigation was inspired by the analogy between the afore mentioned *N*-benzyloxyethyl hexacyclopeptoid, an efficient ionophore agent for Na^+, and the antibiotic valynomicin, a classic transmembrane agent for K^+.

The purpose of this study was to explore the biological effects of the cyclization on the antimicrobial properties of positively charged oligomeric *N*-alkylglycines, in order to mimic the natural amphiphilic peptide antibiotics. Moreover, the modular peptoid backbone was very suitable for the appropriate design of novel antimicrobial compounds.

Experimentally, all the molecules analyzed were more active against fungi than bacteria. In addition, cyclic molecules exhibited better antifungal properties with respect to the linear ones. Finally, within the cyclic compounds, the antifungal potency increased with the net positive charge, as indicated by the fact that compounds **27** and **28** (figure 1.27) possessed the highest net positive charge amongst the peptoids tested and were also the most effective ones.

[52] D. Comegna, M. Benincasa, R. Gennaro, I. Izzo, F. De Riccardis *Biorg. Med. Chem.*, **2010**, *18*, 2010-2018.

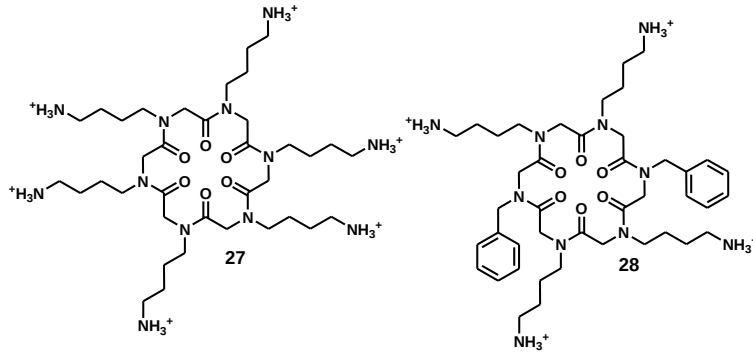

Figure 1.27: Amphiphilic cyclopeptoids resulted to be the most active against fungi in a recent study carried out by De Riccardis and co-workers.

Kirshenbaum and co-workers recently patented some cyclopeptoids with antibacterial activity[53] (figure 1.28) and more recently in 2013 reported some novel amphiphilic cyclopeptoids, exhibiting a strong antibacterial activity against *Staphylococcus aureus*, a multi-drug resistant bacterium.[54] One of the most active cyclopeptoids tested is illustrated in figure 1.29.

[53] U.S.A. Patent Application Pubblication 2010/0222255.

[54] M. L. Huang, M. A. Benson, S. B. Y. Shin, V. J. Torres, K. Kirshenbaum *Eur. J. Org. Chem.*, **2013**, *17*, 3560-3566.

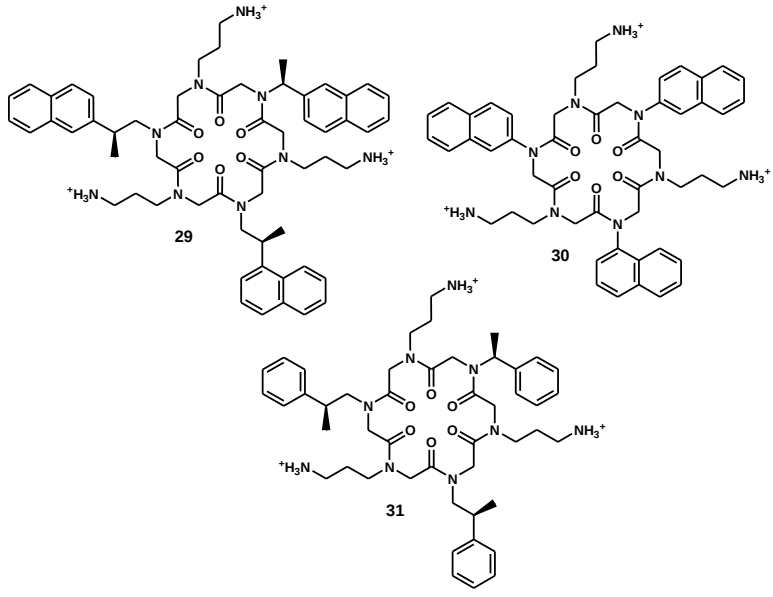

Figure 1.28: Amphiphilic cyclohexapeptoids patented by Kirshenbaum.

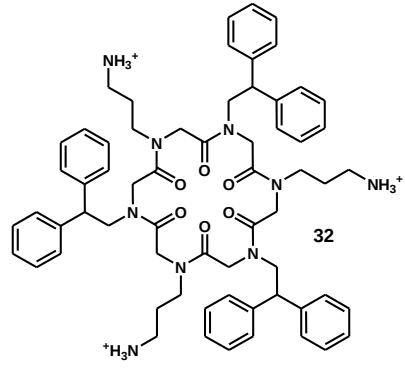

Figure 1.29: Amphiphilic cyclopeptoid resulted to be one of the most active against *Staphylococcus aureus* in a very recent study carried out by Kirshenbaum and co-workers.

In conclusion, these results strongly encourage the research on amphiphilic peptidomimetics with antibiotic properties.

1.2.7 Catalytic properties

In literature there is only one example of peptoids in the role of catalysts, reported by Kirshenbaum and co-workers.

Specifically, Kirshenbaum synthesized a set of helical peptoid oligomers catalyzing the oxidative kinetic resolution (OKR) of 1-phenylethanol induced by the oxidant TEMPO (2,2,6,6-tetramethylpiperidine-1-oxyl) (figure 1.30).[55]

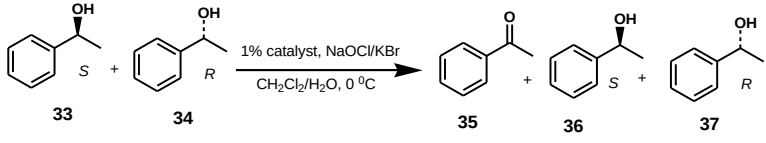

Figure 1.30: Oxidative kinetic resolution of 1-phenylethanol.

TEMPO, a well-known catalyst for oxidative transformations, was covalently linked at various sites along properly designed chiral peptoid backbones which were used as asymmetric catalysts in the oxidative resolution.

It was demonstrated that the enantioselectivity of the process essentially depended on three factors: 1) the handedness of the asymmetric environment derived from the

[55] G. Maayan, M. D. Ward, K. Kirshenbaum *Proc. Natl. Acad. Sci.* U.S.A., **2009**, *106*, 13679-13684.

helical scaffold, 2) the position of the catalytic centre TEMPO along the peptoid backbone, and 3) the degree of conformational ordering of the peptoid scaffold. For istance, the highest activity in the OKR (e.e. > 99%) was observed for the catalytic peptoids with the TEMPO group attached at the N-terminus, as in the case of peptoids **38**, **39** (figure 1.31). These results revealed that the selectivity of the OKR was dictated by the global structure of the catalyst and not solely from the local chirality at sites neighbouring the catalytic centre.

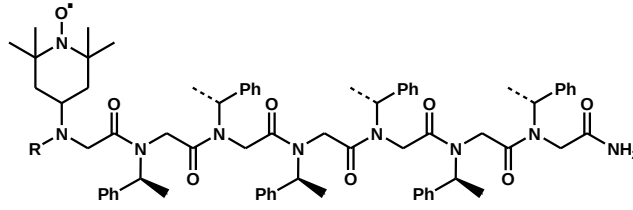

38, right-handed helix (*e.e.* > 99% (*R*))

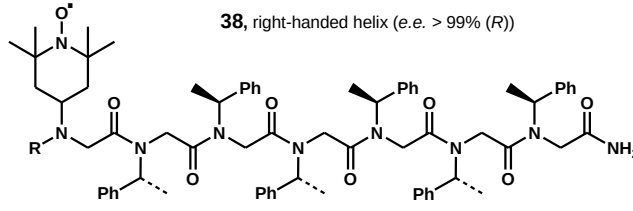

39, left-handed helix (*e.e.* > 99% (*S*))

Figure 1.31: Catalytic peptoid oligomers **38** and **39**.

1.2.8 Nanostructures

Peptoids can also form nanotubular structures as in the case of peptide nanotubes described before.

In 2013 Kirshenbaum's group reported a cyclo-octapeptoid (**40**) which is able to storage and release water molecules from the central channels of a nanotubular structure, realizing the first single-crystal-to-single-crystal transition for a peptoid (figure 1.32).[56]

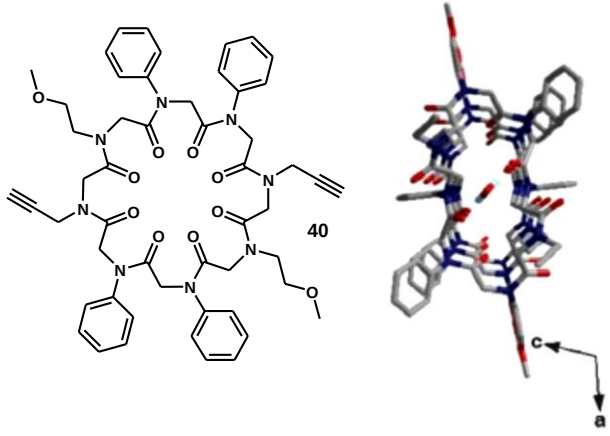

Figure 1.32: Chemical structure of cyclo-octapeptoid **40** (*left*) and X-ray crystal structure of the same compound with view along *b* axis (*right*). Atom designations: red = oxygen; blue = nitrogen; gray = carbon.

Single crystal X-ray determination demonstrated the formation of a monoclinic crystal with C_2 symmetry derived from the backbone sequence. The backbone adopts a planar geometry, and there is a central cavity in the macrocycle. In the crystal lattice, the macrocycle units stack along the *b* axis

[56] S. B. L. Vollrath, C. Hu, S. Brase, K. Kirshenbaum *Chem. Commun.*, **2013**, *49*, 2317-2319.

and in this way the inner macrocycle cavities generate a nanotube structure.

In addition, the crystal contained water molecules within the central channel, which sum up to 19% mol relative to the peptoid. Furhermore, in order to evaluate the possibility to uptake and release water molecules from the nanotubular structure in a cyclic way, a peptoid single-crystal was firstly full dehydrated under ambient conditions with total retention of the single crystalline morphology, and afterwards was effectively rehydrated in a humid environment up to 44% mol.

In conclusion, the nanotubular structure of peptoid **40** is a valid starting point for the future design of new peptoid-based crystalline materials capable of undergoing unusual single-crystal-to-single-crystal transformations.

1.3 The research project

Aim of the research project has been the synthesis of cyclopeptides and cyclopeptoids in order to investigate their structural properties and catalytic activities.

In particular, studies of the arrangement and the cyclopeptoids organization in the crystal structure have been realized. Moreover, the influence of some aminoacidic residues on conformational control of peptoid skeleton was evaluated. In this context, the effect of proline, an aminoacid with an important role in the formation of

secondary protein structures,[57] and of a pseudo-proline residue on the crystal structure and conformational equilibria of some cyclopeptoids was evaluated. In particular, *N*-methoxyethyl cyclic peptoids containing proline and *N*-methoxyethyl hexacyclopeptoid (proline-free) in complexed and uncomplexed form (**41-43**, figure 1.33) were successfully synthesized and characterized by X-ray diffraction. In addition, the synthesis of a cyclohexapeptoid containing a pseudo-proline residue was obtained (**44**, figure 1.33).

Furthermore, two isomeric amphiphilic peptoids (**45, 46**, figure 1.33) were synthesized in order to investigate the effect of amphiphilicity on the crystal frame.

All that will be described in the following two sections.

Moreover, considering the well documented complexation properties of cyclopeptoids towards alkaline metals,[50] the ability of some cyclohexapeptoids to work as phase-transfer catalysts was investigated in a benchmark S_N2 reaction. In particular, the cyclopeptoid which revealed to be the most active was the *N*-[2-(2-methoxyethoxy)ethyl] side chain cyclohexapeptoid (**47**, figure 1.34). Therefore, we also tested some proline-rich cyclopeptoids in asymmetric phase transfer catalysis and the most promising demonstrated to be the cyclopeptoid **48** (figure 1.34) alternating *N*-3,5-dimethyl benzylamine glycine and proline residues.

[57] M. Mutter, G. G. Tuchscherer, C. Miller, K. H. Altmann, R. I. Carey, D. F. Wyss, A. M. Labhardt, J. E. Rivier, *J. Am. Chem. Soc.*, **1992**, *114*, 1463 –1470.

The catalytic studies mentioned will be illustrated in section 4.

Finally, in section 5 is reported a novel synthetic strategy for the synthesis of the biologically active cyclotide kalata B1 (**10**, figure 1.35), based on Fmoc/*t*-Bu solid phase synthesis and on the use of an innovative linker.

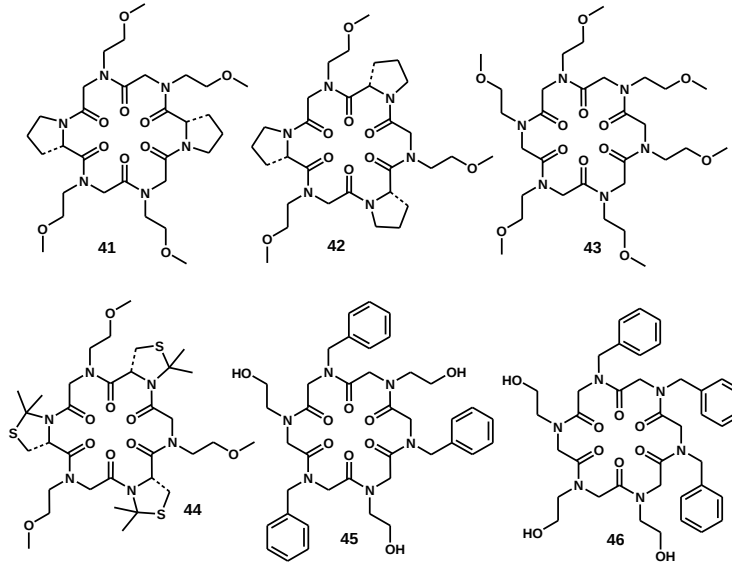

Figure 1.33: Cyclopeptoids synthesized for structural studies.

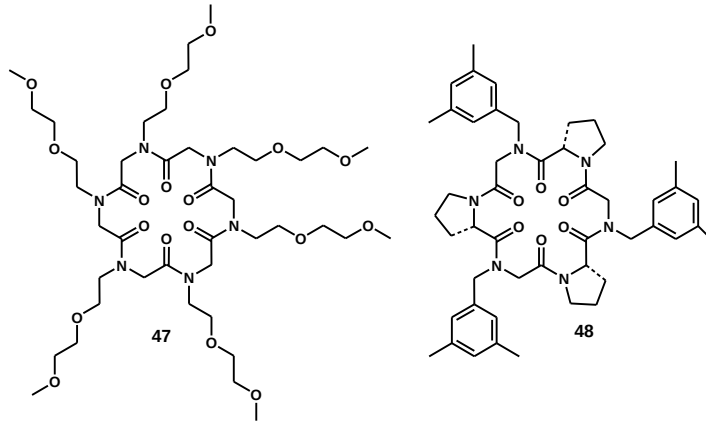

Figure 1.34: Cyclopeptoids resulted to be the most active in the phase-transfer catalysis studies.

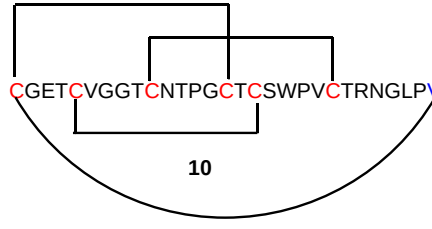

Figure 1.35: Cyclotide kalata B1.

1 INTRODUCTION

2 PROLINE-RICH CYCLOPEPTOIDS

2.1 The role of proline in peptoid conformation

In the last years many efforts have been devoted to restrict backbone conformation for linear and cyclic peptoids,[58] considering that a decreased conformational entropy and a well defined structure could be useful for biological applications such as interaction peptoid-biological target.

Proline is unique among the aminoacids, having the side chain linked to amide nitrogen atom. Its five membered ring imposes rigid constraints on the N-C^{α} bond rotation, playing important role in peptide loops and turns, and confering unique conformational properties to the peptide or protein backbone when compared to the common proteinogenic aminoacids.[47] For example, the structural elements induced by proline are necessary for the formation of compact globular structures in proteins.[57] Futhermore, proline residues lead to *cis-trans* isomerization of the imidic bond formed with the preceding residue (Xaa-Pro) due to the characteristic low activation barrier for isomerization, combined with the small free energy differences between the two peptide bond isomers. This isomerization can produce conformational changes involved in many biological processes such as protein folding and various aspects of

[58] S. A. Fowler, H. E. Blackwell *Org. Biomol. Chem.*, **2009**, *7*, 1508-1524.

protein function (*e.g.* channel gating, membrane binding, etc.).[59]

The biological importance of proline-rich peptides has caused the development of several substituted-proline analogues in order to control the peptoid backbone or to modify the imide *cis-trans* ratio.[60] In this regard, it was recently reported that 2,2-dimethyl-1,3-oxazolidine-4-carboxylic acid and 2,2-dimethyl-1,3-thiazolidine-4-carboxylic acid, named pseudo-prolines ($\Psi^{Me,Me}$Pro) (**49** and **50**, figure 2.1), significantly control the peptide backbone, inducing preferentially the *cis* conformation in the Xaa-ΨPro bond, due to unfavorable steric interactions between the methyl groups and the α-proton of Xaa in the *trans*-conformation.[60]

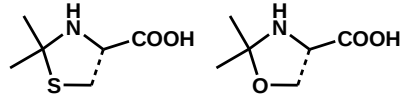

49 **50**

Figure 2.1: 2,2-dimethyl-1,3-thiazolidine-4-carboxylic acid (**49**) and 2,2-dimethyl-1,3-oxazolidine-4-carboxylic acid (**50**) (pseudoprolines, $\Psi^{Me,Me}$Pro).

An intriguing example of pseudo-proline analogue of a biologically active peptide deals with the synthesis of a mimetic of peptide hormone oxytocine (**51**, figure 2.2): a cyclic nonapeptide containing a disulfide bond between two

[59] P. Craveur, A. P. Joseph, P. Poulain, A. G. de Brevern, J. Rebehmed *Amino Acids*, **2013**, *45*, 279-289.
[60] P. Dumy, M. Keller, D. E. Ryan, B. Rohwedder, T. Wohr, M. Mutter *J. Am. Chem. Soc.*, **1997**, *119*, 918-925.

cysteine residues at positions 1 and 6.[61] Oxytocine is a mammalian neurohypophysial hormone which plays roles during child birth and is used clinically to stimulate uterine contractions during labour and to stimulate the secretion of breast milk. Specifically, it was studied the role of the proline residue at position 7 of oxytocine, linked to Cys^6 through a *trans* peptide bond.

Notably, the replacement of Pro^7 in the oxytocine backbone with *cis*-prolyl mimic 2,2-dimethyl-1,3-thiazolidine-4-carboxylic acid yielded an analogue, characterized by a 92-95% *cis* peptide bond conformation between Cys^6 and $\Psi^{Me,Me}$Pro, as demonstrated by 2D NMR studies. In addition, no antagonistic activities were observed for the analogue **52** (figure 2.2), as an evidence of the importance of *cis*/*trans* conformational change in oxytocine receptor binding and activation.

In 2013 Albericio *et al.* reported the synthesis and the biological evaluation of a library of Cys($\Psi^{Me,Me}$Pro)-containing analogues of phakellistatin 19 (**53**, figure 2.3).[62] Phakellistatin 19 is an octacyclopeptide and represents the last isolated member of the class of phakellistatins, biologically active cyclopeptides isolated from marine sponges. Interestingly, the natural phakellistatin 19 exhibits cytotoxicity whereas its synthetic counterpart is inactive. This phenomen could be ascribable to the presence of an impurity

[61] A. Wittelsberger, L. Patiny *J. Med. Chem.*, **2005**, *48*, 6553-6562.

[62] M. Pelay-Gimeno, A. Meli, J. Tulla-Puche, F. Albericio *J. Med. Chem.*, **2013**, *56*, 9780-9788.

in the natural peptide, which is responsible for the antiproliferative activity, or to conformational differences due to the presence of many proline residues in the peptide skeleton. On the basis of the second hypothesis, the effect of the replacement of one to three proline residues in phakellistatin 19 by Cys($\Psi^{Me,Me}$Pro) was studied by Albericio. Substantially, the incorporation of the pseudo-proline moieties increases the percentage of *cis* geometry in the prolyl peptide bonds determining enhanced biological activity in the analogues. In figure 2.3 is reported one of the analogues synthesized (**54**).

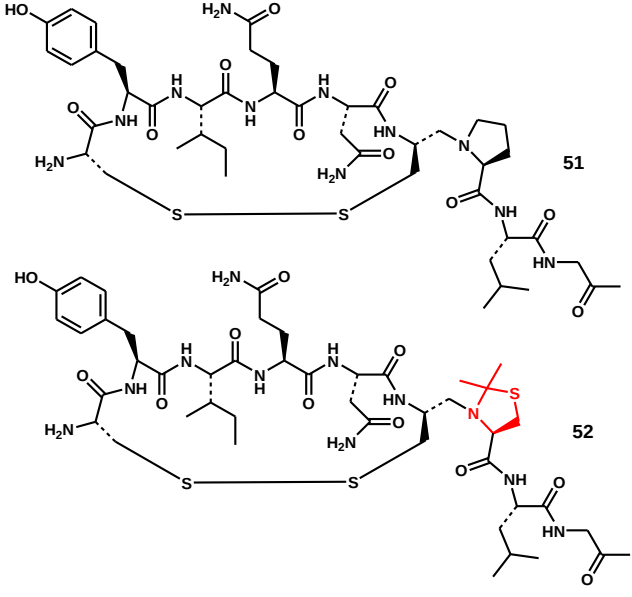

Figure 2.2: Structure of oxytocine (**51**) and its analogue (**52**).

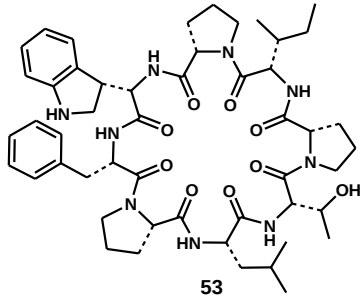

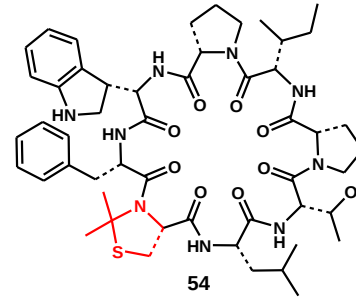

Figure 2.3: Structure of phakellistatin 19 (**53**) and one of its analogues (**54**).

2.2 *Aims of the work*

In order to investigate the structural effects of proline and pseudo-proline residues and metal binding on cyclohexapeptoids with respect to the conformational equilibrium and the crystal structure, the synthesis of the cyclopeptoids **41, 42, 44** and of the proline free macrocycle **43** (figure 2.4) was planned.

The proline and pseudo-proline residues would have imparted conformational rigidity to cyclopeptoid skeleton, forming a stable structure in absence of metal ions. In addition, *N*-methoxyethyl glycine residue was chosen for its propensity to enhance the complexing attitudes of cyclic peptoids as a prerequisite to build coordination-driven metal-organic framework structures.

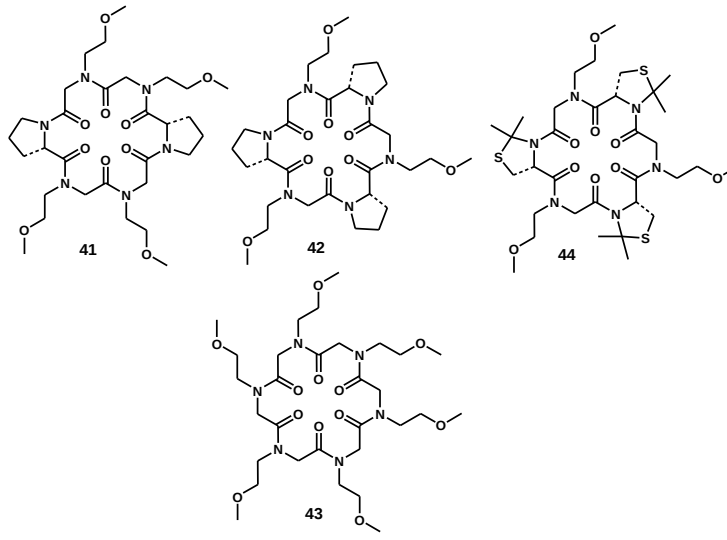

Figure 2.4: Proline-rich cyclopeptoids (**41, 42, 44**) and proline-free macrocycle (**43**).

2.3 *N*-methoxyethyl cyclopeptoids containing proline[63]

2.3.1 Synthesis

The synthesis of the linear precursors of compounds **41**, **42** was accomplished through solid-phase mixed approach (submonomer[34] and monomer approach) (scheme 2.1). *N*-methoxyethyl glycine monomer, prepared on 2-chlorotrithyl resin in standard conditions, was coupled with *N*-Fmoc-L-proline using HATU as condensing agent. Successive couplings DIC or HATU-induced yielded the required

[63] I. Izzo, G. Ianniello, C. De Cola, B. Nardone, L. Erra, G. Vaughan, C. Tedesco, F. De Riccardis *Org. Lett.*, **2013**, *15*, 598-601.

oligomers **55-57** (scheme 2.1 and figure 2.5).

The linear precursor **58** (figure 2.5) of compound **43** was synthesized through a classic solid-phase submonomer approach.

All linear compounds were successfully synthesized as established by HPLC analysis and mass spectrometry, with purities greater than 90%.

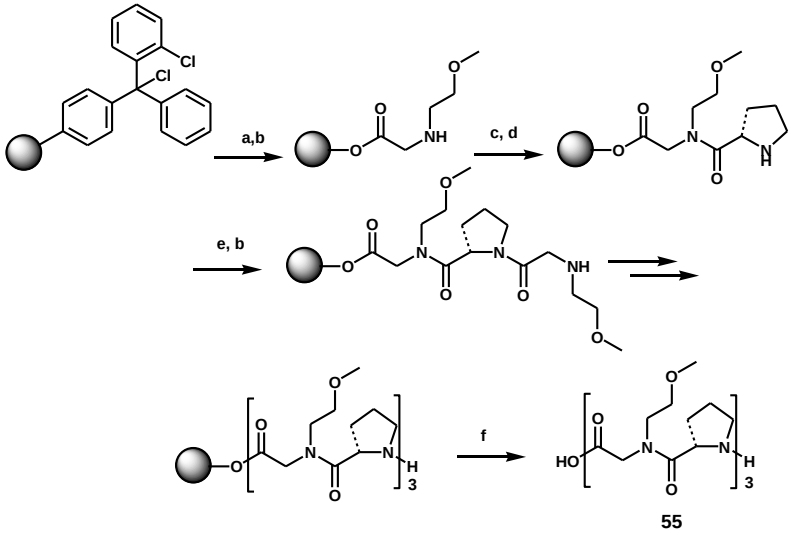

Scheme 2.1: Synthesis of **55**, linear precursor of **42**. Reagents and conditions: (a) bromoacetic acid, DIPEA, DCM; (b) methoxyethylamine, DMF; (c) *N*-Fmoc-L-Proline, HATU, DIPEA, DMF; (d) Piperidine-DMF (1:5); (e) bromoacetic acid, DIC, DMF; (f) HFIP-DCM (1:5).

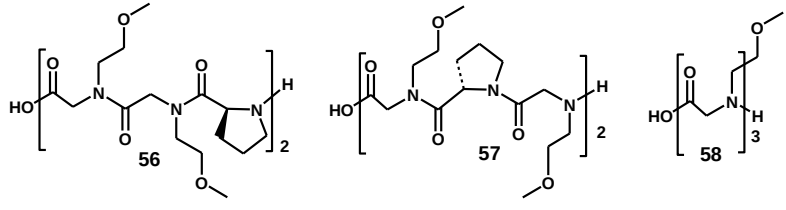

Figure 2.5: Linear precursors **56, 57** of the diprolinate hexapeptoid **41** and linear precursor **58** of the proline-free hexapeptoid **44**.

Head-to-tail macrocyclizations in high dilution conditions of the linear *N*-substituted glycines were realized in the presence of HATU in DMF.

Macrocyclization of the linear precursor **56** afforded **41** in a disappointing 3% yield. In order to improve the yield of the cyclization step, we exchanged the N-terminal proline residue with the less sterically demanding *N*-methoxyethyl glycine residue (peptomer **57**, figure 2.5). The choice was propitious and the cyclization reaction proceeded smoothly affording, after silica gel chromatography, the pure eighteen-membered ring **41** in 20% yield.

The complexity of the rt ^{1}H and ^{13}C NMR spectra recorded for the cycle **41** corroborated the contemporary presence of more than one conformer in slow exchange on the NMR time scale, already observed for structurally related compounds.[50] The stepwise addition of lithium picrate to a 9:1 $CD_3CN/CDCl_3$ solution of **41** determined a simplification of ^{1}H NMR spectrum, reflecting the formation of a conformationally rigid C_1-symmetric[64] lithiated species and confirming the ability of cyclohexapeptoids to complex alkali metals (see section 1.2.5).[50] Observation of the C^{γ} signals of proline residues in ^{13}C NMR spectrum (δ = 25.8 and 25.4 in **41** as lithium salt) indicates a *trans N*-methoxyethyl glycine-proline peptoid junction. Resonances at δ = 21.7 and δ = 24.0 correspond, infact, to the amide *cis* and *trans* X-Pro peptide

[64] The absence of symmetry in **41** as a lithium salt (despite the C_2 symmetry of its chemical structure) is ascribable to a nonsymmetric disposition of the carbonyls around the lithium cation.

bond geometry, respectively.[65]

Overall, the presence of the two proline monomers did not seem to give any conformational restriction to the macrocycle.

Cyclization of oligomer **53** afforded in 28% yield the cyclohexapeptoid **42** directly as metal complex (Na^+[**42**]PF_6^-). It has been the first time that a cyclopeptoid exhibited a so high affinity with sodium to result in complexation during the cyclization step in glass vessels.

Metal complexation was demonstrated by the presence of a 3-fold symmetric species in the rt ^{1}H-NMR spectrum and further by crystallization. The geometry of the *N*-methoxyethyl glycine-Pro bond of the complex was *trans* as inferred by the ^{13}C NMR resonance of the C^γ proline residue signal ($\delta = 25.0$).[65]

Metal-free **42** was obtained through a demetallation procedure starting from the sodium complex (see section 2.3.2).

In order to better understand the influence of the proline residue on the structural properties, the proline-free *N*-methoxyethyl cyclo hexapeptoid **43** was synthesized. Particularly, purification of the crude after macrocyclyzation step by flash chromatography afforded in 19% yield the complexed species Na^+[**43**]PF_6^-.[66] On the other hand, purification by HPLC after cyclization step allowed to obtain

[65] S. K. Sarkar, P. E. Sullivan, C. E. Torchia *Proc. Natl. Acad. Sci. U.S.A.*, **1984**, *81*, 4800-4803.

[66] The affinity of **43** for alkali metals induces complexation during the silica-gel column chromatography.

43 in uncomplexed form (29% yield).

2.3.2 Decomplexation procedure of the triprolinate cyclopeptoid

In order to isolate the uncomplexed species of **42** (the triprolinate cyclopeptoid) some attempts were made. The cyclization reaction and the subsequent work-up were made using polypropylene vessels and ultrapure deionized water (HPLC grade). In this conditions the macrocyclization proved to be less efficient (15% by HPLC analysis), suggesting a metal-templated effect. In any case the crude, containing the desired uncomplexed product, showed in ^{1}H-NMR spectrum the contemporary presence of more than one conformer in slow exchange on the NMR time scale. In order to obtain the uncomplexed hexapeptoid **42** in pure form a decomplexation procedure was realized.

To a 0.006 M solution of the sodium complex Na^{+}[**42**]PF_6^{-} in $CDCl_3$ (figure 2.6 a), $AgNO_3$ in water (0.1 M) was added (in order to exchange the metal present in the complex with silver) . The two phase blend was stirred for 30 min and formation of the silver complex was hypotized (figure 2.6 b). Me_4NI, insoluble in $CDCl_3$, was added to the organic phase containing the silver complex, and formation of a yellow precipitate (AgI) was observed. Filtration afforded **42** in uncomplexed form (figure 2.6 c). ^{1}H NMR spectrum of the desired product was characterized by a complex signal pattern (illustrating the presence of multiple conformers in slow

exchange on the NMR time scale), which highlighted the lack of metal complexation.

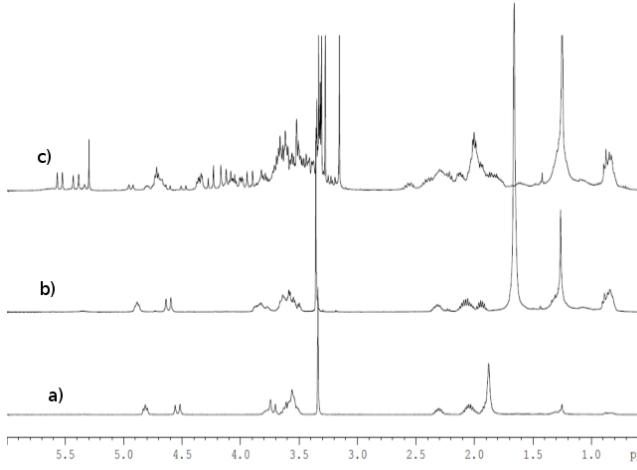

Figure 2.6: a) ^{1}H-NMR spectrum of sodium complex of cyclohexapeptoid **42**. **b)** ^{1}H-NMR spectrum of silver complex of cyclohexapeptoid **42**. **c)** ^{1}H-NMR spectrum of uncomplexed cyclohexapeptoid **42**.

2.3.3 Structural analysis

Compounds Na^{+}[**42**]PF_6^{-}, Na^{+}[**43**]PF_6^{-}, **43** were crystallized and analyzed by X-ray diffraction.

Different crystallization techniques were used:

1. slow evaporation;
2. liquid-phase diffusion;
3. vapour-phase diffusion.

Slow evaporation of a solvent from a saturated solution of the examined compound is a very simple crystallization technique. Typically, two or more solvents are used in order to form single crystals. Solvents should not be too volatile to avoid the formation of microcrystals onto the walls of

crystallization camera, as a consequence of the rapid decreasing of the solvent level.

In the case of liquid-phase diffusion, the solid compound is dissolved into a proper liquid solvent and another liquid solvent (which results to be immiscible) is layered over the solution. The layered liquid slowly diffuses in the solution of the compound determining the precipitation and the following formation of crystals at the interface.

Similarly, in the third crystallization technique mentioned, a non-solvent diffuses from the outer camera to an inner crystallization camera containing the solution of the compound. In this way, a precipitation is induced and crystals are formed.

Tables **2.1**, **2.2** and **2.3** show the obtained results with the crystallization trials**.**

Table 2.1: Results of crystallization of cyclopeptoid Na^{+}[**42**]PF_6^{-}**.**

#	SOLVENT 1	SOLVENT 2	SOLVENT 3	Technique	Results
1	$CHCl_3$	AcOEt		Slow evaporation	Needle-like crystals
2	$CHCl_3$	Hexane		Diffusion in vapor phase	Needle-like crystals
3	$CHCl_3$	AcOEt	Hexane	Slow evaporation	Crystalline precipitate
5	CH_3OH	AcOEt		Slow evaporation	Crystalline precipitate

6	CH_3CN	EtOH		Slow evaporation	Needle-like bundles
7	CH_3CN	Toluene		Slow evaporation	Crystalline precipitate
8	CH_3CN	Hexane		Diffusion in vapor phase	Hexagonal crystals

Table 2.2: Results of crystallization of cyclopeptoid Na^+[**43**]PF_6^-.

#	SOLVENT 1	SOLVENT 2	Technique	Results
1	$CHCl_3$		Slow evaporation	Crystals
2	$CHCl_3$	CH_3CN	Slow evaporation	Precipitate
3	AcOEt	CH_3CN	Slow evaporation	Precipitate
5	AcOEt	CH_3CN	Diffusion in vapor phase	Prismatic crystals
6	CH_3CN	$CH(CH_3)_2OH$	Slow evaporation	Little crystals
7	CH_3CN	MeOH	Slow evaporation	Crystalline precipitate
8	Hexane	CH_3CN	Diffusion between two liquids	Precipitate
9	CH_3CN		Slow evaporation	Crystalline precipitate

Table 2.3: Results of crystallization of cyclopeptoid **43**.

#	SOLVENT 1	SOLVENT 2	Technique	Results
1	AcOEt		Slow evaporation	Crystals

With respect to compound Na^+[**42**]PF_6^-, conditions shown at the entry **8** (table 2.1) produced hexagonal white crystals (see section 2.3.4). In addition, in the case of compound Na^+[**43**]PF_6^-, conditions shown at the entry **5** (table 2.2) afforded prismatic colorless crystals (see section 2.3.5). Finally, compound **43** was crystallized making use of conditions shown at the entry **1** (table 2.3) (see section 2.3.5).

2.3.4 Structural analysis of the triprolinate cyclopeptoid

Rather small needle-like hexagonal crystals of compound Na^+[**42**]PF_6^- (the triprolinate cyclopeptoid), suitable for synchrotron radiation diffraction studies, were harvested using the diffusion in vapour phase of hexane in an acetonitrile solution. Specifically, X-ray diffraction measurements were performed at beam line ID11 of European Synchrotron Radiation Facility (ESRF) located in Grenoble (FRANCE).

The obtained structure demonstrated the complexation of **42** with Na^+ and the presence of PF_6^-, as counter ion derived from macrocyclization coupling agent HATU.

The crystals showed a trigonal lattice (a = 16.382(5)° Å, c = 39.89(2)° Å; space group = *R3*). X-ray diffraction data indicated that crystals correspond to a complexed species, made of three molecules of cyclopeptoid **42**, four sodium cations and one molecule of acetonitrile ($Na_4cPP_3L^{4+}$, *cPP*=cyclopeptoid **42**, L=CH_3CN) which form a triple-decker

salt sandwich (figures 2.7). Such complexed species proved to have C_3 symmetry because a ternary cristallographic axis crosses the four sodium atoms, centers of gravity of the three cyclopeptoid rings and molecular axis of acetonitrile.

In all the three cyclopeptoid rings the conformation of the cyclopeptoid backbone is all-*trans*, the carbonyl groups alternately point toward the sodium cations and force the *N*-linked side chains to assume an alternate pseudo-equatorial arrangement (figure 2.8), as previously observed by De Riccardis and co-workers for the structure of a cyclopeptoid strontium complex (**25**$_2$·[Sr(picr)$_2$]$_3$, section 1.2.5).[50]

It is interesting to notice that the edge sodium ions complete the coordination sphere in two different ways: on one side by coordinating three alternate carbonyl groups and an acetonitrile molecule (bottom face of the complex: Na1 ion, fig. 2.7); on the opposite side by linking all six carbonyl groups (top side of the complex: Na4 ion, fig. 2.7). The distances between the Na ions and the mean planes constituted by C and N atoms of the rings are the following: Na1 1.93Å, Na2 2.17 and 1.84Å, Na3 2.76 and 2.45Å, Na4 0.79Å. The last distance strongly suggests a cation-π interaction between Na4 and the π-bond of the carbonyl groups, in analogy with an enniatin B sodium 1:1 complex (see section 1.1.3).[23]

The unit cell presents three triple-decker metal complexes $Na_4cPP_3L^{4+}$ and twelve anions PF_6^- (to allow for electroneutrality) together with other nine molecules of

acetonitrile, which occupy interstitial positions. The *N*-methoxyethyl side chains are excluded by metal coordination, hampering crystal network extension. Therefore, the formula of crystallized species is $[Na_4cPP_3L^{4+}\ (PF_6^-)_4] \cdot 3(CH_3CN)$. The counter ion nature was justified considering that complex formation occurred during macrocyclization with coupling agent HATU, containing PF_6^-.

The crystal packing is illustrated in figure 2.9.

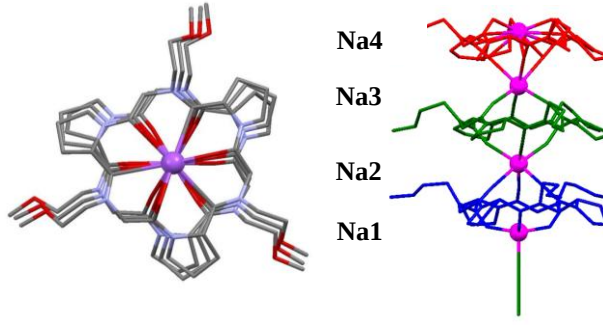

Figure 2.7: X-ray molecular structure of complexed species $Na_4cPP_3L^{4+}$, constituted from three molecules of cyclopeptoid **42**, four sodium cations and one molecule of acetonitrile.

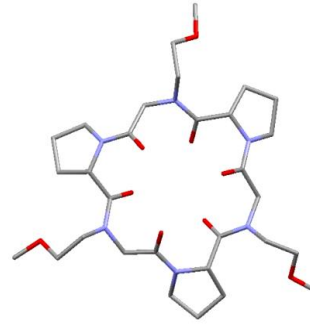

Figure 2.8: X-ray molecular structure of a single cyclopeptoid ring **42** which forms the complexed species $Na_4cPP_3L^{4+}$. Conformation of the backbone is all-*trans*.

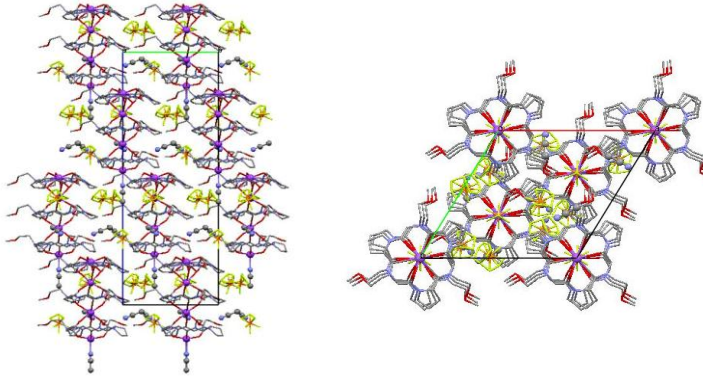

Figure 2.9: Crystal packing for the species $[Na_4cPP_3L^{4+}\ (PF_6^-)_4]$. $3(CH_3CN)$.

2.3.5 *Structural analysis of N-methoxyethy cyclohexapeptoid*

Prismatic colorless crystals of Na^+[**43**]PF_6^-, suitable for X-ray diffraction analysis, were obtained by slow

diffusion of ethyl acetate in an acetonitrile solution.

Even in this case X-ray analysis confirmed the presence of the complexed form. In particular, the complexation took place during silica gel column purification of the crude.

The crystals showed a triclinic lattice (a = 8.805(3) Å, b = 11.014(2) Å, c = 12.477(2) Å, α = 70.97(2)°, β = 77.347(16)°, γ = 89.75(2)°; space group = *P-1*).

The conformation of the cyclopeptoid backbone is all-*trans* as for Na^+[**42]** PF_6^- (figure 2.10).

The metal adduct of **43** is characterized by unique properties, in the following described.

Each sodium ion results to be coordinated to three carbonyl groups and two side chains methoxy groups, one belonging to the same cyclopeptoide molecule and the other from an adiacent one (figure 2.11). Examples of pentacoordinated sodium atom have been observed in G-quadruplex DNA.[67]

Side chain methoxy groups allow the formation of a 1D polymeric chain made of cyclopeptoid molecules and sodium ions extending along *b* axis (figure 2.11).

Two side chains are folded toward the center of the cyclopeptoid ring to bind two sodium ions, two side chains extend outside to bind two other sodium ions and extend the polymeric structure, the remaining two other side chains point outward and are involved in crystal packing interactions.

PF_6^- ions (from HATU) are located in the interstitial space

[67] (a) A. Wrong, G. J. Wu *Phys. Chem. A,* **2003,** *107,* 579-586; (b) J. T. Davis *Angew. Chem. Int. Ed.*, **2004**, *43*, 668-698.

amongst the chains.

The aggregative forces generate the first metal-organic frameworks (MOF) structure based on peptoids as linkers.

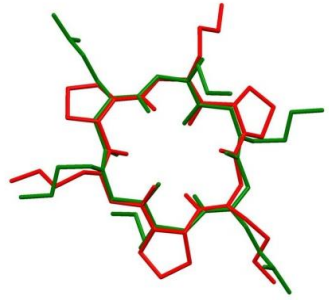

Figure 2.10: Backbone overlay for Na^+[**42**]PF_6^- and Na^+[**43**] PF_6^- (rms = 0.234 Å).

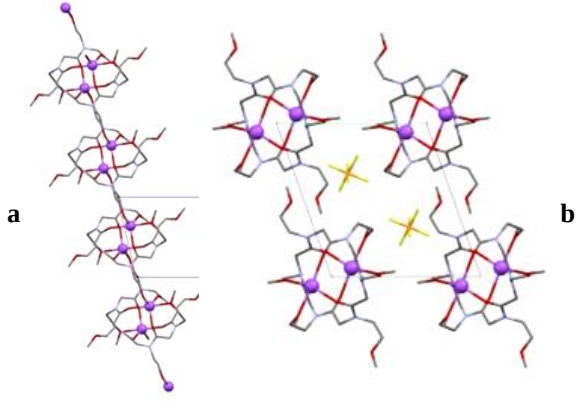

Figure 2.11: a) 1D polymer side chain of Na^+[**43**]PF_6^- as view along *b* axis. b) Crystal packing as view along *a* axis.

Purification by HPLC after cyclization step proved to be successful and **43** was isolated in uncomplexed form and crystallized from ethyl acetate by slow evaporation.

The crystals of **43** in uncomplexed form showed a triclinic lattice (a = 8.358(4) Å, b = 9.176(4) Å, c = 11.623(4) Å, α = 99.636(6)°, β = 101.488(12)°, γ = 104.239(13)°; space group = *P-1*).

In the same way as Na^+[**42**]PF_6^-, the X-ray structure of **43** possesses a crystallographic inversion center (figure 2.12). Instead, the backbone conformation results to be *tcctcc* (figure 2.12), a typical conformation for a decomplexed cyclohexapeptoid (**24**, section 1.2.4).[49]

Indeed, in the case of compound **43** the template effect of metal complexation can be confirmed due to the fact that the presence of Na^+ induces a conformational change in the peptoid bond configuration from the *tcctcc* geometry to the all-*trans* geometry.

From the comparison between the crystal structures of cyclopeptoid **43** in free and complexed form, it is remarkable to notice that in both forms cyclopeptoid molecules are stacked along the *a* axis to form columns (figure 2.13). Therefore, in spite of different ring conformation cyclopeptoid molecules in the free form are pre-organized to stack in columns and to host the metal ion. Substantially, the presence of the cation does not seem to modify the crystal packing.

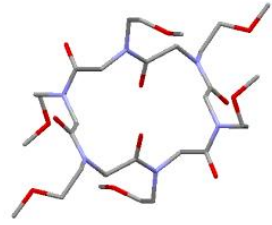

Figure 2.12: X-ray molecular structure of **43.** The backbone conformation is *tcctcc*.

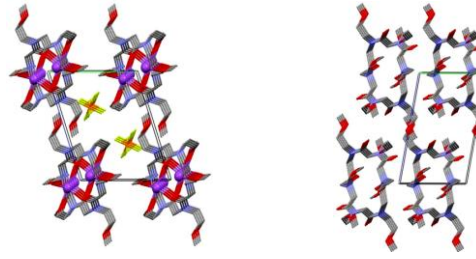

Figure 2.13: Crystal packing of **43** in complexed (*left*) and free form (*right*) as view along *a* axis.

2.4 *N-methoxyethyl cyclopeptoid containing pseudo-proline residues*

In order to perform the solid phase synthesis of the linear precursor of **44**, a dipeptide building block **65** (scheme 2.2) containing the pseudoproline residue **49** was previously prepared. This kind of approach is required because of the low nucleophilicity of the secondary amine in addition to the steric hindrance imposed by the two methyl groups of the 2,2-

dimethyl-1,3-thiazolidine-4-carboxylic acid, as well documented in literature.[68]

The synthesis of the peptoid monomer **62** was realized as shown in scheme 2.2. The 2,2-dimethyl-1,3-thiazolidine-4-carboxylic acid **49** was prepared according to the literature (scheme 2.2).[69,62]

The dipeptide building block **65** was obtained in 58% overall yield forming the Fmoc protected *N*–methoxyethylglycine fluoride of peptoid monomer with (diethylamino)sulfur trifluoride (DAST) and futher coupling it with the seudoproline (scheme 2.2).[70]

[68] A. Wittelsberger, L. Patiny, J. Slaninova, C. Barberis, M. Mutter *J. Med. Chem.* **2005**, *48*, 6553-6562.

[69] N.J. Lewis, R. L. Inloes, J. Hes, *J. Med. Chem.*, **1978**, *21*, 1070-1072.

[70] C. Kaduk, H. Wenschuh, M. Beyermann, K. Forner, L. A. Carpino *Lett. Pept. Sci.* **1996**, *2*, 285-288.

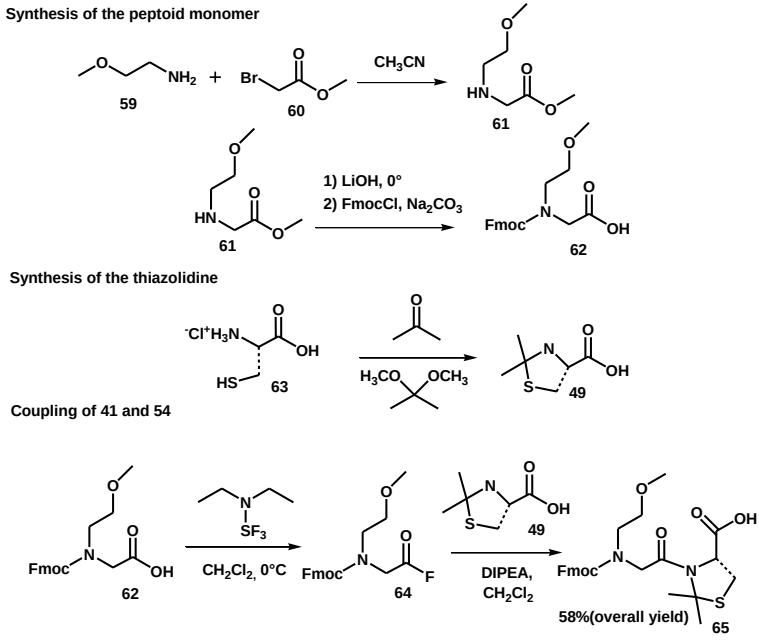

Scheme 2.2: Synthesis of the peptoid-peptide unit **63** (dipeptide building block).

A classic monomer approach on solid phase produced the linear precursor of compound **44** in 40% yield (scheme 2.3).

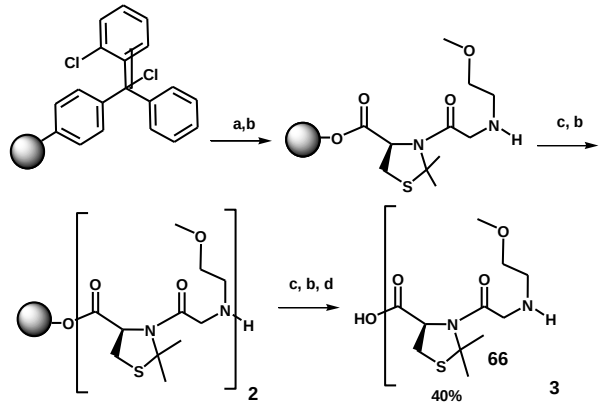

Scheme 2.3: Synthesis of linear precursor for **44**. Reagents and conditions: (a) **65**, DIPEA, DCM; (b) Piperidine-DMF (1:5); (c) **65**, HATU, DIPEA, DMF; (e) $(CF_3)_2CHOH$-DCM (1:5).

The linear compound **66** was subjected to three attempts of cyclization respectively with coupling agents HATU, PyBOP, FDPP (scheme 2.4). HATU and PyBOP are the most used coupling agents, while FDPP is considered to be an efficient coupling agent for the cyclization of cyclopeptides containing pseudo prolines.[71] Unfortunately, in all cases it was obtained a complex mixture which did not contain the target molecule **44** (ES-MS analysis). We realized that, evidently, the impurities contained in the crude could influence the progress of the cyclization reaction.

Futhermore, in order to remove most of the impurities a RP-HPLC purification of the linear precursor **66** was achieved**.** Afterwards, to our delight, the cyclization of the purified linear peptoid with HATU in DMF was successfully

[71] K. A. Fairweather, N. Sayyadi, I. J. Luck, J. K. Clegg, K. A. Joliffe *Org. Lett.*, **2010**, *12*, 3136-3139.

performed. Finally, a RP-HPLC purification on a C_{18} reversed-phase semi-preparative column of the crude cycle afforded **44** in 41% yield.

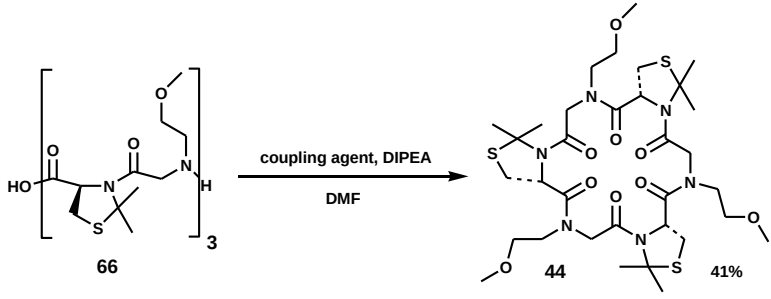

Scheme 2.4: Cyclization of compound **66** in high dilution condition.

The cycle **44** was conformationally flexible in solution as indicated by its ^{1}H NMR spectrum. Therefore, pseudo-proline residues are not able to costrain the peptoid macrocycle as in the case of proline residues.

In order to simplify the ^{1}H NMR spectrum of the compound was tried at first the stepwise addition of lithium picrate, which this time did not induce a simplification of the spectrum through the formation of a rigid complex.

We also registered high temperature ^{1}H NMR spectra of the compound (up to 100 $^{\circ}$C) in order to produce a conversion between rotamers more rapid in the NMR time scale, but a simplification was not obtained.

With respect to the X-ray characterization, the following crystallization trials were unsuccessfully conducted on compound **44**: a) Slow evaporation from a solution of AcOEt: $CHCl_3$ 1:1 (v/v); b) slow evaporation from a solution of

$CHCl_3$; c) slow evaporation from a solution of CH_3CN; d) slow evaporation from a solution of CF_3CH_2OH. In table 2.4 the solubility scale of **44** is reported. In definitive, it was not possible to evaluate the effect of pseudo-proline residues on the crystal structure.

Table 2.4: Solubility scale of **44**.

Solvent	Solubility order
$CHCl_3$	1
CH_3CN, CF_3CH_2OH	2
AcOEt	3

2.5 Conclusions

In this chapter, the synthesis and structural characterization of the proline-rich cyclopeptoids **41, 42** and *N*-methoxyethyl cyclopeptoid **43** (proline-free) were reported. In addition, the synthesis of the pseudo-proline rich cyclopeptoid **44** was successfully obtained.

First of all, NMR analysis of the proline-rich and pseudo-proline rich cyclopeptoids demonstrated that prolines and pseudo-prolines residues are not able to stabilize the conformation of cyclopeptoids in solution with respect to our expectations, on the other hand metal ions such as Na^+ induce conformational rigidity in the macrocycle backbone.

Notably, structural analysis *via* X-ray diffraction emphasized that rigid L-proline and chelating *N*-methoxyethyl

glycine residues determine the formation of fascinating metalated supramolecular frameworks.

In particular, compound **42** was crystallized in the form of sodium complex Na^+**[42]**PF_6^-. The crystal structure was characterized by the formation of a triple-decker salt sandwich metal complex $Na_4cPP_3L^{4+}$ (*cPP*=cyclopeptoid **42**, L=CH_3CN) with a crystallographic 3-fold rotation symmetry. In addition, the geometry of the amide linkages in all three cyclopeptoid macrocycles present in metal complex of **42** is *trans* as in the case of a cyclopeptoid strontium complex synthesized by De Riccardis *et al.* (**25**$_2$.[Sr(picr)$_2$], section 1.2.5).[50]

Compound **43** was crystallized both in the sodium complex and free form. In the sodium complex two sodium ions and one cyclopeptoid molecule are linked to form a 1D-coordination polymer extending along the *a* axis. In addition, the configuration of the amide bonds in the macrocycle is all-*trans*.

With respect to the free form, the crystal packing is practically the same of the complexed form, as an evidence of a pre-organization of the structure. Instead, the amide bond pattern is the typical *tcctcc*. As a consequence, Na^+ is responsible for a template effect determining a conformational change in the peptoid bond pattern from the *tcctcc* to the all-*trans* geometry.

2.6 Experimental section

2.6.1 General procedures

Reagents purchased from commercial sources were used without further purification. All reactions involving air or moisture sensitive reagents were carried out under a dry argon atmosphere. CH_2Cl_2 was distilled from CaH_2. Glassware was flame-dried (0.05 Torr) prior to use. When necessary, compounds were dried in vacuo over P_2O_5 or by azeotropic removal of water with toluene under reduced pressure. Starting materials and reagents purchased from commercial suppliers were generally used without purification. Reactions were monitored by TLC on silica gel plates (0.25 mm) and visualized by UV light or by spraying with ninhydrin solutions or drying with iodine. Flash chromatography was performed on Silica Gel 60 (particle size: 0.040–0.063 mm) and the solvents employed were of analytical grade. HPLC analysis was performed on C_{18} reversed-phase analytical and semipreparative columns (Waters, Bondapak, 10 μm, 125 Å, 3.9 mm × 300 mm and 7.8 × 300 mm, respectively) using a Modular HPLC System JASCO LC-NET II/ADC, equipped with a JASCO Model PU-2089 Plus Pump and a JASCO MD-2010 Plus UV-vis multiple wavelength detector set at 220 nm. Yields refer to chromatographically and spectroscopically (^{1}H and ^{13}C NMR) pure materials. The NMR spectra were recorded on Bruker DRX 400, (^{1}H at 400.13 MHz, ^{13}C at 100.03 MHz), Bruker DRX 250 (^{1}H at 250.13 MHz, ^{13}C at

62.89 MHz), and Bruker DRX 300 (^{1}H at 300.1 MHz, ^{13}C at 75.5 MHz) spectrometers. Chemical shifts (δ) are reported in ppm relatively to the residual solvent peak ($CHCl_3$, δ = 7.26, $^{13}CDCl_3$, δ = 77.0; CD_2HCN, δ = 1.98; $^{13}CD_3CN$, δ = 1.80; CD_2HOD, δ = 4.78, $^{13}CD_3OD$, δ = 49.2, in the case of solvent mixtures, the considered residual peak was that of the most abundant deuterated solvent). The multiplicity of each signal is designated by the following abbreviations: s, singlet; d, doublet; t, triplet; q, quartet; m, multiplet; b, broad. Coupling costants (J) are quoted in Hz. Homonuclear decoupling, COSY-45 and DEPT experiments completed the full assignment of each signal. High resolution ESI-MS spectra were performed on a Q-Star Applied Biosystem mass spectrometer. ESI-MS analysis in positive ion mode was performed using a Finnigan LCQ Deca ion trap mass spectrometer (ThermoFinnigan, San Josè, CA, USA) and the mass spectra were acquired and processed using the Xcalibur software provided by Thermo Finnigan. Samples were dissolved in 1:1 CH_3OH/H_2O, 0.1 % formic acid, and infused in the ESI source by using a syringe pump; the flow rate was 5 μl/min. The capillary voltage was set at 4.0 V, the spray voltage at 5 kV, and the tube lens offset at 4.0 V. The capillary temperature was 220 °C. Data were acquired in MS1and MSn scanning modes. Zoom scan was used in these experiments.

X-ray analysis was performed with a Rigaku AFC11K diffractometer equipped with a Saturn944 CCD detector using

CuKα radiation and with a Rigaku AFC7S diffractometer equipped with a Mercury[72] CCD detector using Mo*K*α radiation.

2.6.2 Solid-phase synthesis

Mixed monomer/submonomer solid-phase synthesis of linear precursors 55-57

Linear peptoids **55-57** were synthesized by alternating submonomer and monomer solid-phase methods using standard manual Fmoc solid-phase peptide synthesis protocols. Typically 0.40 g of 2-chlorotrityl chloride resin (2,α-dichlorobenzhydryl-polystyrene crosslinked with 1% DVB; 100-200 mesh; 1.20 mmol/g) was swelled in dry DCM (4 mL) for 45 min and washed twice in dry DCM (3 mL). To the resin bromoacetic acid (107 mg, 0.77 mmol) and DIPEA (418 µL, 2.4 mmol) in dry DCM (4 mL) were added on a shaker platform for 40 min at room temperature, washes with dry DCM (3 × 4 mL) and then with DMF (3 × 4 mL) followed. To the bromoacetylated resin metoxyethylamine (413 µl, 4.80 mmol) in dry DMF (4 mL), was added. The mixture was left on a shaker platform for 40 min at room temperature, then the resin was washed with DMF (3 × 4 mL). The resin was incubated with a solution of *N*-Fmoc-L-proline (4.85 mg, 1.44 mmol), HATU (529 mmol, 1.39 mmol), DIPEA (333 µl) in dry DMF (4 mL) on a shaker platform for 1 h, followed by extensive washes with DMF (3

[72] CrystalClear, Crystal Structure Analysis Package, Rigaku-Molecular Structure Corp.

× 4 mL), DCM (3 × 4 mL) and DMF (3 × 4 mL). Chloranil test was performed and once the coupling was complete the Fmoc group was deprotected with 20% piperidine/DMF (v/v, 3 mL) on a shaker platform for 3 min and 7 min respectively, followed by extensive washes with DMF (3 × 3 mL), DCM (3 × 3 mL) and DMF (3 × 3 mL). The yields of loading step and of the following coupling steps were evaluated interpolating the absorptions of dibenzofulvene-piperidine adduct (λ_{max} = 301 nm, ε = 7800 M^{-1} cm^{-1}), obtained in Fmoc deprotection step (the average coupling yield was 63-70 %). Subsequent bromoacetylation reactions were accomplished by reacting the oligomer with a solution of bromoacetic acid (690 mg, 4.8 mmol) and DIC (817 μL, 5.28 mmol) in DMF (4 mL) on a shaker platform 40 min at room temperature. Subsequent *N*-Fmoc-L-proline addition and Fmoc deprotection steps were performed as described above, addition of the proline at the fourth and sixth position required longer reaction time (2.5 h) and two treatments. The synthesis proceeded until the desired hexaoligomer was obtained. The oligomer-resin was cleaved in 4 mL of 20% HFIP in DCM (v/v). The cleavage was performed on a shaker platform for 30 min at room temperature the resin was then filtered away. The resin was treated again with 4 mL of 20% HFIP in DCM (v/v) for 5 min, washed twice with DCM (3 mL), filtered away and the combined filtrates were concentrated in vacuo. The final products were dissolved in 50% ACN in HPLC grade water

and analysed by RP-HPLC and ESI mass spectrometry. The linear compounds were subjected to the cyclization without further purification.

✔ *Compound **55***

Purity: >95%.

Yield: 62% (crude residue).

ES-MS: 655.6 *m/z* [M + H^+].

HPLC: t_R: 10.5 min; conditions: 5 → 100% B in 30 min (A, 0.1% TFA in water, B, 0.1% TFA in acetonitrile); flow: 1 mL min^{-1}, 220 nm.

✔ *Compound **56***

Purity: >95%.

Yield: 70% (crude residue).

ES-MS: 673.9 *m/z* [M + H^+].

HPLC: t_R: 10.3 min; conditions: 5 → 100% B in 30 min (A, 0.1% TFA in water, B, 0.1% TFA in acetonitrile); flow: 1 mL min^{-1}, 220 nm.

✔ *Compound **57***

Purity: >95%.

Yield: 40% (crude residue).

ES-MS: 655.6 *m/z* [M + H^+].

HPLC: t_R: 10.2 min; conditions: 5 → 100% B in 30 min (A, 0.1% TFA in water, B, 0.1% TFA in acetonitrile); flow: 1 mL min^{-1}, 220 nm.

Submonomer solid-phase synthesis of linear precursor **58**

Linear peptoid **58** was synthesized using a submonomer solid-phase approach.

Typically 0.40 g of 2-chlorotrityl chloride resin (2,α-dichlorobenzhydryl-polystyrene crosslinked with 1% DVB; 100-200 mesh; 1.20 mmol/g) was swelled in dry DCM (4 mL) for 45 min and washed twice in dry DCM (4 mL). The first sub-monomer was attached onto the resin by adding bromoacetic acid (107 mg, 0.77 mmol) and DIPEA (418 μL, 2.4 mmol) in dry DCM (4 mL) on a shaker platform for 40 min at room temperature, followed by washing with dry DCM (3 × 4 mL) and then with DMF (3 × 4 mL). To the bromoacetylated resin metoxyethylammine (413 μl, 4.80 mmol) in dry DMF (4 mL), was added. The mixture was left on a shaker platform for 40 min at room temperature, then the resin was washed with DMF (3 × 4 mL). Subsequent bromoacetylation reactions were accomplished by reacting the oligomer with a solution of bromoacetic acid (690 mg, 4.8 mmol) and DIC (817 μL, 5.28 mmol) in DMF (4 mL) on a shaker platform 40 min at room temperature. The filtered resin was washed with DMF (3 × 4 mL) and treated again with methoxyethylamine under the same conditions reported above. This cycle of reactions was iterated until the target oligomer was obtained. The oligomer-resin was cleaved in 4 mL of 20% HFIP in DCM (v/v). The cleavage was performed on a shaker platform for 30 min at room temperature the resin

was then filtered away. The resin was treated again with 4 mL of 20% HFIP in DCM (v/v) for 5 min, washed twice with DCM (3 mL), filtered away and the combined filtrates were concentrated in vacuo. The final products were dissolved in 50% ACN in HPLC grade water and analysed by RP-HPLC and ESI mass spectrometry. The linear compound was subjected to the cyclization without further purification.

✔ *Compound **58***

Purity: >95%.

Yield: 65% (crude residue).

ES-MS: 709.0 *m/z* [M + H^+].

HPLC: t_R: 10.4 min; conditions: 5 → 100% B in 30 min (A, 0.1% TFA in water, B, 0.1% TFA in acetonitrile); flow: 1 mL min^{-1}, 220 nm.

Monomer solid-phase synthesis of linear precursor 66

Linear peptoid **66** was synthesized using a monomer solid-phase approach.

Typically 0.30 g of 2-chlorotrityl chloride resin (2,α-dichlorobenzhydryl-polystyrene crosslinked with 1% DVB; 100-200 mesh; 1.20 mmol/g) was swelled in dry DCM (3 mL) for 45 min and washed twice in dry DCM (3 mL). To the resin monomer **65** (99 mg, 0.2 mmol) and DIPEA (139 μL , 0.8 mmol) in dry DCM (3 mL) were added on a shaker platform for 1 h at room temperature, washes with dry DCM (3 × 3 mL) and then with DMF (3 × 3 mL) followed. The resin was capped with a solution of DCM/CH_3OH/DIPEA

17:2:1 (3 mL) on a shaker platform for 30 min at room temperature, followed by extensive washes with DMF (3 × 3 mL), DCM (3 × 3 mL) and DMF (3 × 3 mL). Fmoc group was deprotected with 20% piperidine/DMF (v/v, 3 mL) on a shaker platform for 3 min and 7 min respectively, followed by extensive washes with DMF (3 × 3 mL), DCM (3 × 3 mL) and DMF (3 × 3 mL). The yields of loading step and of the following coupling steps were evaluated interpolating the absorptions of dibenzofulvene-piperidine adduct (λ_{max} = 301 nm, ε = 7800 M^{-1} cm^{-1}), obtained in Fmoc deprotection step (the average coupling yield was 63-70 %). Subsequently, the resin was incubated with a solution of monomer **65** (199 mg, 0.4 mmol), HATU (145 mg, 0.38 mmol), DIPEA (139 µl, 0.8 mmol) in dry DMF (3 mL) on a shaker platform for 2 h at room temperature. Chloranil test was performed and once the coupling was complete the Fmoc group was deprotected in the conditions described above. The last addition of monomer **65** was carried out in the aforementioned conditions. The oligomer-resin was cleaved in 3 mL of 20% HFIP in DCM (v/v). The cleavage was performed on a shaker platform for 30 min at room temperature and the resin was then filtered away. The resin was treated again with 3 mL of 20% HFIP in DCM (v/v) for 5 min, washed twice with DCM (3 mL), filtered away and the combined filtrates were concentrated in vacuo. The final product was dissolved in 50% ACN in HPLC grade water and analysed by RP-HPLC and ESI mass

spectrometry. Linear compound was purified by semipreparative RP-HPLC.

✔ *Compound* ***66***

Yield: 10% (purified by RP-HPLC).

ES-MS: 793.3 *m/z* [M + H^+].

HPLC: t_R: 11.3 min; conditions: 25 →100% B in 30 min (A, 0.1% TFA in water, B, 0.1% TFA in acetonitrile); flow: 2 mL min^{-1}, 220 nm.

2.6.3 General procedure for high dilution cyclization

Synthesis of 41-44

To a stirred solution of HATU (116 mg, 0.31 mmol), DIPEA (0.082 mL, 0.47 mmol) in dry DMF (20 mL) at room temperature, a solution of the linear compounds (crude **55-58**, HPLC purified **66**) (0.08 mmol) in dry DMF (20 mL) was added by syringe pump in 6 h. After 48 h (**41, 42**) or 12 h (**43, 44**) the resulting mixture was concentrated in vacuo, diluted with DCM (20 mL) and washed with 1 M HCl (7 mL × 3). The mixture was extracted with DCM (10 mL × 2) and the combined organic phases were washed three times with water (10 mL), dried ($MgSO_4$) and concentrated in vacuo. The crude residues from the HATU-induced cyclizations were purified by flash chromatography[73] or by RP-HPLC.

[73] The high affinity of cyclohexapeptoids for alkali metals induces complexation during the silica-gel column chromatography or, in case of strongly coordinating compounds, even during their synthesis (and work-up procedures). A useful way to obtain metal-free compounds is to avoid glassware during their synthesis and manipulation (including glass

✔ *Compound **41***

Yield: 20%. The crude residue from the HATU-induced cyclization was purified by flash chromatography (DCM/MeOH, from: 100/0 to 70/30).

ES-MS: 677.0 *m/z* [M+Na^+].

HPLC: t_R: 13.2 min; conditions: 5 → 100% B in 30 min (A: 0.1% TFA in water, B: 0.1% TFA in acetonitrile), flow: 1.0 mL min^{-1}, 220 nm.

^{1}H NMR (400 MHz, CD_3CN:$CDCl_3$ 9:1, mixture of rotamers) δ: 5.38 (0.3H, m, COC*H*N), 5.09-3.37 (29.7H, m, COC*H*N, COCH_2N, NCH_2CH_2O, NCH_2CH_2O, CHCH_2CH_2CH_2N), 3.36-3.20 (12H, bs, OCH_3) 2.45-1.82(8H, m, CH_2CH_2CH_2N, CHCH2CH_2CH_2N).

^{13}C NMR (100 MHz, $CDCl_3$, mixture of rotamers) δ: 172.7, 172.3, 170.6, 169.8, 169.1, 166.8, 166.3, 165.9, 71.8, 71.1, 70.9, 70.5, 70.2, 69.6, 66.8, 59.1, 58.9, 58.7, 58.6, 57.9, 57.8, 57.1, 55.1, 52.2, 51.5, 50.6, 50.3, 50.1, 49.9 49.7, 49.4, 48.2, 47.8, 47.5, 47.1, 46.7, 46.3, 46.2, 43.2, 39.6, 38.8, 32.0, 31.4, 30.1, 29.7, 29.2, 28.7, 25.5, 25.1, 24.4, 23.2, 22.7, 22.1.

✔ *Compound **41** with lithium picrate*

To a 4.0 mM solution of **41** in CD_3CN:$CDCl_3$ 9:1 (0.5 mL), were added 3 mg of lithium picrate. After the addition the

pipettes or vials), use ultrapure water in the work up procedures and avoid silica-gel column chromatography. Sometimes HPLC purification is able to break the complexes and liberate the cyclohexapeptoids from the metals. Cyclohexapeptoids should always be collected in polypropylene tubes and stored in eppendorf vials or falcon tubes. In the case of the highly coordinating cyclopeptoids, the NMR spectra should always be performed in teflon tubes.

suspension was stirred vigorously for 15 minutes and the ^{1}H NMR and ^{13}C NMR spectra was recorded.

^{1}H NMR (400 MHz, $CD_3CN/CDCl_3$ = 9/1) δ: 8.75 (7H, s, protons of picrate present in excess), 4.82 (1H, m, COC*H*N, pro-1), 4.76 (1H, d, *J* = 15.0 Hz, NC*H*HCO), 4.65 (1H, d, *J* = 12.0 Hz, NC*H*HCO), 4.41 (2H d, *J* = 12.0 Hz, NCH*H*CO), 4.34 (1H, d, *J* = 15.0 Hz, NCH*H*CO), 4.34 (m, 1H, COC*H*N, pro-2), 3.89-3.12 (23H, m, NCH*H*CO, NCH_2CH_2O, NCH_2CH_2O, $CHCH_2CH_2CH_2N$), 3.38 (3H, s, OCH_3), 3.35 (3H, s, OCH_3), 3.30 (3H, s, OCH_3), 3.29 (3H, s, OC*H3*), 2.45 (1H, m, CHC*H*HCH_2CH_2N, pro-1), 2.30 (1H, m, CHC*H*HCH_2CH_2N, pro-2) 2.26-1.95 (4H, m, $CHCH_2CH_2CH_2N$, pro-1 and pro-2 overlapped with CD_2HCN), 1.93 (1H, m, CHCH*H*CH_2CH_2N, pro-1), 1.88 (1H, m, CHCH*H*CH_2CH_2N, pro-2).

^{13}C NMR (62.89 MHz, $CD_3CN/CDCl_3$ = 9/1) δ: 173.9, 172.8, 172.2, 171.5, 168.3, 166.6, 71.7, 71.4, 71.2, 70.9, 70.3, 59.9, 59.8, 59.7, 59.3, 59.1, 58.7, 52.2, 51.7, 51.1, 50.3, 50.6, 50.0, 49.6, 49.4, 49.2, 48.0, 30.7, 30.3, 26.3, 25.7.

✔ *Compound **42** with $Na^+PF_6^-$*

Yield: 28%. The crude residue from the HATU-induced cyclization was purified by flash chromatography (DCM/MeOH, from: 98/2 to 70/30).[73]

ES-MS: 659.5 *m/z* [M + Na^+]; 341.4 *m/2z* [M + $2Na^+$].

HPLC: t_R: 13.5 min.; conditions: 5 → 100% B in 30 min (A: 0.1% TFA in water, B: 0.1% TFA in acetonitrile), flow: 1.0 mL min^{-1}, 220 nm.

[α]^D: -6.2 (c =1.0, $CHCl_3$).

^{1}H NMR (400 MHz, $CDCl_3$) δ: 4.81 (3H, m, COC*H*N), 4.51 (3H, d, *J* = 16.6 Hz, NC*H*HCO), 3.74 (3H, m, NC*H*HCH_2O), 3.72 (3H, d, *J* = 16.6 Hz, NCH*H*CO), 3.61-3.50 (15H, m, CHCH_2CH_2C*H*$_2$N, NCH_2C*H*$_2$O and NC*H*$_2$CH_2O), 3.33 (9H, s, OC*H*$_3$), 2.30 (3H, m, CHC*H*HCH_2CH_2N), 2.04 (6H, m, CHCH_2C*H*$_2$CH_2N), 1.92 (3H, m, CHCH*H*CH_2CH_2N).

^{13}C NMR (100 MHz, $CDCl_3$) δ: 174.2 (× 3, q), 168.0 (× 3, q), 70.3 (× 3, CH_2), 58.9 (× 3, CH_3), 58.0 (× 3, CH), 50.3 (× 3, CH_2), 49.4 (× 3, CH_2), 46.5 (× 3, CH_2), 29.2 (× 3, CH_2), 25.0 (× 3, CH_2).

✔ *Compound **43***

Yield: 29%. The crude residue from the HATU-induced cyclization was purified by RP-HPLC on a C_{18} reversed-phase semi-preparative column (t_R: 18.0 min.; conditions: 5 → 100% B in 30 minutes (A: 0.1% TFA in water, B: 0.1% TFA in acetonitrile), flow: 2.0 mL min^{-1}, 220 nm).

ES-MS: 691.8 *m/z* [M + H^+]; 713.7 *m/z* [M + Na^+].

HPLC: t_R: 11.8 min.; conditions: 5 → 100% B in 30 min (A: 0.1% TFA in water, B: 0.1% TFA in acetonitrile), flow: 1.0 mL min^{-1}, 220 nm.

^{1}H-NMR (400 MHz, $CDCl_3$, mixture of rotamers) δ: 10.1 ($CF_3COO\mathit{H}$), 4.92–3.86 (m, 12 H, $COC\mathit{H}_2N$), 3.86–2.80 (m, 42 H, $NC\mathit{H}_2CH_2O$, $NCH_2C\mathit{H}_2O$, $OC\mathit{H}_3$).

^{13}C-NMR (100 MHz, $CDCl_3$, mixture of rotamers) δ: 171. 5, 171.0, 170.6, 170.1, 170.0, 169.8, 169.7, 169.5, 169.3, 169.1, 168.9, 168.7, 168.2, 168.1, 158.7 (q, J = 40 Hz, $CF_3\mathit{C}OOH$), 115.0 (q, J = 285 Hz, $\mathit{C}F_3COOH$), 71.7, 71.5 , 71.4 , 71.3, 71.0, 70.8, 70.6, 70.2, 70.0, 69.8, 69.6, 69.3, 69.1, 68.8, 68.7 , 59.1 , 58.9, 58.6, 58.2, 53.4, 52.5, 52.3, 50.9, 50.7, 50.4, 50.3, 50.2, 49.9, 49.1, 48.7, 48.4 , 48.3, 48.0, 47.6 , 47.4, 47.0, 46.8, 46.6, 45.9, 45.5, 43.3.

✔ *Compound **44***

Yield: 41%. The crude residue from the HATU-induced cyclization was purified by RP-HPLC on a C_{18} reversed-phase semi-preparative column (t_R: 13.2 min.; conditions: 25 → 100% B in 30 min (A: 0.1% TFA in water, B: 0.1% TFA in acetonitrile), flow: 2.0 mL min^{-1}, 220 nm).

ES-MS: 775.2 *m/z* [M + H^+].

[α]^{D}: - 6.7 (c =1.0, $CHCl_3$).

^{1}H-NMR (400 MHz, $CDCl_3$, mixture of rotamers) δ: 5.64-4.03 (18H, m, $COC\mathit{H}_2N$), 3.91-2.89 (27H, m, $NC\mathit{H}_2CH_2O$, $NCH_2C\mathit{H}_2O$, $SC\mathit{H}_2$, $OC\mathit{H}_3$), 1.97-1.84 (18H, m, $C\mathit{H}_3$).

^{13}C-NMR (100 MHz, $CDCl_3$, mixture of rotamers) δ: 172.6, 172.4, 171.9, 171.8, 170.5, 170.4, 170.0, 168.3, 167.4, 167.0, 166.6, 166.4, 166.3, 166.0, 165.3, 75.1, 75.0, 74.5, 74.1, 71.9, 71.7, 71.5, 71.0, 70.6, 70.5, 70.3, 70.1, 69.9, 69.4, 68.0, 66.1, 66.0, 65.9, 64.6, 64.3, 63.6, 63.0, 62.8, 62.4, 59.0, 58.8, 58.7,

54.1, 53.8, 53.3, 53.0, 52.6, 51.8, 51.7, 51.3, 50.9, 50.7, 50.6, 50.3, 50.0, 49.7, 49.4, 49.2, 49.1, 49.0, 48.7, 48.4, 37.2, 31.6, 31.5, 31.1, 31.0, 30.6, 30.5, 30.4, 30.0, 29.8, 29.7, 29.6, 27.3, 26.6, 26.5, 26.3.

Decomplexation procedure of **42** *complex with* $Na^+PF_6^-$

To a solution of the compound **42**, complexed with Na^+ (22.0 mg, 0.027 mmol) in $CDCl_3$ (4.4 mL), a 0.1 M solution of $AgNO_3$ in water (4.4 mL) was added. The two phase mixture was stirred for 30 min. The organic phase was washed with deuterated water and, after recording an ^1H NMR, an excess of Me_4NI (50 mg, 0.25 mmol) was added. The suspension was sonicated for 3 h in a sonicator bath and once filtered the excess of Me_4NI and the AgI formed, the organic phase was again subjected to a ^1H NMR, demonstrating the liberation of the cyclic peptoid from the metal complexation.

✓ *Compound* ***42***

ES-MS: 659.7 *m/z* [M + Na^+]; 341.8 *m/2z* [M + $2Na^+$].

^1H NMR (400 MHz, $CDCl_3$, mixture of rotamers) δ: 5.53 (0.75H, d, *J* = 17.6 Hz, NC*H*HCO), 5.40 (0.34H d, *J* = 18.8 Hz, NC*H*HCO), 5.31 (0.34H, d, *J* = 14.0 Hz, NCH*H*CO), 4.93 (0.34H, d, *J* = 14.0 Hz, NC*H*HCO), 4.79 (0.34H, m, COC*H*N), 4.74-4.61 (1.84H, m, COC*H*N), 4.60 (0.34H, d, *J* = 14.4 Hz NCH*H*CO), 4.48 (0.34H, d, *J* = 16.3 Hz NC*H*HCO), 4.34 (0.85H, m, COC*H*N), 4.25 (0.85H, d, *J* = 18.0 Hz, NC*H*HCO), 4.14 (0.85H, d, *J* = 18.0 Hz, NCH*H*CO), 4.09-3-96 (1.6H, m, NCH*H*CO, NCH_2CH_2O),

3.91 (0.75H, d, *J* = 18.8 Hz, NCH*H*CO), 3.81-3.36 (17.95H, m, NCH_2CH_2O, NCH_2CH_2O, $CHCH_2CH_2CH_2N$), 3.35 (0.44H, bs, OCH_3), 3.34 (0.34H, bs, OC*H3*), 3.32 (1.5H, bs, OCH_3), 3.31 (0.44H, bs, OCH_3), 3.30 (1.5H, bs, OCH_3), 3.27 (2H, bs, OCH_3), 3.15 (2.3H, bs, OCH_3), 2.60-1.73 (12H, m, $CHCH_2CH_2CH_2N$, $CHCHHCH_2CH_2N$).

^{13}C NMR (100 MHz, $CDCl_3$, mixture of rotamers) δ: 172.9, 172.5, 172.0, 171.6, 171.3, 170.45, 168.6, 168.4, 167.6, 167.2, 166.9, 165.8, 71.9, 71.7, 70.6, 70.3, 70.2, 68.8, 59.2, 59.0, 58.7, 58.4, 58.1, 56.3, 56.0, 53.4, 51.7, 51.2, 50.9, 50.7, 50.2, 49.7, 49.4, 49.11, 48.9, 48.5, 47.9, 47.6, 46.9, 47.3, 46.7, 46.3, 32.7, 31.9, 31.5, 31.2, 29.9, 29.2, 28.6, 26.4, 25.7, 25.0.

2.6.4 Synthesis of monomer 65

Synthesis of 61

To a solution of methoxyethylamine (4.1 mL, 47.8 mmol) in acetonitrile (80 mL), DIPEA (8.3 mL, 47.8 mmol) and ethyl bromoacetate (4.0 g, 23.9 mmol) were added. The reaction mixture was stirred overnight, concentrated *in vacuo*, dissolved in DCM (20 mL) and washed with brine solution. The aqueous layer was extracted with DCM (× 3). The combined organic phases were dried over $NaSO_4$, filtered and the solvent evaporated *in vacuo* to give a crude material **61** (3.8 g, 98%) which was used in the next step without further purification.

✔*Compound* ***61***

^{1}H-NMR (400 MHz, $CDCl_3$) δ: 4.18(2H, q, *J* = 7.1 Hz, OCH_2CH_3), 3.50 (2H, t, *J* = 4.7 Hz, CH_2OCH_3), 3.44(2H, s, $COCH_2$), 3.35(3H, s, OCH_3), 2.81(2H, t, *J* = 4.7 Hz, CH_2NHCH_2), 2.29 (1H, bs, CH_2NHCH_2), 1.26 (3H, t, *J* = 7.1 Hz, OCH_2CH_3).

^{13}C-NMR (75 MHz, $CDCl_3$) δ: 171.8, 71.6, 60.6, 58.6, 50.6, 48.5, 14.0.

Synthesis of 62

To a solution of **61** (0.48 g, 2.99 mmol) in 1,4-dioxane-water 1:1 (30 mL) at 0°C, $LiOH.H_2O$ (0.21 g, 5.08 mmol) was added. After two hours, $NaHCO_3$ (0.30 g, 3.59 mmol) and Fmoc-Cl (0.93 g, 3.59 mmol) were added. The reaction mixture was stirred overnight. Subsequently, $KHSO_4$ (until pH= 3) was added and the mixture was concentrated *in vacuo*, dissolved in DCM (20 mL) and washed with brine solution. The aqueous layer was extracted with DCM (× 3). The combined organic phases were dried over $NaSO_4$, filtered and the solvent evaporated *in vacuo* to give a crude material (1.4 g, yellow oil), which was purified by flash chromatography (DCM/MeOH, from: 100/0 to 80/20, 0.1% ACOH) to give **62** (0.86 g, 81%).

✔*Compound* ***62***

^{1}H-NMR (400 MHz, $CDCl_3$, mixture of rotamers) δ: 7.55-7.25 (8H, m, ArFmoc), 4.54 (2H, d, *J* = 6.4 Hz, CH_2Fmoc), 4.43 (2H, d, *J* = 6.4 Hz, CH_2Fmoc), 4.26 (1H, t, *J* = 6.4 Hz, CHFmoc), 4.20 (1H, t, *J* = 6.4 Hz, CHFmoc), 4.10 (2H, s,

NCH_2COOH), 4.04 (2H, s, NCH_2COOH), 3.54 (4H, s, CH_2OCH_3), 3.34 (2H, s, NCH_2CH_2O), 3.31(3H, s, OCH_3), 3.24 (2H, s, NCH_2CH_2O), 3.22 (3H, s, OCH_3).

^{13}C-NMR (100 MHz, $CDCl_3$, mixture of rotamers) δ: 174.2 (× 2), 156.3, 155.9, 143.8 (× 2), 141.4, 141.3, 127.7 (× 4), 127.1 (× 2), 127.0 (× 2), 124.9 (× 2), 124.8 (× 2), 119.9 (× 4), 71.5, 71.3, 67.9, 67.5, 58.6 (× 2), 50.4 (× 2), 48.9, 48.3, 47.2, 47.1.

Synthesis of 49

L-Cysteine hydrochloride monohydrate (**63**) (4.8 g, 22.8 mmol) and 57 mL of 2,2-dimethoxypropane were refluxed for 1 h at 60°C in 286 mL of acetone. Then, the reaction mixture was allowed to cool down to 25°C, filtered and the white solid washed with cold acetone to yield **49** (3.04 g, 68%).

✔ *Compound **49***

^{1}H-NMR (400 MHz, D_2O) δ: 4.80 (1H, m, C*H*, overlapped with water signal), 3.67 (1H, dd, *J* = 12.1, 7.4 Hz, SCH*H*), 3.52 (1H, dd, *J* = 12.1, 7.4 Hz, SC*H*H), 1.86 (3H, s, CH_3), 1.84 (3H, s, CH_3).

^{13}C-NMR (100 MHz, D_2O, 1,4-dioxane as internal standard) δ: 170.9, 73.5, 63.1, 32.3, 28.2, 27.2.

Synthesis of 64

To a solution of **62** (0.95 g, 2.67 mmol) in dry DCM (27 mL) at 0 °C, DAST (0.211 mL, 1.602 mmol) was added and the mixture was stirred for 1h. Then, after monitoring the reaction by TLC, more DAST was added (0.211 mL, 1.602 mmol) and the resulting mixture was allowed to react for 1h more. The

reaction was quenched by adding H_2O, and the organic layer was washed with brine (× 1), dried over $MgSO_4$, filtrated and concentrated under *vacuum* to give a crude material **64** which was used in the next step without further purification.

Coupling of 62 *and* 49

To a solution of **49** (0.788 g, 3.99 mmol) in dry DCM (80 mL), **62** (0.95 g, 2.66 mmol) and DIPEA (1.02 mL, 5.85 mmol) were added and the resulting mixture was stirred overnight under a N_2 atmosphere. After, the organic layer was washed with a 5% aqueous solution of citric acid (× 1) and with brine (× 1), dried over $MgSO_4$, filtrated and concentrated under *vacuum*. The residue was purified by silica flash (DCM/MeOH, from: 98/2 to 85/15) to give **65** (0.73 g, 55%).

✔ *Compound **65***

ES-MS: 499.6 *m/z* [M+H^+].

[α]^D: -22.0 (c = 1.0, $CHCl_3$).

^{1}H-NMR (300 MHz, $C_2D_2Cl_4$, 100°C) δ: 7.62-7.15 (8H, m, ArFmoc), 4.74 (1H, bs, C*H*COOH), 4.35 (2H, m, CH_2Fmoc), 4.10 (1H, m, C*H*Fmoc), 3.94 (1H, d, *J* = 7.9 Hz, NCH*H*CO), 3.82 (1H, d, *J* = 7.9 Hz, NC*H*HCO), 3.34-3.25 (4H, m, NCH_2CH_2OCH$_3$), 3.16 (2H, m, SCH_2), 3.13 (3H, s, OCH_3), 1.74 (3H, s, CH_3), 1.70 (3H, s, CH_3).

^{13}C-NMR (75 MHz, $C_2D_2Cl_4$, 100°C) δ: 172.9, 165.1, 154.7, 142.3, 139.5, 127.2, 126.4, 123.0, 118.0, 69.3, 65.9, 65.8, 62.6, 56.7, 49.8, 46.1, 45.8, 29.5, 28.2, 26.0.

2.6.5 X-ray analysis

Table 2.5: Crystal data and structure refinement details for compounds Na^+[**42**]PF_6^-, Na^+[**43**]PF_6^-, **43**.

Compound	Na^+[**42**]PF_6^-	Na^+[**43**]PF_6^-	**43**
CCDC	897772	897773	897774
Formula	$C_{98}H_{156}F_{24}N_{22}Na_4O_{27}P_4$	$C_{15}H_{27}F_6N_3NaO_6P$	$C_{30}H_{54}N_6O_{12}$
P.M. (g mol^{-1})	2746.29	513.36	690.79
λ (Å)	0.30060	Cu*K*α	Mo*K*α
Cristal system	trigonal	triclinic	triclinic
Space group	*R3*	*P-1*	*P-1*
***a* (Å)** ***b* (Å)** ***c* (Å)** **α (°)** **β (°)** **γ (°)**	16.382(5) 16.382(5) 39.89(2) 90 90 120	8.805(3) 11.014(2) 12.477(2) 70.97(2) 77.347(16) 89.75(2)	8.358(4) 9.176(4) 11.623(4) 99.636(6) 101.488(12) 104.239(13)
***V* (Å^3)**	97271(6)	1131(5)	824.5(6)
Z	3	2	1
D_X (g cm^{-3})	1.476	1.532	1.391
μ (mm^{-1})	0.016	2.105	0.107
F(000)	4302	532	372

Indep. refl. measured	11518	2648	3734
Param. / restraints	519 / 1	290 / 0	217 / 0
R1[F_0>4σ(F_0)], $_w$R2(all refl)	0.1436, 0.485	0.116, 0.396	0.046, 0.1295
GooF	2.29	1.396	1.075
Δρ min (e Å^{-3}), Δρ max (e Å^{-3})	-0.594, 1.141	-0.412, 0.598	-0.314, 0.274

Compound Na^+[**42**]PF_6^- was crystallized by slow diffusion of hexane in an acetonitrile solution. Rather small needle-like crystals resulted to be suitable for synchrotron radiation diffraction studies. A crystal of Na^+[**42**]PF_6^- was mounted on a cryo-loop and measured at 100 K at the European Synchrotron Radiation Facility beam line ID11.

Data reduction was performed with the Bruker package (SMART, Saint, SADABS)[74]. Data have been corrected for Lorentz, polarization and absorption.

Compound Na^+[**43**]PF_6^- was crystallized by slow diffusion of ethyl acetate in an acetonitrile solution. Small crystals of Na^+[**43**]PF_6^- were analyzed using a rotating anode as X-ray source available at IBB-CNR (Naples, Italy). A suitable crystal was selected and glued on a glass fiber and measured at room temperature with a Rigaku AFC11K diffractometer equipped with a Saturn944 CCD detector using CuKα

[74] Bruker AXS Inc., Madison, Wisconsin, USA.

radiation. Data reduction was performed with the crystallographic package CrystalClear.[74]

X-ray diffraction quality single crystals of **43** were obtained by slow evaporation of a solution of ethyl acetate.

A suitable crystals of **43** was selected and glued on a glass fiber and measured at room temperature with a Rigaku AFC7S diffractometer equipped with a Mercury[75] CCD detector using Mo*K*α radiation. Data reduction was performed with the crystallographic package CrystalClear.

In all case collected data have been properly corrected for Lorentz, polarization and absorption.

The structures of all three compounds were solved by direct methods using the program SIR2002[76] and refined by means of full matrix least-squares based on F2 using the program SHELXL97.[77]

All non-hydrogen atoms were refined anisotropically, hydrogen atoms were positioned geometrically and included in structure factors calculations but not refined.

Refinement details are summarized in Table 2.5.

R-indices for compound Na^+[**42**]PF_6^- are rather high due to the presence of disordered PF_6^- ions, whose associated electron density resulted to be rather difficult to model. This reflects also on an undetermined Flack parameter for compound Na^+[**42**]PF_6^-.

[75] CrystalClear, Crystal Structure Analysis Package, Rigaku-Molecular Structure Corp.

[76] M. C. Burla, M. Camalli, B. Carrozzini, G. Cascarano, C. Giacovazzo, G. Polidori, R. Spagna, *J. Appl. Cryst.* **2001,** *34,* 523-526.

[77] G. M. Sheldrick, *Acta Cryst*. **2008**, *A64,* 112-122.

2 PROLINE-RICH CYCLOPEPTOIDS

3 AMPHIPHILIC CYCLOPEPTOIDS

3.1 Introduction

Amphiphilic peptides and peptoids represent a fascinating class of molecules with broad-spectrum applications in many fields such as material science and biomedicine.[78,79]

For example, a very interesting application of amphiphilic peptides consists in the design of supramolecular micelles of different size and shape, called "peptide amphiphile micelles" (PAs).[79] A typical PA molecule contains a biologically active hydrophilic peptide "headgroup" which is linked through an amide bond to a hydrophobic "tail". The tails can be double-chain lipids, single-chain fatty acids, hydrophobic peptides, polymers. In some cases a linker of different length and flexibility (*e.g.* PEG, polyproline linker, polyalanine linker) is introduced between the headgroup and the tail.

In aqueous solution the self assembly of PA molecules determines the formation of nanofibers, whose core is made of packed tails while the surface contains the hydrophilic portion. The main driving force for the self assembly process is the hydrophobic aggregation of the hydrocarbon tails, dictated by their shielding from the aqueous solvent.

[78] R. Kudirka, H. Tran, K. T. Nam, B. Sanii, P. H. Choi, N. Venkateswaran, R. Chen, S. Whitelam, R. N. Zuckermann *Peptide Science*, **2011**, *96*, 586-595.
[79] A. Trent, R. Marullo, B. Lin, M. Black, M. Tirrel *Soft Matter*, **2011**, *7*, 9572-9582.

The hydrophilic peptide regions can interact generating α-helix or β-sheet secondary structures. Notably, the peptide secondary structure was demonstrated to influence PA micelle morphology.

An intriguing family of PAs, whose self assembly is reversibly induced through pH changes or addition of Ca^{++}, was reported by Stupp and co-workers.[80]

They prepared a set of PA molecules containing cysteine-rich hydrophilic peptide sequences with biologically active RGD motif linked to a fatty acid of various length. One of the PA molecules synthesized (**67**) is reported in figure 3.1.

These molecules were solubilized in water at pH 8 exploiting the negative charges located on aspartate and the C-terminal carboxylate. Upon full reduction of the PA molecules with dithiothreitol (DTT), on pain of the formation of intramolecular disulfide bridges unfavouring the self assembly, and acidification at pH below 4.5 it was found the formation of a gel phase containing micelles, as shown in figures 3.2 and 3.3. The gel is disassembled at neutral and basic pH, so the gelification process is reversible. The effect of pH can be explained as follows.

In essence, the self assembly process is favourite at low pH due to the fact that in these conditions the peptides do not posses negative charges, which inhibit in basic media the micelle formation as a result of electrostatic repulsion phenomena.

[80] J. D. Hartgerink, E. Beniash, S. I. Stupp *Proc. Natl. Acad. Sci.* U.S.A. **2002**, *99*, 5133-5138.

It was also possible to form micelles adding Ca^{++} to an aqueous solution at pH 8 of the PA molecule. In this case the divalent cation acts as gelator agent shielding the negative charges of the peptide chains.

Very interestingly, it was realized a reversible linkage of the nanofibers oxidating the cysteine residues with I_2 (figure 3.3). In this way intermolecular disulfide bridges were produced, generating a very stable supramolecular structure which is preserved in a broad range of pH values.

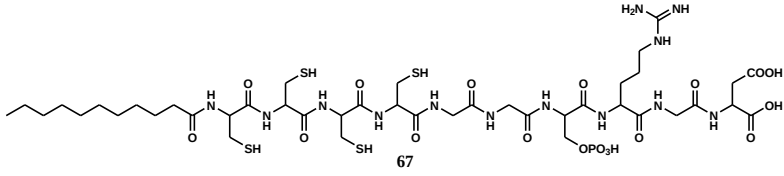

67

Figure 3.1: Chemical structure of an amphiphilic peptide synthesized by Stupp and co-workers.

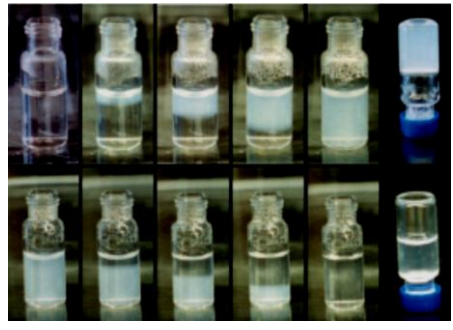

Figure 3.2: Time sequence of pH-controlled PA self assembly and disassembly. (*Upper*) From left to right PA molecule dissolved in water at pH 8 is exposed to HCl vapour. The diffusion of the acid causes the formation of a gel phase (*far left*). (*Lower*) The same gel is treated with NH_4OH vapour, which disassembles the gel.

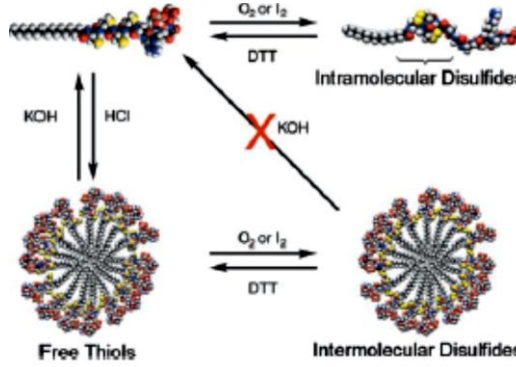

Figure 3.3: Schematic representation of the self-assembly and covalent linkage of the PAs based on pH and oxidation state.

3.2 *Aims of the work*

The great interest engendered by amphiphathic peptide and peptoid structures suggested us to prepare some amphiphilic cyclopeptoids.

In particular, with the aim to evaluate the effect of side chain polarity and orientation on the organization in the crystal structure, the synthesis of amphiphilic cyclopeptoids containing at the same time an hydrophobic molecular portion and a polar one was planned. The choice fell to cyclohexapeptoids decorated with three side chains of benzylamine and ethanolamine in alternate and continuous positions (**45** and **46**, figure 3.4).

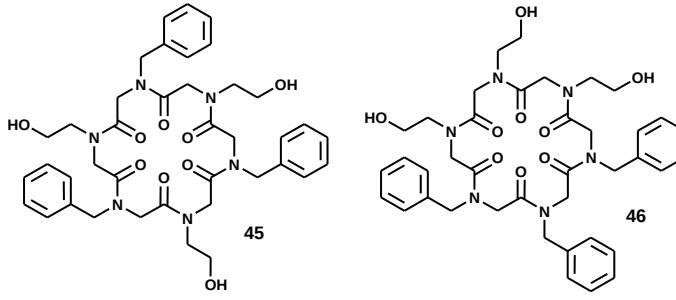

Figure 3.4: Amphiphilic cyclopeptoids synthesized.

3.3 Synthesis

In order to carry out the classic submonomer solid phase synthesis it was necessary to prepare a protected ethanolamine (figure 3.5). The nucleophilic alcoholic function could indeed lead to secondary reactions during the coupling reaction.

The protecting group which in our experience proved to be the most suitable was the *t*-butylchlorodiphenylsilane (TBDPS). It assures a good resistance both to basic and acidic conditions, which will be used during elongation and cleavage of the resin respectively.

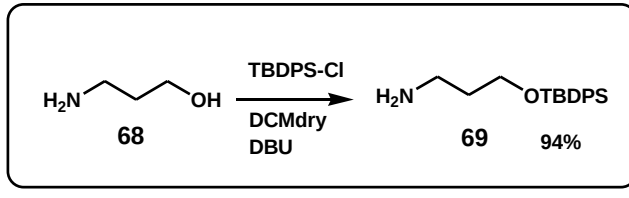

Figure 3.5: Protection reaction of ethanolamine with *t*-butylchlorodiphenylsilane.[81]

[81] M. Rayesh, J. Sen, M. Srujan, K. Mukherjee, B. Sreedhar, A.Chaudhuri *J. Am. Chem. Soc*., **2007**, *129*, 11408-11420.

Synthesis of linear precursor, followed by the cyclization step in high dilution, gave protected compounds **71** and **73** (scheme 3.1and figure 3.6).

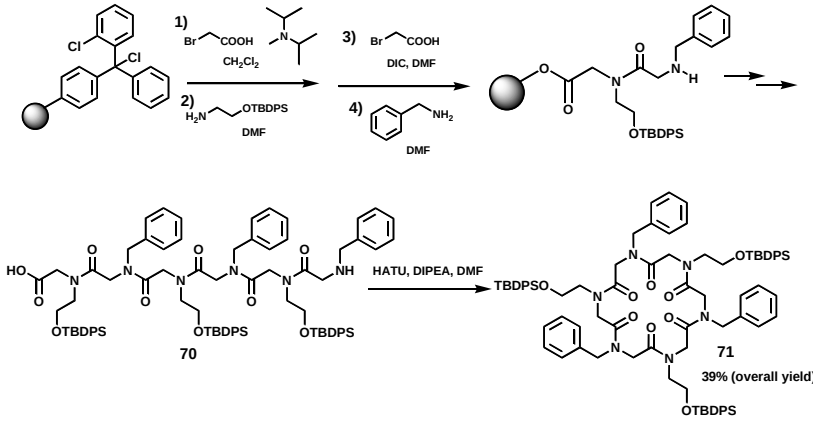

Scheme 3.1: Synthesis of **71** (alternate protected hexacyclopeptoid). Cleavage of the resin is conducted with 20% $(CF_3)_2CHOH$ in DCM. Purification was performed by precipitation in CH_3CN:H_2O 3:1.

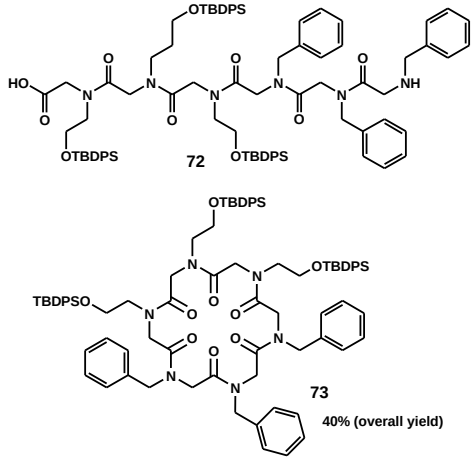

Figure 3.6: Compound **73** (continuous protected hexacyclopeptoid) and its linear precursor (**72**). The synthesis of **73** is performed in the same way as compound **71** (scheme 3.1). Purification was conducted through silica flash chromatography.

The deprotection of compounds **71, 73** revealed to be quite difficult.

Classic deprotection conditions of silylether protecting groups (HF/Piridine, NaOH/MeOH, TBAF (tetra-*n*-butylammonium fluoride) unexpectedly failed. Finally, deprotection of the compounds **71** and **73** was successful achieved with a 3% solution of HCl/MeOH (scheme 3.2).[82]

[82] E. M. Nashed, C. P. J. Glaudemans *J. Org. Chem.*, **1987**, *52*, 5255-5260.

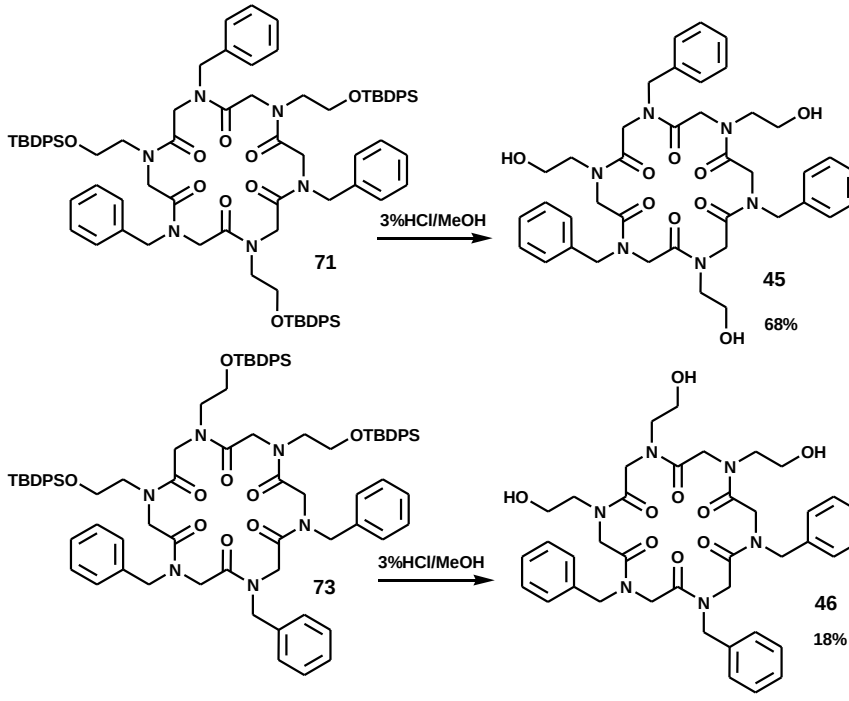

Scheme 3.2: Deprotection reaction of compounds **71** and **73**. Target molecules **45** and **46** were purified via RP- HPLC.

3.4 Structural analysis of the alternate protected cyclopeptoid

Table 3.1: Solubility scale for the compound **71.**

Solvent	Solubility order
$CHCl_3$	1
AcOEt	2
MeOH	3
CH_3CN	4
Hexane	5

The solubility scale of **71** (table 3.1) indicates that ethylacetate is a good crystallization solvent and, at the same time, MeOH can play the role of non solvent. Indeed, sparkling crystals of compound **71** (the alternate protected cyclopeptoid), suitable for X-ray structure analysis, were obtained by vapour phase diffusion of methanol in a solution of ethylacetate.

The crystals showed a triclinic lattice (a = 14.707(4) Å, b = 16.200(5) Å, c = 18.353(5) Å, α = 99.654(9)°, β = 90.154(5)°, γ = 100.828(10)°; space group = *P-1*; cavities volume = 40 Å^3 (probe radius 1.2 Å)). X-ray diffraction data indicated that the crystals correspond to an uncomplexed species devoid of a co-crystallization solvent. The conformation of the peptoid backbone is *tcctcc* (figure 3.7), similarly to cyclopeptoid **43** in uncomplexed form (see section 2.3.5). Moreover, it is interesting to notice that in the X-ray structure are present T shaped interactions between aryl rings (figure 3.7). In addition, there is some positional disorder around a specific aryl ring. The discussed disorder arises from one of the aryl moieties which can adopt two different positions in the crystal structure. The movement is allowed by the void space present in the crystal (figure 3.8). Interestingly, *t*-butyl groups lead to some complications in crystal packing and as a consequence the crystal structure exhibits empty cavities of 40 Å^3 volume (probe radius = 1.2 Å). The porosity of the structure under investigation is a so-called closed porosity because only closed pores (non-connected cavities) are present.

The dimension of the cavities permits to accommodate tiny molecules like water.

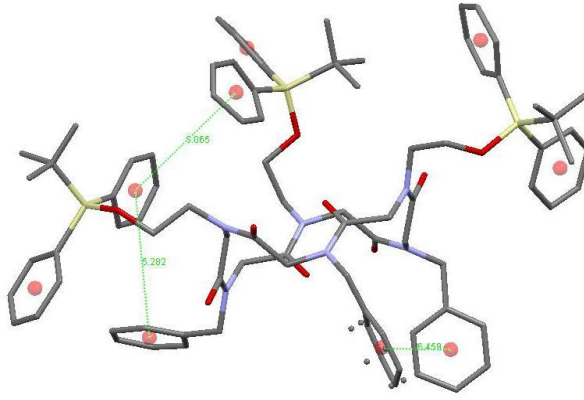

Figure 3.7: X-ray molecular structure of **71**. Distances between centroids of aryl rings are reported in Å. It is reported the positional disorder around a specific aryl ring.

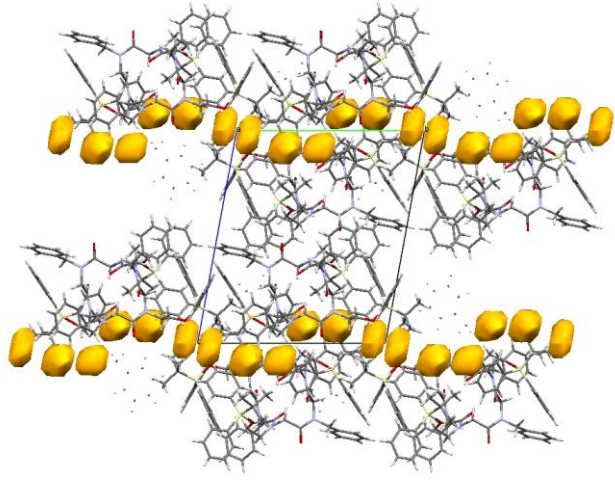

Figure 3.8: Crystal packing of **71** with the void space (40 $Å^3$) represented by Van Der Waals spheres. It is reported the positional disorder around a specific aryl ring.

3.5 Crystallization trials for 73

The compound **73** (the continuous protected cyclopeptoid) contained some impurities derived from HATU. In CH_3CN the impurities are soluble whereas the product **73** precipitates as a white powder. Later, the solubility scale (table 3.2) for **73** was determined and some crystallization trials were unsuccessfully carried out:

a) Slow evaporation from a solution $CH_3CN/CHCl_3$ 1:1; b) slow evaporation from a solution of $CHCl_3$; c) slow evaporation from a solution of toluene.

Table 3.2: Solubility scale for the compound **73**.

Solvent	Solubility order
$CHCl_3$	1
AcOEt, Toluene	2
CH_3CN	3
MeOH	4
Hexane	5

3.6 Crystallization trials for 45

The solubility scale for the compound **45** (the alternate amphiphilic cyclopeptoid) is illustrated in table 3.3. Some crystallization trials were unsuccessfully performed: a) Slow evaporation from a solution of EtOH/hexane 1:1 (v/v); b) diffusion in vapour phase of hexane in a solution MeOH/$CHCl_3$ 2:1 (v/v); c) diffusion in vapour phase of hexane in a solution AcOEt/$CHCl_3$ 1:1 (v/v).

Table 3.3: Solubility scale for the compound **45**.

Solvent	Solubility order
EtOH, MeOH	1
$CHCl_3$, H_2O	2
CH_3CN	3
AcOEt	4

3.7 Crystallization trials for 46

The solubility scale for the compound **46** (the continuous amphiphilic cyclopeptoid) is illustrated in table 3.4. Some crystallization trials were unsuccessfully performed: a) Slow evaporation from a solution of EtOH/hexane 1:1 (v/v); b) slow evaporation from a solution of EtOH/acetone 1:1 (v/v); c) slow evaporation from a solution of EtOH/H_2O 1:1 (v/v).

Table 3.4: Solubility scale for the compound **46**.

Solvent	Solubility order
EtOH, MeOH	1
$CHCl_3$, H_2O	2
CH_3CN	3
AcOEt	4

3.8 Conclusions

The synthesis of the continuous and alternate amphiphilic cyclopeptoids (**45, 46**) was successfully performed. The final aim was to crystallize amphiphatic peptoid structures, and at the same time to compare the

crystal structure of a specific amphiphilic isomer with that of its protected precursor. Unfortunately, only the alternated protected compound **71** was crystallized whereas all the crystallization attempts carried out on the other three cyclic molecules failed.

Notably, the crystal structure of **71** is characterized by a *tcctcc* conformation, typical of a decomplexed cyclohexapeptoid, and a closed porosity with a void space of 40Å^3.

3.9 Experimental section[83]

3.9.1 Submonomer solid-phase synthesis of linear precursors 70 and 72

Linear peptoid precursors of **70, 72** were synthesized using a submonomer solid-phase approach. Typically 0.40 g of 2-chlorotrityl chloride resin (2,α-dichlorobenzhydryl-polystyrene crosslinked with 1% DVB; 100-200 mesh; 1.30 mmol/g) was swelled in dry DCM (4 mL) for 45 min and washed twice in dry DCM (4 mL). The first sub-monomer was attached onto the resin by adding bromoacetic acid (107 mg, 0.77 mmol) and DIPEA (418 μL, 2.4 mmol) in dry DCM (4 mL) on a shaker platform for 40 min at room temperature, followed by washing with dry DCM (3 × 4 mL) and then with DMF (3 × 4 mL). To the bromoacetylated resin benzylamine (524 μl, 4.80 mmol) in dry DMF (4 mL), was added. The mixture was left on a shaker platform for 40 min at room

[83] See section 2.6.1 for general procedures.

temperature, then the resin was washed with DMF (3 × 4 mL). Subsequent bromoacetylation reactions were accomplished by reacting the oligomer with a solution of bromoacetic acid (690 mg, 4.8 mmol) and DIC (817 μL, 5.28 mmol) in DMF (4 mL) on a shaker platform 40 min at room temperature. The filtered resin was washed with DMF (3 × 4 mL) and treated again with benzylamine under the same conditions reported above in the case of linear precursor of **70**, or with amine **67** (864 mg, 2.88 mmol) in the case of linear precursor of **69**. This cycle of reactions was iterated until the target oligomer was obtained. The oligomer-resin was cleaved in 4 mL of 20% HFIP in DCM (v/v). The cleavage was performed on a shaker platform for 30 min at room temperature the resin was then filtered away. The resin was treated again with 4 mL of 20% HFIP in DCM (v/v) for 5 min, washed twice with DCM (4 mL), filtered away and the combined filtrates were concentrated in vacuo. The final product was dissolved in 50% ACN in HPLC grade water and analysed by RP-HPLC and ESI mass spectrometry. The linear compounds were subjected to the cyclization without further purification.

✔ *Compound **70***

Purity: >95%.

Yield: 76% (crude residue).

ES-MS: 1477.7 *m/z* [M + H^+].

HPLC: t_R: 26.4 min; conditions: 5 → 100% B in 30 min (A, 0.1% TFA in water, B, 0.1% TFA in acetonitrile); flow: 1 mL min^{-1}, 220 nm.

✔ *Compound **72***

Purity: 76%.

Yield: 74% (crude residue).

ES-MS: 1477.7 *m/z* [M + H^+].

HPLC: t_R: 23.6 min; conditions: 5 → 100% B in 30 min (A, 0.1% TFA in water, B, 0.1% TFA in acetonitrile); flow: 1 mL min^{-1}, 220 nm.

3.9.2 General procedure for high dilution cyclization. Synthesis of 71 and 73

To a stirred solution of HATU (116 mg, 0.31 mmol), DIPEA (0.082 mL, 0.47 mmol) in dry DMF (20 mL) at room temperature, a solution of the linear compounds (crude **70**, **72**) (0.08 mmol) in dry DMF (20 mL) was added by syringe pump in 6 h. After 12 h the resulting mixture was concentrated in vacuo, diluted with DCM (20 mL) and washed with 1 M HCl (7 mL × 3) was added. The mixture was extracted with DCM (10 mL × 2) and the combined organic phases were washed three times with water (10 mL), dried ($MgSO_4$) and concentrated in vacuo. The crude residues of **71**, **73** from the HATU-induced cyclizations were respectively purified by precipitation in CH_3CN/H_2O 3:1 (v/v) and flash chromatography (DCM/MeOH, from: 100/0 to 96/4).

✔ *Compound **71***

Yield: 51%. The crude residue from the HATU-induced cyclization was purified by precipitation in CH_3CN/H_2O 3:1 (v/v).

ES-MS: 1481.7 *m/z* [M + Na^+].

HPLC: t_R: 28.2 min; conditions: 5 → 100% B in 30 min (A, 0.1% TFA in water, B, 0.1% TFA in acetonitrile); flow: 1 mL min^{-1}, 220 nm.

^{1}H-NMR: (400 MHz, $CDCl_3$, mixture of rotamers) δ: 7.68–6.89 (45 H, m, Ar), 5.36–5.24, 4.75–2.71 (30 H, m, COC*H*$_2$N, NC*H*$_2$CH$_2$O, NCH$_2$C*H*$_2$O, C*H*$_2$Ph), 1.25–0.82 (27 H, m, SiC(C*H*$_3$)$_3$).

^{13}C-NMR: (100 MHz, $CDCl_3$, mixture of rotamers) δ: 171.8, 171.3, 170.4, 170.2, 170.1, 169.7, 169.5, 169.1, 168.9, 168.6, 168.1, 167.8 , 167.7, 167.6, 167.2, 167.0, 137.1, 136.7, 135.4, 134.7, 133.5, 133.0, 132.8 , 129.9, 129.8, 129.6 , 129.0, 128.6, 128.3, 127.9, 127.7 , 127.2 , 126.9 , 126.8, 125.3, 82.8–79.7, 63.3, 62.9, 62.6, 62.3, 62.0, 61.7, 61.3, 61.0, 60.6, 53.2, 52.6, 51.8, 51.5, 51.1, 50.8, 50.5, 50.0, 49.7, 49.1, 48.3, 48.1, 47.7, 47.4, 47.0, 46.6, 46.2, 32.0, 31.6 , 31.4, 31.2, 30.9, 30.6, 29.7, 26.9.

✔ *Compound **71** with sodium picrate*

To a 4.0 mM solution of **71** in CD_3CN:$CDCl_3$ 9:1 (0.5 mL), were added 3 mg of sodium picrate. After the addition the suspension was stirred vigorously for 15 min and the ^{1}H NMR and ^{13}C NMR spectra was recorded.

^{1}H-NMR: (400 MHz, $CD_3CN/CDCl_3$ = 9/1) δ: 8.73 (s, protons of picrate present in excess), 7.75–7.16 (45H, m, Ar), 4.74 (3H, d, *J* = 17.4 Hz, C*H*HPh or NC*H*HCO), 4.69 (3H, d, *J* = 16.9 Hz, C*H*HPh or NC*H*HCO), 4.68 (3H, d, *J* = 16.6 Hz, C*H*HPh or NC*H*HCO), 4.17 (3H, d, *J* = 17.4 Hz, CH*H*Ph or NC*H*HCO), 3.67 (9H, m, NCH*H*CH$_2$O and NCH$_2$C*H*$_2$O,

overlapped), 3.61 (3H, d, *J* = 16.6 Hz, CH*H*Ph or NCH*H*CO), 3.53 (3H, d, *J* = 16.9 Hz, CH*H*Ph or NCH*H*CO), 3.17 (3H, d, *J* = 12.2 Hz, NC*H*HCH$_2$O), 0.91 (27H, s, SiC(C*H*$_3$)$_3$).

^{13}C-NMR: (62.89 MHz, CD$_3$CN/CDCl$_3$ = 9/1) δ: 171.1 (× 3), 170.6 (× 3), 163.3 (picrate), 143.3 (picrate), 137.0 (× 3), 136.7 (× 12), 134.1 (× 6), 131.3 (× 6), 130.2 (× 9), 129.2 (× 15), 129.1 (× 3), 128.3 (picrate), 127.2 (picrate), 63.1 (× 3), 53.7 (× 3), 51.8 (× 3), 50.6 (× 3), 50.4 (× 3), 30.7 (× 3), 27.6 (× 9).

✓ *Compound **73***

Yield: 54%. The crude residue from the HATU-induced cyclization was purified by flash chromatography (DCM/MeOH, from: 100/0 to 96/4).[84]

ES-MS: 1481.7 *m/z* [M + Na$^+$].

HPLC: t_R: 26.5 min; conditions: 5 → 100% B in 30 min (A, 0.1% TFA in water, B, 0.1% TFA in acetonitrile); flow: 1 mL min^{-1}, 220 nm.

^{1}H-NMR: (400 MHz, CDCl$_3$, mixture of rotamers) δ: 7.62–6.91 (45 H, m, Ar), 5.30–5.28, 4.71–2.79 (30 H, m, COC*H*$_2$N, NC*H*$_2$CH$_2$O, NCH$_2$C*H*$_2$O), 1.12–0.83 (27 H, m, SiC(C*H*$_3$)$_3$).

^{13}C-NMR: (100 MHz, CDCl$_3$, mixture of rotamers) δ: 169.9, 169.8, 169.6, 169.5, 135.4, 135.3, 135.0, 134.6, 134.5, 132.6, 132.4, 130.0, 129.5, 129.0, 127.9, 127.4, 127.3, 126.5, 120.7, 62.1, 61.8, 61.6, 61.3, 61.2, 52.6, 52.5, 50.9, 50.1, 49.6, 49.3, 48.9, 48.8, 48.7, 38.0, 36.5, 32.7, 31.9, 30.2, 29.6, 29.3, 29.0, 26.9.

[84] With flash chromatography it was not possible to separate well the product **73** from HATU byproducts.

3.9.3 Deprotection reaction of 71 and 73

To a flask containing the compound **71** or **73** (45 mg, 0.031 mmol), 9 mL of 3% HCl solution in MeOH was added and the resulting mixture was stirred at room temperature for 48h. The reaction was monitored *via* RP-HPLC. Later, the reaction mixture was neutralized with Amberlite IR-45 (OH^-), concentrated, and purified by RP-HPLC on a C_{18} semi-preparative reversed-phase column. Thus, compounds **45** and **46** were obtained.

✓ *Compound **45***

Yield: 68%. The crude residue was purified by RP-HPLC on a C_{18} reversed-phase semi-preparative column (t_R: 8.6 min.; conditions: 25 → 100% B in 30 min (A: 0.1% TFA in water, B: 0.1% TFA in acetonitrile), flow: 3.0 mL min^{-1}, 220 nm).

ES-MS: 767.4 *m/z* [M + Na^+].

^{1}H-NMR: (400 MHz, CD_3OD, mixture of rotamers) δ: 7.72–7.21 (45 H, m, Ar), 4.55–2.60 (30 H, m, $COCH_2N$, NCH_2CH_2O, NCH_2CH_2O).

✓ *Compound **46***

Yield: 18%.[85] The crude residue was purified by RP-HPLC on a C_{18} reversed-phase semi-preparative column (t_R: 10.8 min.; conditions: 25 → 100% B in 30 min (A: 0.1% TFA in water, B: 0.1% TFA in acetonitrile), flow: 3.0 mL min^{-1}, 220 nm).

[85] The low yield is due to the fact that the purified protected-precursor **73** contained HATU byproducts.

ES-MS: 767.4 *m/z* [M + Na^+].

^{1}H-NMR: (400 MHz, CD_3CN, mixture of rotamers) δ: 7.38–7.06 (45 H, m, Ar), 4.16–2.45 (30 H, m, COC*H*$_2$N, NC*H*$_2$CH$_2$O, NCH$_2$C*H*$_2$O).

3.9.4 Synthesis of 69

A solution of 2-aminoethanol (**68**) (0.5 g, 8.2 mmol) dissolved in 9 mL of dry DCM was transferred to a flask, and the solution was cooled to 0 °C. DBU (3.7 g, 24.6 mmol) was addedto this cold solution at 0 °C. *t*-butylchlorodiphenylsilane (6.8 g, 24.6 mmol) was added to the cold reaction mixture and stirred for 15 min

at 0 °C. The temperature was gradually raised to room temperature, and stirring was continued for additional 12 h. The reaction mixture was then diluted with DCM (100 mL) and washed with water (2 × 50 mL). The organic layer was separated, dried over anhydrous Na_2SO_4, and concentrated on a rotary evaporator. The residue, upon chromatographic purification by flash silica (DCM/MeOH, from: 100/0 to 91/9), afforded the amine **69** as a light brown liquid (2.3 g, 94%).

✓ *Compound **69***

^{1}H-NMR: (250 MHz, $CDCl_3$) δ: 7.68-7.66 (4H, m, Ar*H*), 7.43-7.38 (6H, m, Ar*H*), 3.69 (2H, t, *J* = 4.3 Hz, C*H*$_2$OSi), 2.83 (2H, t, *J* = 4.3 Hz, t, C*H*$_2$NH$_2$), 1.83 (2H, bs, N*H*$_2$), 1.06 (9H, s, SiC(C*H*$_3$)$_3$).

3.9.5 X-ray analysis

Table 3.5: Crystal data and structure refinement details for compound **71**.

Compound	**71**
Formula	$C_{87}H_{102}N_6O_9Si_3$
P.M. (g mol^{-1})	1460.02
λ (Å)	0.7107
Space group	*P-1*
Cristal system	triclinic
Space group	*P-1*
***a* (Å)**	14.707(4)
***b* (Å)**	16.200(5)
***c* (Å)**	18.353(5)
α (°)	99.654(9)
β (°)	90.154(5)
γ (°)	100.828(10)
***V* (Å^3)**	42321(2)
Z	2
D_X (g cm^{-3})	1.546
μ (mm^{-1})	0.114
F(000)	1560
Indep. refl. measured	17970
Param. / restraints	9 / 1
R1[F_0>4σ(F_0)], $_w$R2(all refl)	0.1104, 0.3830

GooF	1.046
Δρ min (e Å^{-3}) , Δρ max (e Å^{-3})	-0.03, 0.032

X-ray diffraction quality single crystals of **71** were obtained by slow diffusion of methanol in an ethyl acetate solution.

A suitable crystals of **71** was selected and glued on a glass fiber and measured at room temperature with a Rigaku AFC7S diffractometer equipped with a Mercury[74] CCD detector using Mo*K*α radiation. Data reduction was performed with the crystallographic package CrystalClear.[75]

Collected data have been properly corrected for Lorentz, polarization and absorption. The structures was solved by direct methods using the program SIR2002[76] and refined by means of full matrix least-squares based on F2 using the program SHELXL97.[77]

All non-hydrogen atoms were refined anisotropically, hydrogen atoms were positioned geometrically and included in structure factors calculations but not refined. Refinement details are summarized in Table 3.5.

3 AMPHIPHILIC CYCLOPEPTOIDS

4 CYCLOPEPTOIDS AS PHASE TRANSFER CATALYSTS

4.1 Introduction

Phase-transfer catalysis (PTC) is a laboratory scale synthetic method and industrial process which is employed in a variety of organic reactions (*e.g.* alkylation, Michael addition, aldol condensation, oxidation, etc.).[86] Some areas of application are the production of polymers, pharmaceuticals, dyes, perfumes, agrochemicals. The advantages of PTC in industial context are operational simplicity, mild conditions, high reaction rates, waste reduction and catalyst reuse.[87] Most commercially available phase-transfer catalysts are quaternary ammonium and phosphonium salts, crown ethers and open chain polyethers.

Phase-transfer catalysis was first introduced in the 1960's as an efficient strategy to carry out organic reactions between water soluble inorganic reagents and organic substrates in a biphasic liquid-liquid system. [87,88] In a typical PT reaction, such as the S_N2 reaction of 1-chlorooctane (RY) with NaCN (MX) in an aqueous-organic system, the quaternary phosphonium PT catalyst $(C_6H_{13})P^+Br^-$ (Q^+Y^-)

[86] M. Halpern "Phase-Transfer Catalysis" in Ullmann's Encyclopedia of Industrial Chemistry **2002**, Wiley-VCH, Weinheim.

[87] G. Pozzi, S. Quici, R.H. Fish *J. of Fluorine Chem.* **2008**, *129*, 920–929.

[88] T. Ooi, K. Maruoka *Angew. Chem. Int. Ed.*, **2007**, *46*, 4222-4266; S. Shikarawa, K. Maruoka *Angew. Chem. Int. Ed.*, **2013**, *52*, 4312-4348.

induces a many thousand fold increase of the reaction rate. According to the first general PTC mechanism proposed by Starks (scheme 4.1)[87], the PT catalyst, partitioned between the two immiscible liquid phases, in water forms the lipophilic ion-pair $(C_6H_{13})P^+CN^-$ (Q^+X^-), in which the anion interacts very weakly with the bulky cation and as a consequence its reactivity is enhanced. In this way, the reacting anion (CN^-) is transferred from the aqueous to the organic phase where the reaction happens and the catalyst is regenerated.

Altough the exact mechanism of PTC is elusive, many different mechanisms can be hypothesized depending on the catalyst and the organic reaction analyzed. Indeed, it was proposed a revision of the Starks mechanism, in which the anion exchange between the catalyst (Q^+Y^-) and the inorganic salt (MX) occurred at the phase boundary, and the following reaction between Q^+Y^- and RY takes place in the bulk organic phase.[87] This interphase mechanism is valid also in the case of a neutral PT catalyst, such as lipophilic cyclic and acyclic polyethers (scheme 4.2).

Another possible mechanism for liquid-liquid PTC reactions was proposed by Mazoska and it can be applied when aqueous solutions of alkali hydroxides (M^+OH^-) are employed to form the reactive organic species from weakly acidic substates (SH), as illustrated in scheme 4.3.[87] In essence, OH^- anion can not migrate in the organic phase by the action of lipophilic onium salts due to its high hydrophilicity. So, the deprotonation of SH occurs at the aqueous-organic interphase

resulting in the formation of the ion pair M^+S^-, which is unable to leave the phase boundary because M^+ can not be extracted in non-polar organic solvents and S^- is unsoluble in the MOH solution. The ion exchange with a PT catalyst allows the formation of a lipophilic ion-pair (Q^+S^-), which migrates from the interface to the bulk organic phase, where the anion reacts with the electrophilic substrate (RX).

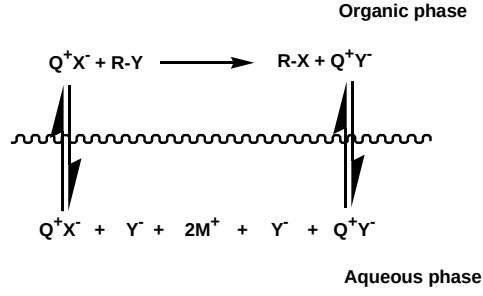

Scheme 4.1: Starks mechanism of PTC.

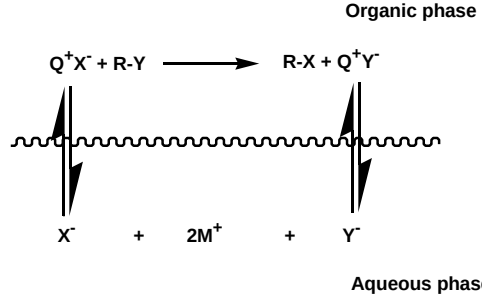

Scheme 4.2: Revision of the Starks mechanism of PTC.

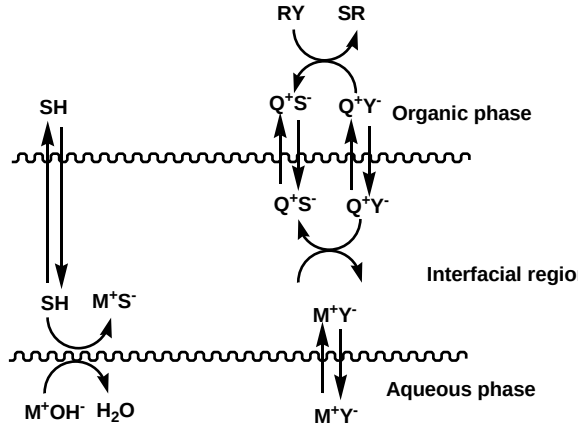

Scheme 4.3: Mazoska mechanism of PTC.

In addition to liquid-liquid phase-transfer catalysis, it is also possible to perform reactions under solid-liquid PTC conditions.[87] Particularly, this reaction is conducted suspending a solid salt in an anhydrous organic solution containing the substrate and the PT catalyst. Substantially, the PT catalyst extracts the reacting anion from the solid salt causing the collapse of the crystal lattice.

In the PTC context, asymmetric phase-transfer catalysis represents a very active research field and in the past few decades several chiral PT catalysts have been designed and used in different asymmetric reactions.[88]

A very important PT asymmetric reaction is the enantioselective alkylation of active methylene compounds, and its development was aroused from a pioneering study of a

Merck research group.[89] Specifically, Dolling and co-workers performed the methylation of the phenylindanone derivative **74** under phase-transfer conditions making use of the chinconine-derived quaternary ammonium salt **75** as asymmetric PT catalyst, obtaining the corresponding alkylated product **76** in high yield and enantiomeric excess (scheme 4.4). The first step of the alkylation is the interfacial deprotonation of the α-proton of **74** with NaOH to generate the corresponding metal enolate, which is localized at the interface between the two liquid phases. Further cation-exchange forms the lipophilic ionic complex **77** between the enolate and the catalyst (scheme 4.4), which goes in the organic phase where the reaction occurs. This complex is stabilized *via* hydrogen bonding, electrostatic and Π-Π stacking interactions. The enantioselective pathway of the reaction occurs through a selective attack of the electrophile (RCl) to the least sterically hindered face of the enolate (*si*-face) belonging to the complex **77**, so that a chiral product is afforded. The *re*-face of the enolate is blocked by the quinoline ring.

[89] S. Jew, H. Park *Chem. Commun.*, **2009**, *46*, 7090-7103.

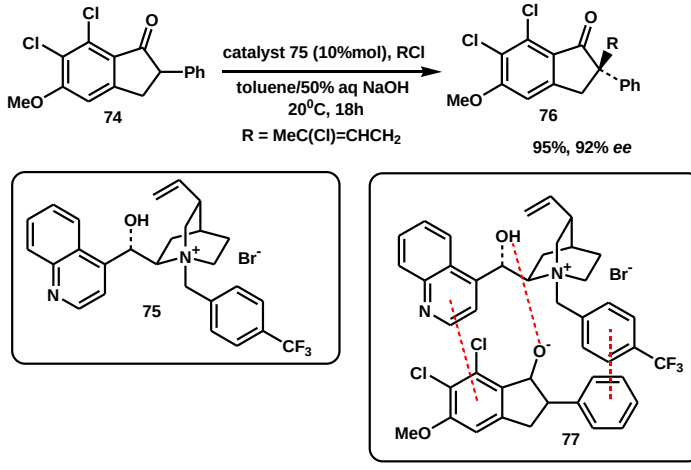

Scheme 4.4: Asymmetric PT alkylation of an indanone derivative.

Another example of enantioselective alkylation of active methylene compounds is the alkylation of *N*-(diphenylmethylene)glycine *t*-buthyl ester, which allows to obtain the iminic precursor of an α-aminoacid. This reaction is usually performed in presence of a chiral catalyst making use of the alkylating agent benzyl bromide and employing an organic solvent and an aqueous solution of an alkaline hydroxide (scheme 4.5). During the years different catalysts were tested in this reaction and in scheme 4.5 are reported some examples of catalysts: *N*-antracenylmethylammonium salt **80** developed by Lygo[88], the binaphtyl N-spiro catalyst **81** developed by Maruoka[88] and the more recent catalyst **82** developed by Grover[90], which contains two chiral elements (tartaric acid and 2,5-dimethylpyrroline rings). **80** and **81** are

[90] W. E. Kowtoniuk, D. K. MacFarland, G. N. Grover *Tetrahedron Lett.*, **2005**, *46*, 5703-5705.

classic asymmetric PT catalyst whereas **82** represents a novel catalytic system. Specifically, as illustrated in table 4.1, high enantioselectivity was obtained with **80** and **81** while the catalyst **82** leaded to a modest enantioselectivity.

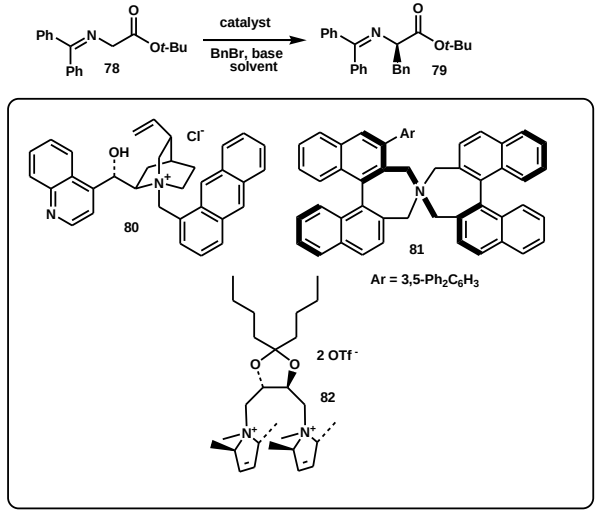

Scheme 4.5: Asymmetric PT alkylation of *N*-(diphenylmethylene)glycine *t*-buthyl ester.

Table 4.1: Catalytic activities of **80-82** in the alkylation of *N*-(diphenylmethylene)glycine *t*-buthyl ester.

Catalyst	Base	Solvent	Temperature (°C)	Time (h)	Yield (%)	*ee* (%)
80 (10 mol %)	KOH	toluene	20	18	63	89
81 (0.05 mol	KOH	toluene	0	3	90	98
82 (5 mol %)	CsOH	DCM	0	1	55	32

Another reaction of great interest in asymmetric PTC is the asymmetric Michael addition. In particular, the first

successful Michael addition in phase-transfer conditions was carried out making use of a chiral crown ether (**85**) in the role of asymmetric catalyst. So, in the presence of **85**, the Michael addition of the β-keto ester **83** to metyl vinyl ketone goes in moderate yield but with excellent enantioselectivity (scheme 4.6).[88]

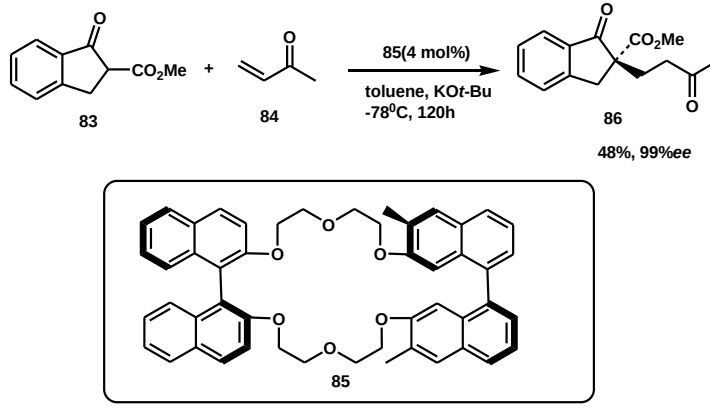

Scheme 4.6: Asymmetric phase-transfer Michael addition catalyzed by a chiral crown ether.

Recently, Makò *et al.* reported the PT epoxidation of *trans*-chalcone analogues making use of a α-D-glucose-based crown ether catalyst (**87**) and a α-D-mannose-based crown ether catalyst (**89**).[91] **87** and **89** are lariat ether catalyst derived from the corresponding monosaccaride. The reaction was performed at

[91] A. Makò, Z. Rapi, G. Keglevich, A. Szöllosky, L. Drahos, L. Hegedus *Tetrahedron,* **2010**, *21*, 919-925.

0°C using *t*-BuOOH as oxidant and employing toluene and 20% aq NaOH solution. Specifically, in presence of the catalyst **87** and with the chalcone **86** it was obtained the enantiomer α*R*-β*S* with an excellent enantioselectivity and a moderate yield (scheme 4.7). On the other hand, the catalyst **89** leaded to the opposite enantiomer α*S*-β*R* with worse enantioselectivity (scheme 4.7).

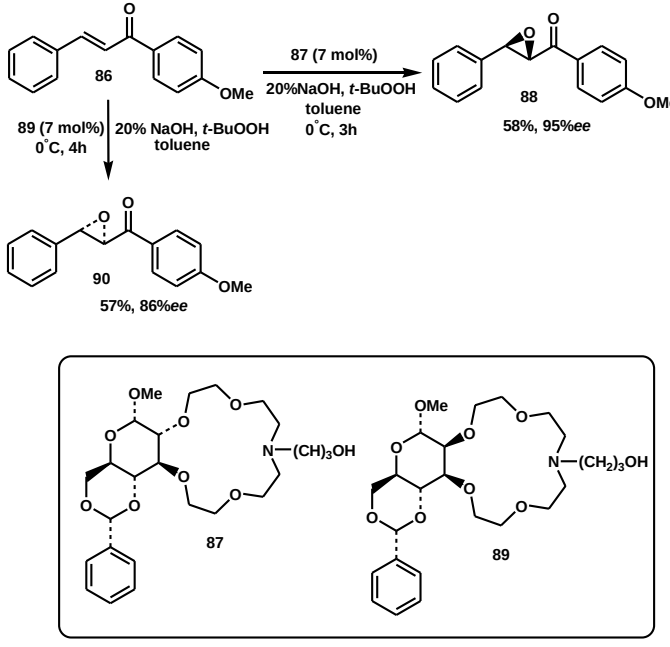

Scheme 4.7: Asymmetric phase-transfer epoxidation of a *trans*-chalcone derivative catalyzed by chiral crown ethers derived from monosaccharides.

4.2 Aims of the work

Cyclopeptoids appear as an ideal platform for the design of new phase-transfer catalysts because of their

versatility of decoration, the high-yield solid phase synthesis, and their attitude to chelate alkali metal ions. In section 1.2.5 the complexation properties towards metal ions and ionophoric activities in the HPTS assay of the *N*-benzyloxyetyl cyclohexapeptoid (**25**, figure 4.1) synthesized by De Riccardis *et al.* has been described.[50] Specifically, the cyclohexapeptoid **25** is characterized by a good affinity to Na^+ and a transmembrane transport selectivity for the same ion.

In spite of the large use of peptides in catalysis, peptoids oligomers of *N*-substituted glycines have been narrowly covered with respect to the catalytic applications and only one example is reported in the literature (see section 1.2.7).[55]

Therefore, we decided to find out the use of cyclopeptoids as novel PT catalysts. In particular, in section 4.3 the binding affinities and catalytic activities of cyclohexapeptoids **43, 47, 71, 91, 92** (figure 4.1) in a liquid-liquid two phase benchmark S_N2 reaction in comparison with classic phase-transfer catalysts have been reported.

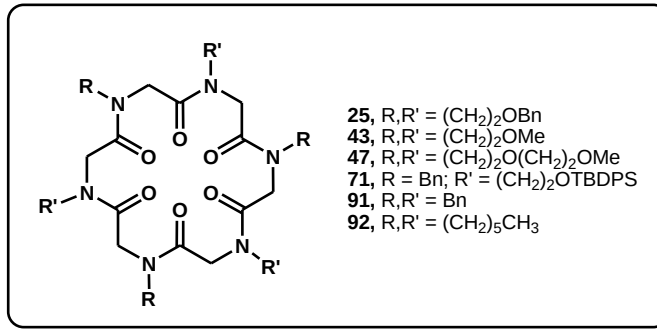

Figure 4.1: Cyclopeptoids (**43, 47, 71, 91, 92**) tested as PT catalysts in a benchmark S_N2 reaction. Cyclopeptoid **25**, synthesized by De Riccardis *et al.*, exhibits a good affinity to sodium ion.

In section 4.4 the catalytic activities of some proline-rich cyclopeptoids (**42, 93-95**, figure 4.2) and of a cyclopeptoid containing valine (**96**, figure 4.2), employed as chiral catalysts in two common asymmetric phase-transfer reactions, have been discussed. Moreover, these results prompted us to investigate the catalytic activities in asymmetric PTC of some structural analogues of *N*-benzyl proline-rich cyclopeptoid **85** (**48** and **97-100**, figure 4.2), affording a promising candidate compound (**48**).

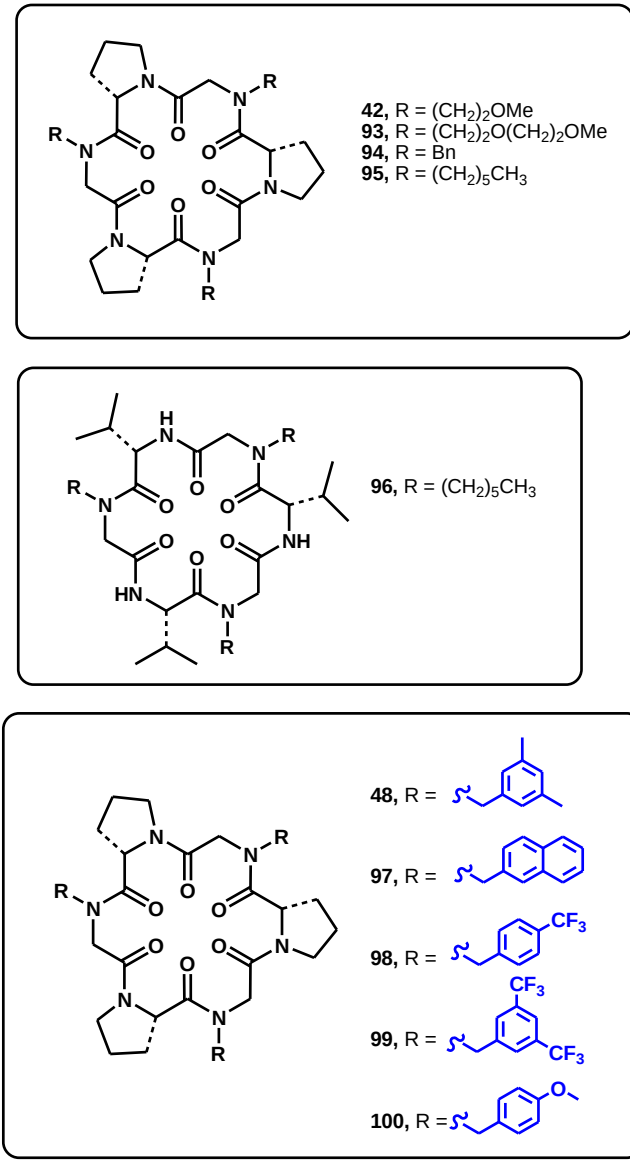

Figure 4.2: Cyclopeptoids examined in the role of asymmetric PT catalysts.

4.3 Cyclopeptoids as PT catalysts in a benchmark S$_N$2 reaction[92]

4.3.1 Design and synthesis of the new catalysts

The purpose was to evaluate the potential of cyclopeptoids as PT catalysts, and, for this reason, we prepared a series of structurally different cyclohexapeptoids (**43, 47, 71, 91, 92**), decorated with various *N*-alkyl side chains, making use of the submonomer approach[34] (figure 4.3) and finally purifying the cycle *via* RP-HPLC. All the amines are commercially available except for the 2-(2-methoxyethoxy)ethanamine (**106**), which was prepared through a rapid two step sequence (scheme 4.4), as well described in the literature.[93] The choice of the side chains was dictated from the intention of providing a good degree of lipophilicity (benzyl and *n*-hexyl appendages) or cation affinity (methoxyethyl and methoxyethoxyethyl pendant groups).

In order to assess the catalytic activity of complexed cyclopeptoids in the phase-transfer reactions in comparison with metal free cyclopeptoids, it was decided to synthesize the sodium hexafluorophosphate adducts **107** and **108** shown in figure 4.4 (from neutral **43** and **91**, respectively).

[92] G. Della Sala, B. Nardone, F. De Riccardis, I. Izzo *Org. Biomol. Chem.* **2013**, *11(5)*, 726-731.
[93] J. R. Harjani, C. Liang, P. G. Jessop *J. Org. Chem.*, **2011**, *76*, 1683–1691.

In figure 4.4 the commercial phase-transfer catalysts, compared with the synthesized cyclopeptoids in this study, are reported.

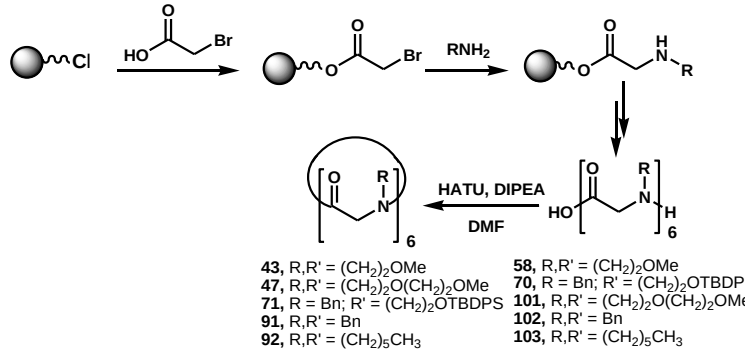

Figure 4.3: Submonomer solid-phase synthesis of **43, 47, 71, 91, 92**.

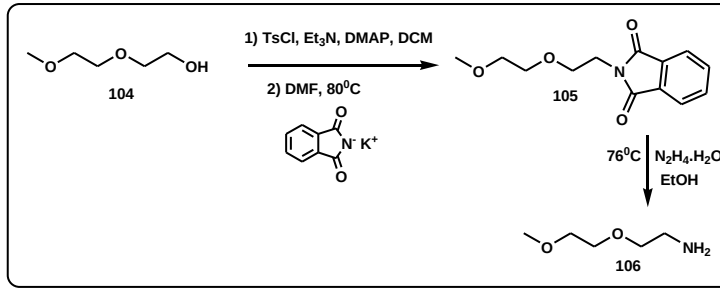

Scheme 4.8: Two step synthesis of 2-(2-methoxyethoxy)ethanamine.

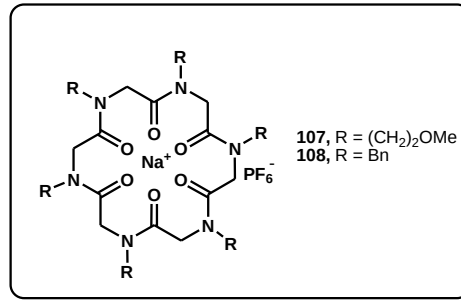

Figure 4.4: Complexed cyclopeptoids.

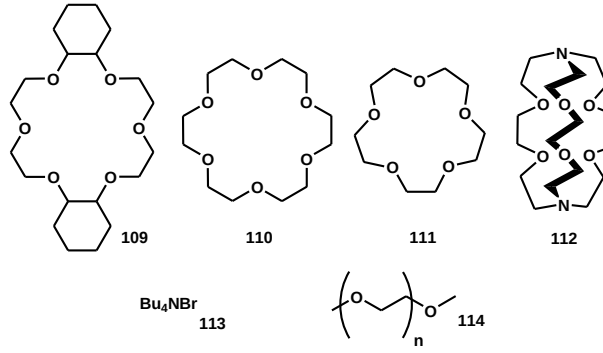

Figure 4.5: Commercial PT catalysts discussed.

4.3.2 Determination of association constants by Cram's method

It is noteworthy to underline that a PT catalyst can not prescind from an efficient metal complexation. Table 4.2 reports the association constants (K_a) together with $-\Delta G^0$ and R_{CHCl_3} values, which were determined for the complexation of **43, 47, 91, 92** to Li^+, Na^+ and K^+ in $H_2O/CHCl_3$ biphasic system according to Cram's method[51], and in comparison with the well-known complexing agents[51] such as dicyclohexyl-18-crown-6 and 15-crown-5 (**109** and **111**,

figure 4.5). Particularly, in Cram's method it is evaluated the ability of a macrocycle to extract picrate salts of a specific cation from bulk water to a chloroformic phase. The results indicate a good degree of selectivity towards Na^+ for 15-crown-5 (**111**) and all the synthesized cyclopeptoids apart from macrocycle **91**, as previously observed for **25**[50] ($K_a \times 10^{-6}$ $[M^{-1}] = 3.3$, see section 1.2.5). Specifically, the macrocycle **47** resulted to be the best complexing agent, showing a K_a value for Na^+ higher than that determined for 15-crown-5 (**111**) and more than six times greater than that calculated for dicyclohexyl-18-crown-6 (**109**). Differently from cyclopeptoids **43, 47, 92** dicyclohexyl-18-crown-6 macrocycle **100** and the other structurally related compounds[51] possess a far more higher association constant with K^+ instead of Na^+.

Table 4.2: Parametres for association between hosts and picrate salts in $CHCl_3$ at 25 °C.

Entry	Host	M^+	R_{CHCl_3} [a]	$K_a \times 10^{-6}$ [M^{-1}]	$-\Delta G^0$ (kcal/mol)
1	**43**	Li^+	0.07	0.27	7.4
		Na^+	0.31	2.5	8.7
		K^+	0.03	0.51	6.4
2	**47**	Li^+	0.38	4.9	9.1
		Na^+	0.55	15	9.8
		K^+	0.48	5.9	9.2
3[b]	**91**	Li^+	0.13	0.63	7.9
		Na^+	0.22	1.2	8.3
		K^+	-	-	-
4	**92**	Li^+	0.24	1.7	8.5
		Na^+	0.32	2.6	8.8
		K^+	0.12	0.31	7.5
5[c]	**109**	Li^+	0.0530	0.192	7.20
		Na^+	0.308	2.34	8.68
		K^+	0.809	200	11.3
6[d]	**111**	Li^+	<0.01	<0.03	-
		Na^+	0.49	8.8	9.5
		K^+	0.10	0.23	7.3

[a] [Guest]/[Host] in $CHCl_3$ layer at equilibrium obtained by direct measurement, or calculated by difference from measurement made on aqueous phase. [b] For compound **91** it was not possible to determine the association constant with the potassium picrate for the formation of a precipitate (probably an insoluble complex with the salt). [c] See reference 51. [d] For compound **111** it was not possible to determine the association with the lithium picrate because the amount of it extracted in organic phase was too low.

4.3.3 *Evaluation of ionophoric activities with the HPTS assay*

The general correlation between the complexing properties of macrocycles towards metal ions and their

ionophoric activities suggested us to evaluate the transport properties through a phospholipid membrane for cyclopeptoids **43, 47, 91, 92**. Experimentally, the ionophoric properties were investigated using the pH-sensitive fluorescent dye HPTS (HPTS = 8-hydroxypyrene-1,3,6-trisulfonic acid, p*K*a = 7.2).[94] This experiment was performed at the University of Trieste, precisely in the laboratory of Prof. Paolo Tecilla.

In this assay the dye is entrapped inside phospholipid vesicles buffered at pH = 7 and, after addition of the ionophore, a pH shock of 0.6 pH units is applied by external addition of NaOH. The suppression of this transmembrane pH-gradient determines basification of the liposome inner water pool which is indicated by an increase of the HPTS fluorescence emission. The basification process may stem from H^+ efflux or OH^- influx and this transmembrane charge translocation must be counterbalanced, determining four possible processes: H^+/Na^+ antiport, OH^-/Cl^- antiport, H^+/Cl^- symport and Na^+/OH^- symport.[50]

The ionophoric activity of the cyclic peptoids under study with respect to sodium ion is reported in figure 4.5. In the presence of NaCl as added salt (figure 4.6), the cyclopeptoids examined are poorly active differently from compound **25**[50] (see section 1.2.5), which in a previous investigation exhibited a good ionophoric activity in the case of sodium

[94] N. Sakai , S. Matile, *J. Phys. Org. Chem.*, **2006**, *19*, 452-460.

ion. Anyway, the scale of ionophoric activity of the cyclopeptoids tested for the sodium ion is: **47>92>91>43**. This scale partially agrees with the Cram data, infact the compound **47** exhibits at the same time the highest K_a and the best ionophoric activity among the cyclopeptoids examined.

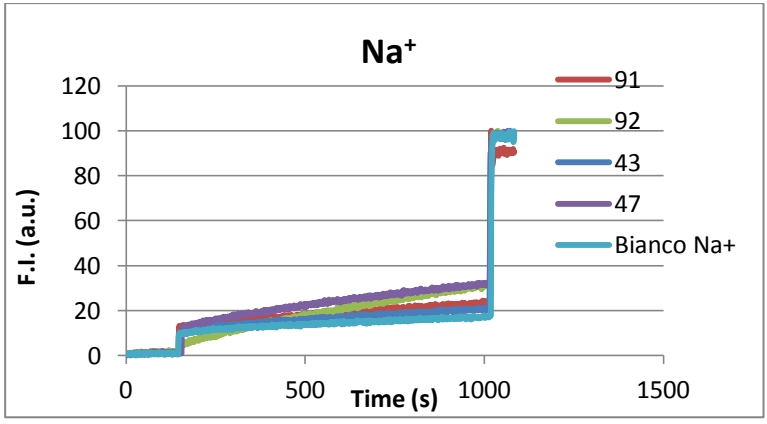

Figure 4.6: Normalized fluorescence change in HPTS emission (FI, λ_{ex} = 460 nm, λ_{em} = 510 nm) as a function of time. The time course of fluorescence was recorded for 200s and then 50 μL of 0.5 M NaOH were rapidly added to 95:5 EYPC/EYPG LUVs (100 nm diameter) loaded with HPTS (0.1 mM HPTS, 0.17 mM total lipid concentration, 25 mM HEPES, 100 mM NaCl, pH 7.0, total volume 3 mL), in the presence of cyclic peptoids **43, 47, 91, 92**. The concentration of the ionophore was 2% with respect to the total concentration of lipids. Maximal changes in dye emission were obtained by final lysis of the liposomes with detergent (40 μL of 5% aqueous Triton® X-100). (HEPES: 4-(2-hydroxyethyl)-1-piperazine ethanesulfonic acid; EYPC: egg yolk phosphatidyl choline; EYPG: egg yolk phosphatidyl glycerol, LUVs = large, unilamellar vesicles).

4.3.4 Catalytic activities and comparison with commercial phase transfer catalysts

With the aim of testing the ability of the cyclopeptoids in the role of PT catalysts we chose the substitution reaction of *p*-nitrobenzyl bromide, in a liquid-liquid two phase system, using sodium or potassium thiocyanate as nucleophilic species (table 4.3). These phase-transfer reactions follow pseudo-first order kinetics. In addition, the observed rates of the reaction are proportional to the amount of the catalyst and the process occurs in the organic layer.[95]

All reactions were performed in a $CHCl_3/H_2O$ two-phase system, with 5 mol% of catalyst. The reactions were monitored via TLC to evaluate the time necessary for total conversion. All the reactions were stopped within 24h and the conversion % was measured by ^{1}H-NMR. Table 4.3 illustrates the activities of the synthesized cyclohexapeptoids compared to some commercially available PT catalysts, such as dicyclohexyl-18-crown-6 (**109**), 18-crown-6 (**110**), 15-crown-5 (**111**), crypt-222 (**112**), tetrabutylammonium bromide (**113**), poly(ethyleneglycol) (average M_n 300, **114**) (figure 4.4).

All compounds (**43, 47, 71, 91, 92, 107** and **108**, entries 2-8) catalyzed the substitution reaction, as it is possible to infer from the comparison with the uncatalyzed reaction (entry 1).

[95] C. M. Starks, R. M. Oweres, *J. Am. Chem. Soc.* **1973**, *5*, 3613-3617.

4 CYCLOPEPTOIDS AS PHASE-TRANSFER CATALYSTS

It is remarkable to point out that whereas all the commercially available PT catalysts (**109-114**) demonstrated to be more efficient in the presence of potassium thiocyanate, with almost all the new cyclohexapeptoids the reaction is quicker with sodium thiocyanate. Cyclopeptoid **91** represents an exception, both in the free or complexed form (entries 5 and 8, respectively). Interestingly, the catalysts in the complexed form (**107** and **108**, entries 7 and 8) revealed to be less efficient than those in the free form (**43** and **91**, entries 2 and 5). All the uncomplexed cyclopeptoids proved to be more effective catalysts than the known poly(ethylene glycol) (**114**).

The most active cyclopeptoids (**43, 47, 92**) exhibited activities close to the crown ethers. And, icing on the cake, macrocycle **47**, containing *N*-[2-(2-methoxyethoxy)ethyl] side chains, showed, in the reaction with NaSCN, higher efficiency than crown ethers, and an activity comparable to that observed for cryptand **112**, one of the best amongst the PTC catalysts. A high activity, although lower, was also obtained with KSCN as reagent.

Table 4.3: S_N2 reaction with NaSCN or KSCN catalyzed by cyclopeptoids and common PT catalysts.[a)]

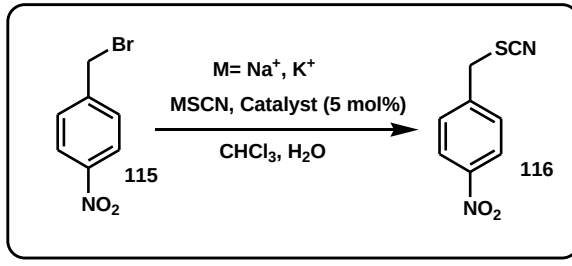

		NaSCN		KSCN	
Entry	Catalyst	time(h)	Conversion(%)	time(h)	Conversion(%)
1	-	24	10	24	5
2	**43**	8	> 99	24	91
3	**47**	2.5	>99	7.5	> 99
4	**71**	12	> 99	24	71
5	**91**	24	95	13	>99
6	**92**	4.5	> 99	24	53
7	**107**	24	55	24	79
8	**108**	24	78	24	30
9	**109**	4.5	> 99	4.5	> 99
10	**110**	24	> 99	7.5	> 99
11	**111**	8	> 99	1	> 99
12	**112**	6.5	> 99	3	> 99
13	**113**	2	> 99	1	> 99
14	**114**	24	81	24	85

[a)] All the reactions were carried out using a 0.25 M solution of *p*-nitrobenzyl bromide (**106**) in $CHCl_3$ (0.4 mL, 0.10 mmol), a 0.75 M aqueous solution of NaSCN or KSCN (0.2 mL, 0.15 mmol) and catalyst (0.005 mmol).

The observed experimental data can be interpreted making the following considerations.

The weak performance of the complexed catalysts **107** and **108** could be ascribed to the low solubility of such compounds in the reaction medium. This observation also stems from the comparison of reactions carried out with the macrocycles **43, 47, 71, 91, 92**. The better solubility for the compounds **43, 47, 71, 83** relative to the products **91**, **107** and **108**, obtained with the introduction of a more lipophilic *N*-alkyl chain, determined reduced reaction times.

Nevertheless, the solubility in chloroform is not the only parameter to be taken into account. The very soluble compound **71**, indeed, proved to be less active than **43, 47, 92** likely because of the presence of the sterically hindered silyl group. It is more difficult to rationalize the data collected for the *N*-benzyl glycine hexacyclopeptoid both in free and complexed form (**91** and **108**), which showed an opposite trend to that of the other macrocycles. In fact, shorter reaction times and a higher conversion, were observed using potassium thiocyanate. Unfortunately, for the macrocycle **91** was not possible to determine the K_a for K^+, in order to compare it with those estimated for the other ions. Anyhow, K_a values for Na^+ was lower than that of the other macrocycles, and that might explain the poorer activity of the discussed catalyst. Ultimately, the data determined by Cram's method agree with the results observed in catalysis since the

compound **47,** which shows the greatest K_a values, resulted to be the best catalyst.

4.4 Cyclopeptoids in the role of asymmetric PT catalyst

4.4.1 Design and synthesis of the first generation catalysts

We decided to evaluate the catalytic activity in phase-transfer conditions of some chiral cyclopeptoids: the prolinated cyclohexapeptoids **42, 93-95** and a cyclohexapeptoid containing residues of L-valine (**96**). The choice of incorporating L-proline in the peptoid backbone was mainly dictated by the ability to complex sodium exhibited by the proline-rich cyclopeptoid **42**, as illustrated in section 2.3.4. On the other hand, L-valine was introduced in order to establish the effect of an hydrogen-bond donor secondary nitrogen on the asymmetric induction. Futhermore, the side chains of cyclopeptoids **42, 93-96** are exactly the same of cyclopeptoids earlier tested in a benchmark S_N2 reaction (**43, 47, 91, 92**).

Two well-known PT asymmetric reactions were considered: i) the enantioselective epoxidation of *trans*-chalcone (scheme 4.9), which represents an useful synthetic route to prepare chiral epoxides; ii) the alkylation of *N*-(diphenylmethylene)glycine *t*-buthyl ester (scheme 4.5), which allows to obtain the iminic precursor of an α-aminoacid. These reactions are often reported in literature in

order to evaluate the activities of new asymmetric PTC catalysts.[88]

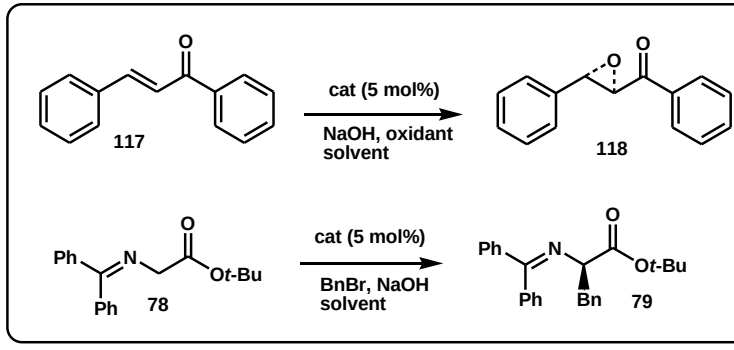

Scheme 4.9: Asymmetric PT reactions examined.

The synthesis of the cyclopeptoids tested was performed making use of a solid-phase mixed approach (submonomer[34] and monomer approach) (scheme 4.10) with the only exception of **96**. Specifically, compound **96** containing L-valine was prepared with a modified mixed approach[96] (scheme 4.11) due to side reactions of alklylation undergone by the primary nitrogen of L-valine, which were observed in previous attempts of synthesis carried out with the general mixed approach. Usually, during submonomer synthesis, the alkylation side reaction is not observed because acylation of an N-terminal secondary amine by means of bromoacetic acid is not reversible and is 1000 times faster than alkylation. On the other hand, acylation of an N-terminal

[96] T. S. Burkoth, A. T. Fafarman, D. H. Charych, M. D. Connolly, R. N. Zuckermann *J. Am. Chem. Soc.*, **2003**, *125*, 8841-8845.

primary amine (L-valine) is reversible and, as a consequence, the alkylation reaction can occur leading to the accumulation of alkylation side products during the acylation step. So, in order to avoid the formation of alkylation byproducts, according to the Zuckermann protocol[96], chloroacetic acid was used in place of bromoacetic acid. In this way, the alkylation is less favoured because chloride is a worse leaving group than bromide. In addition, the displacement step must be conducted in presence of KI to convert the less reactive chloride species in iodide. Zuckermann made use of this protocol[96] for the submonomer synthesis of peptoid oligomers containing aromatic amine submonomers such as aniline and 5-amino-2-methoxypyridine.

With respect to the synthesis of **96** (scheme 4.11), the general mixed approach was used until the dipeptide unit and further the submonomer method was accomplished using chloroacetic acid at 45°C for the acetylation step and a solution of KI and the required amine in DMF at 35°C for the following displacement step.

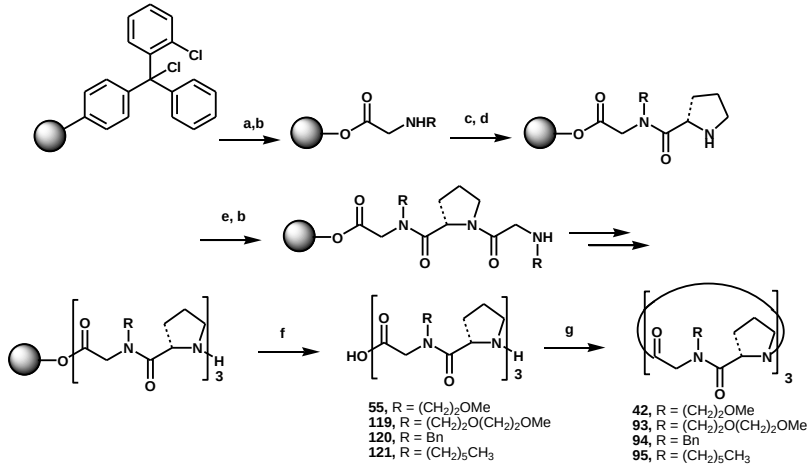

Scheme 4.10: Solid-phase mixed approach for the synthesis of **42, 93-95**. Reagents and conditions: (a) bromoacetic acid, DIPEA, DCM; (b) RNH_2, DMF; (c) *N*-Fmoc-L-proline, HATU, DIPEA, DMF; (d) Piperidine-DMF (1:5); (e) bromoacetic acid, DIC, DMF; (f) HFIP-DCM (1:5); (g) HATU, DIPEA, DMF.

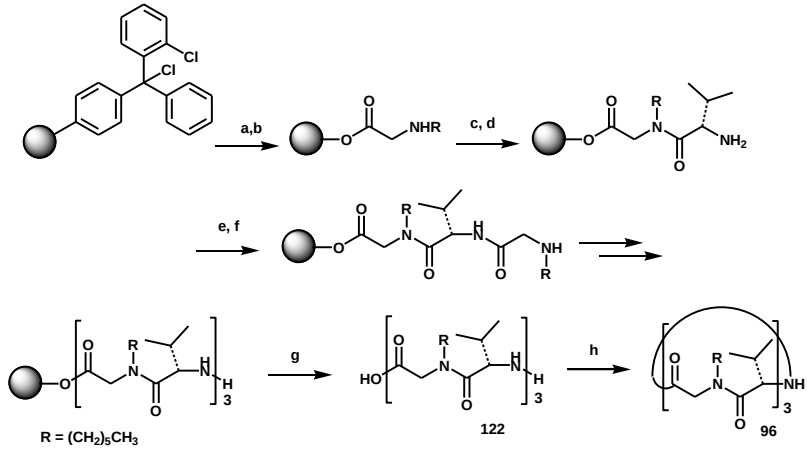

Scheme 4.11: Solid-phase mixed approach for the synthesis of **96**. Reagents and conditions: (a) bromoacetic acid, DIPEA, DCM; (b) hexilamine, DMF; (c) *N*-Fmoc-L-valine, HATU, DIPEA, DMF; (d) Piperidine-DMF (1:5); (e) chloroacetic acid, DIC, DMF, 45°C; (f) hexanamine, KI, DMF, 35°C; (g) HFIP-DCM (1:5), (h) HATU, DIPEA, DMF.

4.4.2 Catalytic activities in the enantioselective epoxidation

Cyclopeptoids **42, 93-95** were initially tested as chiral PT catalyst in the enantioselective epoxidation of *trans*-chalcone (table 4.4). The reactions were monitored *via* TLC in order to evaluate the time required for total conversion. The slow reactions (entry 2, 4, 8, 9) were stopped within 24h (with the only exception of entry 8) and the percentage of conversion was measured by ^{1}H-NMR. The crude was purified by flash cromatography. It was employed as reaction mixture both a liquid-liquid system with a 50% water solution of NaOH and a solid-liquid system with NaOH(s). The reactions were conducted at 0°C with the only exception of a test performed at room temperature with worse results. The first solvent used was DCM in order to properly solubilize the catalyst and, as a result of the very low enantioselectivity obtained with this solvent (entry 2), toluene was employed. It was also tried Bu_2O to evaluate the effect of the solvent on the asymmetric induction, but with this solvent a racemic mixture was obtained (entry 7). *t*-BuOOH was employed as oxidant agent and only a test was performed with NaOCl, which demonstrated to be less efficient.

In general, the only noteworthy enantioselectivity, although low, was the 14% *ee* obtained with the catalyst **94** (entry 6). Nevertheless, the *ee* % measured are clearly worse than those reported in literature for other PT asymmetric catalysts. So, the cyclopeptoids examined revealed to be poor

active chiral catalyst in the asymmetric PT reaction considered. In the epoxidation reaction it is observed the formation of the enantiomer α*S*β*R*, as it is possible to infer from the comparison with the retention times reported in literature.[97]

Table 4.4: Enantioselective epoxidation of *trans*-chalcone catalyzed by cyclopeptoids **42, 93-95**.[a)]

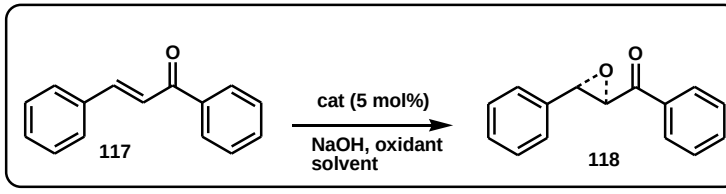

Entry	Catalyst	Base	Solvent	Time (h)	Yield (%)	*ee* (%)
1	**42**	NaOH aq.	toluene	3	78	10
2	**93**	NaOH aq.	toluene	23	81	4
3	**94**	NaOH (s)	DCM	4	83	rac.
4	**94**	NaOH aq.	DCM	26	54	5
5	**94**	NaOH (s)	toluene	2	81	rac.
6	**94**	NaOH aq.	toluene	3.5	83	14
7	**94**	NaOH aq.	Bu_2O	3	80	rac.
8[b)]	**94**	-	toluene	100	78	10
9	**95**	NaOH aq.	toluene	25	79	8

[a)] The reactions were carried out at 0°C using a 0.1 M solution of *trans*-chalcone (**117**) in the organic solvent (0.8 mL), 1.2 eq of *t*-BuOOH (5.5 M in decane), a 50% aqueous solution of NaOH or 3eq of NaOH(s) and catalyst (0.005 mmol). [b)] The reaction was carried out at room temperature with a 11% aqueous solution of NaOCl as oxidant.

[97] M. Yoo, D. Kim, M. W. Ha, S. Jew, H. Park *Tetrahedron Letters*, **2010**, *51*, 5601-5603.

4.4.3 Catalytic activities in the enantioselective alkylation

Cyclopeptoids **42, 93-95** were further employed in a second asymmetric reaction, namely the enantioselective alkylation of *N*-(diphenylmethylene)glycine *t*-buthyl ester (table 4.5). In this case also the compound **96** containing L-valine was tested. The reactions were monitored *via* TLC and stopped after 24h, with the only exception of entry 1. The percentage of conversion was measured by ^{1}H-NMR. The crude was purified by flash cromatography. It was employed as reaction mixture both a liquid-liquid system with a 50% water solution of NaOH and a solid-liquid system with NaOH(s). The reactions were conducted at 0°C and at room temperature in order to evaluate the effect of temperature on the asymmetric induction. The unique solvent used was toluene, which resulted to be the best solvent in the previous study. Compound **94** was first tested as catalyst in this reaction.

As illustrated in table 4.5, in presence of oxygen it was observed a low *ee* (14%) and a low yield due to the decomposition of the substrate **78**. Specifically, **78** in aerobic atmosphere converts into benzophenone, as demonstrated by ^{1}H NMR. From the comparison with the retention times reported in literature, it is deduced the formation of the enantiomer *R*.[98] Analogous decompositions of glycine imines

[98] T. Ooi, M. Kameda, K. Maruoka *J.Am. Chem. Soc.* , **1999**, *121*, 6519-6520.

in presence of oxygen were reported and Maruoka solved the problem operating in inert atmosphere.[99] As a consequence, the reaction was firstly performed under nitrogen registering a better *ee* equal to 36% for **94** (entry 6) and a significative reduction of the benzophenone formation. Afterwards, to prevent the decomposition, the deoxygenation of reagents and solvents was carried out. In this way the enantioselectivity was increased up to 38% (entry 7) and the side reaction of decomposition was effectively inhibited.

From the results illustrated in table 4.5 it is possible to infer that the compounds **42, 93, 95, 96** are characterized by a worse catalytic activity with respect to **94**, both in terms of yield and *ee*. On the other hand, cyclopeptoid **93** leads to a higher yield in relation to **94**, but the *ee* is clearly lower. So, the methoxyethoxyethyl side chains of **93** determine a positive effect on the reaction rate in a similar manner to what happened in the benchmark S_N2 reaction studied before (section 4.3.4).

In conclusion, cyclopeptoid **94** with L-proline and benzyl chains in alternate positions resulted to be the best catalyst in terms of asymmetric induction with a 38% *ee* (table 4.5).

[99] T. Ohshima, T. Shibuguchi, Y. Fukuta, M. Shibasaki *Tetrahedron*, **2004**, *60*, 7743-7754.

Table 4.5: Enantioselective alkylation of *N*-(diphenylmethylene)glycine *t*-buthyl ester catalyzed by cyclopeptoids **42, 93-96**.[a)]

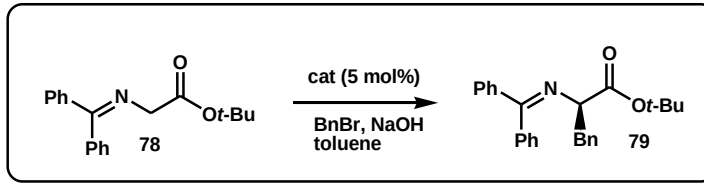

Entry	Catalyst	Time (h)	Yield (%)	*ee*(%)
1[d)]	**42**	44	7	rac.
2[d)]	**93**	21	66	10
3[b)]	**94**	23	29	14
4[c)]	**94**	25	28	rac.
5	**94**	20	36	29
6[d)]	**94**	23	39	36
7[e)]	**94**	19	54	38
8[e)]	**95**	21	36	10
9[e)]	**96**	18	11	8

[a)] The reactions were carried out at 0°C using a 0.1 M solution of *N*-(diphenylmethylene)glycine *t*-buthyl ester (**78**) in toluene (0.8 mL), 1.2 eq of BnBr, a 50% aqueous solution of NaOH or 3eq of NaOH(s) and catalyst (0.005 mmol).

[b)] The reaction was carried out at room temperature.

[c)] The reaction was carried out at room temperature with NaOH(s).

[d)] The reaction was conducted under nitrogen atmosphere.

[e)] Reagents and solvents have been deoxygenated.

4.4.4 Catalytic activities in the enantioselective alkylation: second generation catalysts

On the wake of the promising result obtained with the catalyst **94**, we prepared some structural analogues of **94** (**48**

and **97-100**), containing variously functionalized aromatic side chains. Particularly, the substituents on the aromatic rings present different stereoelectronic features so that it was possible to evaluate the effect on the asymmetric induction. The synthesis of the cyclopeptoids **48, 97-100** was performed making use of a solid-phase mixed approach (submonomer[34] and monomer approach) (scheme 4.12).

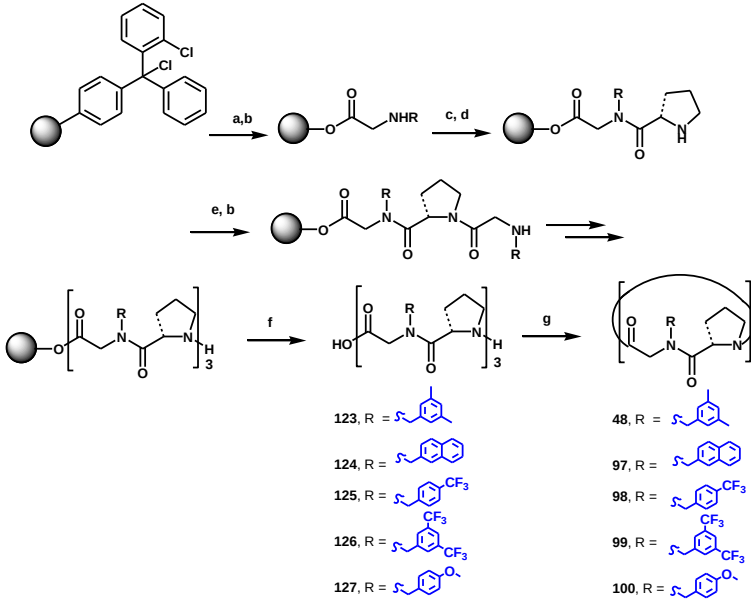

Scheme 4.12: Solid-phase mixed approach for the synthesis of **48, 97-100**. Reagents and conditions: (a) bromoacetic acid, DIPEA, DCM; (b) RNH_2, DMF; (c) *N*-Fmoc-L-Proline, HATU, DIPEA, DMF; (d) Piperidine-DMF (1:5); (e) bromoacetic acid, DIC, DMF; (f) HFIP-DCM (1:5); (g) HATU, DIPEA, DMF.

The novel catalysts were tested in the same asymmetric alkylation reaction in which the first generation catalysts were

employed (table 4.6). The reactions were carried out identically to the best conditions (entry 7, table 4.5).

Observing the results in table 4.6, it is possible to make the following considerations. With the compound **97** it was achieved an higher *ee* and a lower yield with respect to the reaction catalyzed by **94**, reasonably due to the increased steric hindrance of the naphthyl group and to the presence of a more large aromatic system. The electron-withdrawing group $–CF_3$ of **98** exercises a negative effect both on the reaction rate and the *ee*. With two electron-withdrawing groups $–CF_3$ (compound **99**) the reaction rate is higher, but the enantioselectivity is scarce.

The electron-donating group –OMe of **100** leads to low reaction rates and the *ee* is comparable with that obtained with **97**. The two electron-donating groups –Me of **48** play a favourable effect in the asymmetric induction, resulting in an higher *ee* in relation to **97** (66% *ee*).

Table 4.6: Enantioselective alkylation of *N*-(diphenylmethylene)glycine *t*-buthyl ester catalyzed by cyclopeptoids **48** and **97-100**, in comparison with **94**.[a)]

Entry	Catalyst	Time (h)	Yield (%)	*ee* (%)
1	**94**	19	54	38
2	**48**	20	38	66
3	**97**	18	12	50
4	**98**	18	7	30
5[b)]	**98**	20	30	10
6	**99**	19	65	28
7	**100**	18	8	46

[a)] The reactions were carried out at 0°C using a 0.1 M solution of *N*-(diphenylmethylene)glycine *t*-buthyl ester (**78**) in toluene (0.8 mL), 1.2 eq of BnBr, a 50% aqueous solution of NaOH or 3eq of NaOH(s) and catalyst (0.005 mmol). Reagents and solvents were deoxygenated.
[b)] The reaction was performed at room temperature.

Finally, a screening of the reaction conditions was conducted making use of the best catalyst (**48**) in order to improve the enantioselectivity. It is a brief study in which a few experimental parameters were modified. Specifically, in table 4.7 are reported the reactions conducted with different solvents (DCM, $CHCl_3$, mesitylene, *o*-xylene, *m*-xylene) and employing an aqueous solution of NaOH with concentration of 50% and 33%.

It is possible to deduce from the results the following information. First of all, both the yield and the *ee* get worse employing a 33% aqueous solution of NaOH. Futhermore, the enantioselectivity in all the solvents used is by far lower

than that obtained in toluene. Specifically, DCM and $CHCl_3$ determine a strong decrease of the *ee*. In addition, the yield with DCM is the same of that in toluene and with $CHCl_3$ is lower. With respect to the aromatic solvents proved, in mesitylene the reaction resulted to be very rapid (yield = 68%) but a racemic mixture is formed. Futhermore, with *o*-xylene the yield is moderate (51%) but the *ee* is scarce. In the case of *m*-xylene both the yield and the *ee* are low.

Table 4.7: Enantioselective alkylation of *N*-(diphenylmethylene)glycine *t*-buthyl ester catalyzed by cyclopeptoid **48**. Screening of the reaction conditions.[a)]

Entry	Solvent	Time (h)	Yield (%)	*ee* (%)
1	toluene	20	38	66
2[b)]	toluene	20	4	22
3[b)]	toluene	44	10	14
4	DCM	20	38	8
5	$CHCl_3$	18	14	8
6	mesitylene	20	68	rac.
7	*o*-xylene	22	51	16
8	*m*-xylene	22	12	2

[a)] The reactions were carried out at 0°C using a 0.1 M solution of *N*-(diphenylmethylene)glycine *t*-buthyl ester (**78**) in the organic solvent (0.8 mL), 1.2 eq of BnBr, a 50% aqueous solution of NaOH or 3eq of NaOH(s) and catalyst (0.005 mmol). Reagents and solvents were deoxygenated.
[b)] 30% aqueous solution of NaOH was employed.

4.5 Conclusions

In the first part of this chapter, the binding affinities and the catalytic activities of some cyclopeptoids with different side chains (**43, 47, 71, 91, 92**) in the liquid-liquid two phase nucleophilic substitution reaction of *p*-nitrobenzyl bromide with thiocyanate salts and in comparison with classic phase-transfer catalysts were reported. Later, the catalytic activities of some proline-rich cyclopeptoids (**42, 48, 93-95, 97-100**) and of a cyclopeptoid containing valine (**96**), employed as chiral catalysts in two common asymmetric phase-transfer reactions, were described.

With respect to the first subject, compound **47** with *N*-[2-(2-methoxyethoxy)ethyl] side chains showed K_a values for Na^+ greater than that reported for the efficient complexing agents dicyclohexyl-18-crown-6 (**109**) and 15-crown-5 (**111**), and, in agreement with Cram data, the best ionophoric activity towards Na^+ among the cyclopeptoids tested in the HPTS assay. More interestingly, **47** exhibited high catalytic activity in the reaction with NaSCN, comparable to that evaluated for cryptand **112** and higher than those displayed by commonly used crown ethers and the tetrabutylammonium bromide. A good activity was also achieved in the reaction with the KSCN. This is the first example of the use of cyclopeptoids in PTC.

Regarding the challenging studies in PT asymmetric catalysis, the proline-rich cyclopeptoid **94** containing benzyl

side chains resulted to be the best catalyst in terms of enantioselectivity (38% *ee*) among the first generation chiral catalysts (**42, 93-96**) tested in the enantioselective alkylation of *N*- diphenylmethylene)glycine *t*-buthyl ester. On the wake of the promising result, some structural analogues of **94** (**48, 97-100**) were prepared and used as second-generation chiral PT catalyst in the aforementioned reaction. To our delight, the proline-rich cyclopeptoid **48**, containing a 3,5-dimethyl benzylamine side chain, revealed to be the most active asymmetric PT catalyst proved with a 66% *ee* at 0°C in toluene and employing a 50% NaOH solution. The moderate enantioselectivity obtained with **48** represents an interesting result in the vast aerea of asymmetric PT catalysis considering that cyclopeptoids constitute a totally new class of chiral phase-transfer catalysts with respect to the well-known cinchona alkaloids, whose great potential mainly derives from modulability of their backbone. Finally, this work opens the doors for a future employment of more efficient cyclopeptoids in various asymmetric PT reactions.

4.6 Experimental section[83]

4.6.1 Solid-phase synthesis

Submonomer solid-phase synthesis of linear precursors 101-103

Linear precursors **101-103** were synthesized using a submonomer solid-phase approach. In a typical synthesis 0.60

g of 2-chlorotrityl chloride resin (2,α-dichlorobenzhydryl-polystyrene crosslinked with 1% DVB; 100–200 mesh; 1.3 mmol/g) was swelled in dry DCM (6 mL) for 45 min and washed twice with dry DMF (6 mL). The first submonomer was attached onto the resin by adding bromoacetic acid (173 mg, 1.25 mmol) in dry DCM (6 mL) and DIPEA (680 μL, 3.9 mmol) on a shaker platform for 60 min at room temperature, followed by washing with dry DCM (6 mL) and then with DMF (3 × 6 mL). To the bromoacetylated resin was added a DMF solution of the desired amine (1 M, 6 mL). All the amines are commercially available except for the methoxyethoxyethyl amine, which was prepared through a rapid two step sequence, as described in section 4.6.5. The mixture was left on a shaker platform for 30 min at room temperature, then the resin was washed with DMF (3 × 3 mL). Subsequent bromoacetylation reactions were accomplished by reacting the aminated oligomer with a solution of bromoacetic acid (1.08 g, 7.80 mmol) in DMF (6 mL) and of DIC (1.3 mL, 8.40 mmol) for 40 min at room temperature. The filtered resin was washed with DMF (3 × 6 mL) and treated again with the amine under the same conditions reported above. This cycle of reactions was iterated until the target oligomer was obtained. The cleavage was performed by treating twice the resin, previously washed with DCM (3 × 6 mL), with a solution of HFIP in DCM (20% v/v, 8 mL) on a shaker platform at room temperature for 30 min and 5 min,

respectively. The resin was then filtered away and the combined filtrates were concentrated in vacuo. The final products were dissolved in 50% acetonitrile in
HPLC grade water and analysed by RP-HPLC. The linear oligomers were subjected to the cyclization reaction without further purification with the exception of **97** which was purified by semipreparative RP-HPLC.

✔ *Compound **101***

Yield: 69% (purified by RP-HPLC).

ES-MS: 973.5 *m/z* [M + H^+].

HPLC: t_R: 7.8 min; conditions: 25 → 100% B in 30 min (A, 0.1% TFA in water, B, 0.1% TFA in acetonitrile); flow: 2 mL min^{-1}, 220 nm.

✔ *Compound **102***

Purity: >95%.

Yield: 71% (crude residue).

ES-MS: 902.1 *m/z* [M + H^+].

HPLC: t_R: 16.0 min; conditions: 5 → 100% B in 30 min (A, 0.1% TFA in water, B, 0.1% TFA in acetonitrile); flow: 1 mL min^{-1}, 220 nm.

✔ *Compound **103***

Purity: >95%.

Yield: 61% (crude residue).

ES-MS: 865.9 *m/z* [M + H^+].

HPLC: t_R: 20.3 min; conditions: 5 → 100% B in 30 min (A, 0.1% TFA in water, B, 0.1% TFA in acetonitrile); flow: 1 mL min^{-1}, 220 nm.

Mixed monomer/submonomer solid-phase synthesis of linear precursors 55 *and* 119-127

Linear precursors **55**, **119-127** were synthesized by alternating submonomer solid-phase method using standard manual Fmoc solid-phase peptide synthesis protocols. Typically 0.40 g of 2-chlorotrityl chloride resin (2,α-dichlorobenzhydryl-polystyrene crosslinked with 1% DVB; 100-200 mesh; 1.20 mmol/g) was swelled in dry DCM (4 mL) for 45 min and washed twice in dry DCM (3 mL). To the resin bromoacetic acid (107 mg, 0.77 mmol) and DIPEA (418 μL, 2.4 mmol) in dry DCM (4 mL) were added on a shaker platform for 40 min at room temperature, washes with dry DCM (3 × 4 mL) and then with DMF (3 × 4 mL) followed. To the bromoacetylated resin metoxyethylamine (413 μl, 4.80 mmol) in dry DMF (4 mL), was added. The mixture was left on a shaker platform for 40 min at room temperature, then the resin was washed with DMF (3 × 4 mL). The resin was incubated with a solution of *N*-Fmoc-L-proline (4.85 mg, 1.44 mmol), HATU (529 mmol, 1.39 mmol), DIPEA (333 μl) in dry DMF (4 mL) on a shaker platform for 1 h, followed by extensive washes with DMF (3 × 4 mL), DCM (3 × 4 mL) and DMF (3 × 4 mL). Chloranil test was performed and once the coupling was complete the Fmoc group was deprotected with 20%

piperidine/DMF (v/v, 3 mL) on a shaker platform for 3 min and 7 min respectively, followed by extensive washes with DMF (3 × 3 mL), DCM (3 × 3 mL) and DMF (3 × 3 mL). The yields of loading step and of the following coupling steps were evaluated interpolating the absorptions of dibenzofulvene-piperidine adduct (λ_{max} = 301 nm, ε = 7800 M^{-1} cm^{-1}), obtained in Fmoc deprotection step (the average coupling yield was 63-70 %). Subsequent bromoacetylation reactions were accomplished by reacting the oligomer with a solution of bromoacetic acid (690 mg, 4.8 mmol) and DIC (817 μL, 5.28 mmol) in DMF (4 mL) on a shaker platform 40 min at room temperature. Subsequent *N*-Fmoc-L-proline addition and Fmoc deprotection steps were performed as described above, addition of the proline at the fourth and sixth position required longer reaction time (3 h) for all the linear peptoids and two treatments only in the case of **55**. The synthesis proceeded until the desired hexaoligomer was obtained. The oligomer-resin was cleaved in 4 mL of 20% HFIP in DCM (v/v). The cleavage was performed on a shaker platform for 30 min at room temperature the resin was then filtered away. The resin was treated again with 4 mL of 20% HFIP in DCM (v/v) for 5 min, washed twice with DCM (3 mL), filtered away and the combined filtrates were concentrated in vacuo. The final products were dissolved in 50% ACN in HPLC grade water and analysed by RP-HPLC and ESI mass spectrometry. The linear compounds were subjected to the cyclization without further purification.

✔ *Compound* **55**[100]

✔ *Compound* **119**

Purity: >60%.

Yield: 60% (crude residue).

ES-MS: 405.4 *m/2z* [M + H^++Na^+].

HPLC: t_R: 11.7 min; conditions: 5 → 100% B in 30 min (A, 0.1% TFA in water, B, 0.1% TFA in acetonitrile); flow: 1 mL min^{-1}, 220 nm.

✔ *Compound* **120**

Purity: >80%.

Yield: 34% (crude residue).

ES-MS: 751.8 *m/z* [M + H^+].

HPLC: t_R: 13.1 min; conditions: 5 → 100% B in 30 min (A, 0.1% TFA in water, B, 0.1% TFA in acetonitrile); flow: 1 mL min^{-1}, 220 nm.

✔ *Compound* **121**

Purity: >88%.

Yield: 63% (crude residue).

ES-MS: 733.4 *m/z* [M + H^+].

HPLC: t_R: 15.9 min; conditions: 5 → 100% B in 30 min (A, 0.1% TFA in water, B, 0.1% TFA in acetonitrile); flow: 1 mL min^{-1}, 220 nm.

✔ *Compound* **122**

Purity: >83%.

Yield: 52% (crude residue).

[100] See section 2.6.2.

ES-MS: 739.3 *m/z* [M + H^+].

HPLC: t_R: 15.9 min; conditions: 5 → 100% B in 30 min (A, 0.1% TFA in water, B, 0.1% TFA in acetonitrile); flow: 1 mL min^{-1}, 220 nm.

✔ *Compound* **123**

Purity: >70%.

Yield: 39% (crude residue).

ES-MS: 835.0 *m/z* [M + H^+].

HPLC: t_R: 15.3 min; conditions: 5 → 100% B in 30 min (A, 0.1% TFA in water, B, 0.1% TFA in acetonitrile); flow: 1 mL min^{-1}, 220 nm.

✔ *Compound* **124**

Purity: >70%.

Yield: 42% (crude residue).

ES-MS: 901.0 *m/z* [M + H^+].

HPLC: t_R: 15.6 min; conditions: 5 → 100% B in 30 min (A, 0.1% TFA in water, B, 0.1% TFA in acetonitrile); flow: 1 mL min^{-1}, 220 nm.

✔ *Compound* **125**

Purity: >82%.

Yield: 48% (crude residue).

ES-MS: 955.0 *m/z* [M + H^+].

HPLC: t_R: 15.4 min; conditions: 5 → 100% B in 30 min (A, 0.1% TFA in water, B, 0.1% TFA in acetonitrile); flow: 1 mL min^{-1}, 220 nm.

✔ *Compound* **126**

Purity: 78%.

Yield: 55% (crude residue).

ES-MS: 1159.0 *m/z* [M + H^+].

HPLC: t_R: 17.2 min; conditions: 5 → 100% B in 30 min (A, 0.1% TFA in water, B, 0.1% TFA in acetonitrile); flow: 1 mL min^{-1}, 220 nm.

✔ *Compound* **127**

Purity: >85%.

Yield: 38% (crude residue).

ES-MS: 841.0 *m/z* [M + H^+].

HPLC: t_R: 12.9 min; conditions: 5 → 100% B in 30 min (A, 0.1% TFA in water, B, 0.1% TFA in acetonitrile); flow: 1 mL min^{-1}, 220 nm.

4.6.2 General procedure for high dilution cyclization

Synthesis of 47, 48 *and* 91-100

To a stirred solution of HATU (116 mg, 0.31 mmol), DIPEA (0.082 mL, 0.47 mmol) in dry DMF (20 mL) at room temperature, a solution of the linear compounds (crude **101-103**, **119-127**) (0.08 mmol) in dry DMF (20 mL) was added by syringe pump in 6 h. After 12 h the resulting mixture was concentrated in vacuo, diluted with DCM (20 mL) and washed with 1 M HCl (7 mL × 3) was added. The mixture was extracted with DCM (10 mL × 2) and the combined organic phases were washed three times with water (10 mL),

dried ($MgSO_4$) and concentrated in vacuo. The crude residues from the HATU-induced cyclizations were purified by HPLC. Compounds **91**, **92** were purified by precipitation in CH_3CN/H_2O 1:1 (v/v).

✔ *Compound* **47**

Yield: 42%. The crude residue was purified by RP-HPLC on a C_{18} reversed-phase semi-preparative column (t_R: 15.4 min.; conditions: 25 → 100% B in 50 min (A: 0.1% TFA in water, B: 0.1% TFA in acetonitrile), flow: 2.0 mL min^{-1}, 220 nm).

ES-MS: 955.5 *m/z* [M + H^+].

^{1}H-NMR: (400 MHz, $CDCl_3$, mixture of rotamers) δ: 4.94–3.32 (42 H, m, $COCH_2N$, OCH_2CH_2O, OCH_2CH_2O, NCH_2CH_2O, NCH_2CH_2O, OCH_3).

^{13}C-NMR: (100 MHz, $CDCl_3$, mixture of rotamers) δ: 172.6, 172.3, 171.3, 170.9, 170.7, 170.5, 170.1, 169.7, 169.4, 169.0, 168.9, 168.4, 168.3, 168.0, 71.8, 71.8, 70.4, 70.3, 70.2, 70.1, 69.8, 69.7, 69.4, 69.2, 69.0, 68.8, 68.7, 68.5, 68.0, 67.8, 67.4, 58.9, 52.4, 51.0, 50.3, 49.5, 49.3, 48.8, 48.1, 47.3, 46.3.

✔ *Compound* **48**

Yield: 43%. The crude residue was purified by RP-HPLC on a C_{18} reversed-phase semi-preparative column (t_R: 17.2 min.; conditions: 25 → 100% B in 30 min (A: 0.1% TFA in water, B: 0.1% TFA in acetonitrile), flow: 2.0 mL min^{-1}, 220 nm).

ES-MS: 817.6 *m/z* [M + H^+].

^{1}H-NMR: (400 MHz, $CDCl_3$, mixture of rotamers) δ: 7.26-6.72 (9H, m, Ar*H*), 5.75-3.22 (27H, m, COC*H*N, NC*H*HCO, NCH*H*CO, NCH_2Ar, CHCH$_2$CH$_2$CH_2N), 2.66-0.94 (30H, m, CHCH_2CH$_2$CH$_2$N, CHCH$_2$CH_2CH$_2$N, ArCH_3).

^{13}C-NMR: (100 MHz, $CDCl_3$, mixture of rotamers) δ: 173.9, 173.4, 172.6, 171.9, 171.6, 171.5, 168.5, 168.3, 167.6, 167.4, 166.1, 165.8, 138.8, 138.7, 138.6, 138.3, 138.1, 137.8, 136.9, 136.8, 135.9, 129.5, 129.3, 129.1, 128.6, 126.3, 125.9, 125.5, 125.0, 124.5, 124.4, 124.2, 58.4, 58.1, 57.5, 56.8, 56.1, 53.6, 53.0, 52.8, 52.0, 51.3, 50.5, 50.1, 48.8, 48.1, 47.9, 47.6, 47.1, 46.7, 46.4, 46.2, 37.4, 37.1, 32.8, 32.2, 31.9, 31.4, 30.0, 29.7, 29.4, 29.2, 28.3, 27.4, 25.0, 24.9, 24.8, 23.0, 22.7, 22.0, 21.7, 20.9, 19.7, 18.3.

✔ *Compound* **91**

Yield: 39%. The crude residue was purified by precipitation in CH_3CN/H_2O 1:1 (v/v).

ES-MS: 883.9 *m/z* [M + H$^+$].

^{1}H-NMR: (400 MHz, $CDCl_3$, mixture of rotamers) δ: 3.25-4.87 (24 H, m, COCH_2N, NCH_2Ar), 7.06-7.40 (m, 30 H, Ar*H*).

^{13}C-NMR: (100 MHz, $CDCl_3$, mixture of rotamers) δ: 171.9, 171.3, 169.6, 168.9, 168.6, 167.9, 137.2–135.4 ,129.3, 125.4, 53.0, 51.6, 50.2, 48.9, 48.6, 48.4, 47.7, 47.5.

HPLC: t_R: 19.9 min; conditions: 5 → 100% B in 30 min (A, 0.1% TFA in water, B, 0.1% TFA in acetonitrile); flow: 1 mL min^{-1}, 220 nm.

✔ *Compound* **92**

Yield: 37%. The crude residue was purified by precipitation in CH_3CN/H_2O 1:1 (v/v).

ES-MS: 869.7 *m/z* [M + Na^+].

^{1}H-NMR: (400 MHz, $CDCl_3$, mixture of rotamers) δ: 4.73–3.76 (m, 12 H, $COCH_2N$), 3.58–2.70 (m, 12 H, $NCH_2(CH_2)_4CH_3$), 2.05–1.20 (m, 48 H, $NCH_2(CH_2)_4CH_3$), 0.89–0.83 (bs, 18 H, $NCH_2(CH_2)_4CH_3$).

^{13}C-NMR: (100 MHz, $CDCl_3$, mixture of rotamers) δ: 171. 8, 171.5, 171.0, 170.5, 170.3, 170.2, 169.9, 169.5, 169.2, 169.1, 168.8, 168.6, 168.4, 168.3, 168.2, 168.0, 167.6, 167.4, 167.3, 166.8, 166.7, 166.4, 166.3, 51.5, 51.1, 50.9, 50.4, 50.0, 49.7, 49.5, 49.3, 49.0, 48.8, 48.7, 48.6, 48.3,48.2, 47.9, 47.7, 47.5, 47.3, 47.1, 46.8, 46.6, 46.3, 46.0, 43.3, 32.7, 31.6, 31.5, 30.1, 30.0, 29.9, 29.7, 29.4, 29.1, 29.0 , 28.9, 28.7, 28.5, 28.1 , 28.0 , 27.7, 27.6, 27.5, 27.3, 27.2, 27.0 , 26.9, 26.5 , 22.60, 14.0.

HPLC: t_R: 23.2 min; conditions: 5 → 100% B in 30 min (A, 0.1% TFA in water, B, 0.1% TFA in acetonitrile); flow: 1 mL min^{-1}, 220 nm.

✔ *Compound* **93**

Yield: 28%. The crude residue was purified by RP-HPLC on a C_{18} reversed-phase semi-preparative column (t_R: 9.0 min.; conditions: 40 → 100% B in 30 min (A: 0.1% TFA in water, B: 0.1% TFA in acetonitrile), flow: 2.0 mL min^{-1}, 220 nm).

ES-MS: 404.0 *m/2z* [M + H^+ + K^+].

[α]^{D}: -0.72 (c =1.1, $CHCl_3$).

^{1}H-NMR: (400 MHz, $CDCl_3$, mixture of rotamers) δ: 4.82 (3H, bs, COC*H*N), 4.17 (6H, bd, *J* = 16.0 Hz, NC*H*HCO), 4.00-2.76 (36H, m, NCH_2CH_2O, NCH_2CH_2O, OCH_2CH_2O, OCH_2CH_2O, NCH*H*CO, $CHCH_2CH_2CH_2N$,), 3.57 (9H, bs, OCH_3), 2.34-1.10 (12H, m, $CHCH_2CH_2CH_2N$, $CHCH_2CH_2CH_2N$)**.**

^{13}C-NMR: (100 MHz, $CDCl_3$, mixture of rotamers) δ: 173.5, 167.9, 71.9, 70.7, 69.5, 59.0, 57.8, 57.5, 50.4, 49.6, 49.0, 46.8, 31.9, 29.7, 29.3, 27.3, 25.1, 22.6, 19.1.

✔ *Compound* **94**

Yield: 49%. The crude residue was purified by RP-HPLC on a C_{18} reversed-phase semi-preparative column (t_R: 14.8 min.; conditions: 25 → 100% B in 30 min (A: 0.1% TFA in water, B: 0.1% TFA in acetonitrile), flow: 2.0 mL min^{-1}, 220 nm).

ES-MS: 755.2 *m/z* [M + Na^+].

[α]^{D}: +25.5 (c =1.0, $CHCl_3$).

^{1}H-NMR: (300 MHz, $CDCl_3$, mixture of rotamers) δ: 7.85-6.96 (15H, m, Ar*H*), 5.88-3.24 (27H, m, COC*H*N, NC*H*HCO, NCH*H*CO, NCH_2Ar, $CHCH_2CH_2CH_2N$), 2.55-1.30 (12H, m, $CHCH_2CH_2CH_2N$, $CHCH_2CH_2CH_2N$).

^{13}C-NMR: (75 MHz, $CDCl_3$, mixture of rotamers) δ: 174.2, 173.8, 173.2, 172.7, 172.6, 172.2, 171.9, 170.9, 169.9, 168.9, 168.4, 168.1, 167.9, 167.7, 167.3, 167.1, 166.8, 166.7, 165.4, 137.0, 136.7, 136.6, 136.5, 136.4, 136.2, 136.1, 135.7, 129.3,

129.0, 128.7, 128.5, 128.4, 128.3, 128.2, 128.0, 127.8, 127.7, 127.6, 127.5, 127.3, 127.1, 126.9, 126.7, 126.6, 126.4, 126.2, 116.7, 113.8, 58.9, 58.8, 57.9, 57.8, 57.3, 56.7, 56.5, 56.1, 53.6, 53.3, 53.1, 53.0, 52.3, 51.7, 51.4, 50.8, 50.1, 50.0, 49.9, 49.8, 49.4, 49.1, 48.8, 48.4, 48.1, 47.8, 47.7, 47.6, 47.4, 47.1, 46.9, 46.8, 46.4, 46.3, 46.2, 32.2, 32.0, 31.9, 31.4, 31.3, 29.9, 29.6, 29.4, 29.2, 28.9, 28.6, 28.2, 25.9, 25.4, 25.2, 25.0, 24.8, 24.6, 22.9, 22.7, 22.6, 22.0, 21.6.

✔ *Compound* **95**

Yield: 64%. The crude residue was purified by RP-HPLC on a C_{18} reversed-phase semi-preparative column (t_R: 17.6 min.; conditions: 40 → 100% B in 30 min (A: 0.1% TFA in water, B: 0.1% TFA in acetonitrile), flow: 2.0 mL min^{-1}, 220 nm).

ES-MS: 737.5 *m/z* [M + Na^+].

[α]^D: -2.3 (c =1.0, $CHCl_3$).

^{1}H-NMR: (400 MHz, $CDCl_3$, mixture of rotamers) δ: 5.66-4.50 (15H, m, NC*H*HCO, NCH*H*CO, COC*H*N), 4.36-3.08 (15H, m, $CH_3(CH_2)_4CH_2N$, $CHCH_2CH_2CH_2N$), 2.51-1.47 (12H, m, $CHCH_2CH_2CH_2N$, $CHCH_2CH_2CH_2N$), 1.28 (24H, m, $CH_3(CH_2)_4CH_2N$), 0.86 (9H, m, $CH_3(CH_2)_5N$).

^{13}C-NMR: (75 MHz, $CDCl_3$, mixture of rotamers) δ: 173.3, 172.8, 172.1, 171.6, 168.3, 167.8, 167.5, 167.0, 166.7, 58.9, 58.3, 57.7, 56.5, 50.5, 50.2, 49.8, 49.4, 49.0, 48.8, 48.5, 48.2, 47.8, 47.6, 47.3, 47.1, 46.8, 32.1, 31.9, 31.6, 31.4, 30.2, 29.8,

29.7, 29.5, 29.3, 29.2, 29.0, 28.7, 28.4, 27.8, 27.5, 27.2, 27.0, 26.9, 26.5, 26.4, 26.2, 25.5, 25.1, 24.9, 22.9, 22.6, 22.1, 13.9.

✔ *Compound* **96**

Yield: 18%. The crude residue was purified by RP-HPLC on a C_{18} reversed-phase semi-preparative column (t_R: 18.6 min.; conditions: 25 → 100% B in 30 min (A: 0.1% TFA in water, B: 0.1% TFA in acetonitrile), flow: 2.0 mL min^{-1}, 220 nm).

ES-MS: 721.3 *m/z* [M + Na^+].

[α]^D: +5.7 (c =0.8, $CHCl_3$).

^{1}H-NMR: (400 MHz, $CDCl_3$, mixture of rotamers) δ: 7.68-6.88 (3H, m, CON*H*), 4.76-3.39 (21H, m, NC*H*HCO, NCH*H*CO, COC*H*N, $CH_3(CH_2)_4CH_2N$), 2.05-1.25 (m, $CH_3(CH_2)_4CH_2N$, $(CH_3)_2CH$, $(CH_3)_2CH$) , 1.00-0.88 (m, $(CH_3)_2CH$), 0.86 (9H, m, $CH_3(CH_2)_5N$).

^{13}C-NMR: (75 MHz, $CDCl_3$, mixture of rotamers) δ: 173.4, 172.4, 171.9, 171.4, 170.0, 169.9, 169.5, 168.8, 168.2, 167.7, 54.6, 54.5, 54.0, 52.1, 51.7, 51.4, 50.8, 50.5, 50.4, 50.1, 49.8, 48.2, 47.9, 47.4, 32.1, 31.9, 31.4, 31.1, 30.5, 29.9, 28.9, 28.7, 28.2, 27.0, 26.3, 22.5, 19.8, 19.7, 19.6, 18.3, 17.8, 17.7, 17.5, 13.9.

✔ *Compound* **97**

Yield: 22%. The crude residue was purified by RP-HPLC on a C_{18} reversed-phase semi-preparative column (t_R: 17.4 min.; conditions: 40 → 100% B in 30 min (A: 0.1% TFA in

water, B: 0.1% TFA in acetonitrile), flow: 2.0 mL min^{-1}, 220 nm).

ES-MS: 905.4 *m/z* [M + Na^+].

[α]^D: +8.3 (c =0.9, $CHCl_3$).

^{1}H-NMR: (400 MHz, $CDCl_3$, mixture of rotamers) δ: 8.30-6.96 (21H, m, Ar*H*), 6.10-3.13(27H, m, COC*H*N, NC*H*HCO, NCH*H*CO, NCH_2Ar, $CHCH_2CH_2CH_2N$), 2.74-0.84 (12H, m, $CHCH_2CH_2CH_2N$, $CHCH_2CH_2CH_2N$).

^{13}C-NMR: (100 MHz, $CDCl_3$, mixture of rotamers) δ: 175.5, 174.4, 173.7, 173.4, 173.2, 173.0, 172.2, 172.1, 171.8, 171.4, 169.9, 169.8, 169.1, 168.9, 168.5, 168.3, 168.0, 167.6, 166.9, 166.1, 166.0, 165.8, 133.8, 133.7, 133.0, 132.6, 132.5, 132.3, 132.1, 131.9, 131.7, 131.5, 131.3, 131.2, 131.0, 130.9, 130.8, 130.6, 130.3, 129.2, 129.0, 128.7, 128.4, 128.3, 128.2, 127.8, 127.6, 127.0, 126.8, 126.6, 126.3, 125.9, 125.6, 125.4, 125.3, 125.2, 124.4, 123.6, 123.5, 123.1, 122.9, 122.6, 122.5, 122.3, 121.7, 59.0, 58.9, 58.6, 57.9, 57.8, 57.4, 57.3, 56.9, 56.7, 56.6, 56.1, 55.8, 51.6, 51.5, 51.1, 50.7, 50.5, 50.1, 50.0, 49.3, 48.9, 48.7, 48.5, 47.9, 47.6, 47.5, 47.3, 47.2, 46.8, 46.6, 46.4, 46.2, 45.6, 32.0, 31.9, 31.6, 31.3, 31.2, 31.1, 30.0, 29.7, 29.3, 29.1, 28.7, 28.3, 27.5, 27.3, 27.1, 25.8, 25.4, 25.2, 25.1, 24.8, 23.2, 23.0, 22.6, 22.1, 21.4, 20.6, 20.1, 19.7.

✔ *Compound* **98**

Yield: 18%. The crude residue was purified by RP-HPLC on a C_{18} reversed-phase semi-preparative column (t_R: 17.5 min.; conditions: 25 → 100% B in 30 min (A: 0.1% TFA in

water, B: 0.1% TFA in acetonitrile), flow: 2.0 mL min^{-1}, 220 nm).

ES-MS: 975.0 *m/z* [M + K^+].

[α]^D: +28.6 (c =0.9, $CHCl_3$).

^{1}H-NMR: (400 MHz, $CDCl_3$, mixture of rotamers) δ: 7.78-7.26 (12H, m, Ar*H*), 5.90-2.85(27H, m, COC*H*N, NC*H*HCO, NCH*H*CO, NCH_2Ar, $CHCH_2CH_2CH_2N$), 2.55-1.00 (12H, m, $CHCH_2CH_2CH_2N$, $CHCH_2CH_2CH_2N$).

^{13}C-NMR: (100 MHz, $CDCl_3$, mixture of rotamers) δ: 174.4, 173.9, 173.8, 173.6, 173.5, 172.9, 172.4, 172.1, 171.9, 171.5, 171.0, 169.9, 169.8, 169.7, 169.2, 168.8, 168.5, 168.2, 167.7, 167.0, 166.8, 166.6, 166.3, 165.9, 165.6, 165.3, 141.5, 141.3, 141.1, 140.9, 140.5, 140.1, 139.8, 139.6, 139.1, 130.8, 130.3, 130.0, 129.7, 129.4, 129.2, 128.5, 128.3, 127.9, 127.7, 127.4, 127.1, 126.9, 126.7, 126.5, 126.0, 125.6, 125.5, 125.3, 122.5, 59.5, 58.9, 57.7, 57.5, 57.3, 56.6, 56.5, 56.2, 53.3, 53.2, 52.7, 52.3, 51.8, 51.7, 51.5, 51.0, 50.7, 50.5, 50.6, 50.4, 49.8, 49.6, 49.3, 49.0, 48.8, 48.4, 48.3, 48.1, 47.8, 47.6, 47.4, 47.2, 46.9, 46.6, 46.5, 46.3, 37.4, 32.7, 32.1, 31.9, 31.6, 31.4, 30.3, 30.0, 29.6, 29.3, 28.9, 28.7, 28.3, 27.8, 27.3, 27.1, 26.3, 25.9, 25.6, 25.4, 25.2, 25.0, 24.8, 23.0, 22.9, 22.6, 22.1, 21.6, 21.1, 19.7.

✔ *Compound* **99**

Yield: 23%. The crude residue was purified by RP-HPLC on a C_{18} reversed-phase semi-preparative column (t_R: 19.0 min.; conditions: 25 → 100% B in 30 min (A: 0.1% TFA in

water, B: 0.1% TFA in acetonitrile), flow: 2.0 mL min^{-1}, 220 nm).

ES-MS: 1141.0 *m/z* [M + H^+].

[α]^D: +22.9 (c =1.0, $CHCl_3$).

^{1}H-NMR: (400 MHz, $CDCl_3$, mixture of rotamers) δ: 8.17-7.56 (9H, m, Ar*H*), 5.73-2.79 (27H, m, COC*H*N, NC*H*HCO, NCH*H*CO, NCH_2Ar, CHCH$_2$CH$_2$CH_2N), 2.34-1.03 (12H, m, CHCH_2CH$_2$CH$_2$N, CHCH$_2$CH_2CH$_2$N).

^{13}C-NMR: (100 MHz, $CDCl_3$, mixture of rotamers) δ: 174.4, 173.7, 172.8, 172.4, 169.9, 169.7, 168.4, 168.2, 167.4, 168.2, 167.4, 166.3, 166.1, 159.6, 159.3, 139.6, 139.1, 138.3, 133.0, 132.7, 132.4, 132.1, 131.8, 131.5, 128.5, 128.3, 127.5, 127.2, 127.0, 126.5, 124.6, 124.5, 124.3, 122.2, 121.9, 121.6, 121.4, 119.2, 118.9, 116.6, 113.7, 59.6, 58.0, 57.8, 57.8, 56.6, 56.3, 53.4, 53.1, 52.4, 52.0, 51.9, 50.7, 50.4, 49.8, 49.2, 48.8, 48.5, 47.6, 46.9, 46.8, 46.6, 37.4, 37.1, 32.7, 31.9, 31.6, 31.3, 30.0, 29.7, 29.5, 29.3, 28.5, 27.8, 27.6, 27.3, 27.0, 25.5, 25.4, 25.1, 24.4, 22.8, 22.7, 20.8, 19.7.

✔ *Compound* **100**

Yield: 57%. The crude residue was purified by RP-HPLC on a C_{18} reversed-phase semi-preparative column (t_R: 14.1 min.; conditions: 25 → 100% B in 30 min (A: 0.1% TFA in water, B: 0.1% TFA in acetonitrile), flow: 2.0 mL min^{-1}, 220 nm).

ES-MS: 823.5 *m/z* [M + H^+].

[α]^D: +30.8 (c =1.0, $CHCl_3$).

^{1}H-NMR: (400 MHz, $CDCl_3$, mixture of rotamers) δ: 7.54-6.59(12H, m, Ar*H*), 5.87-3.16(36H, m, COC*H*N, NC*H*HCO, NCH*H*CO, NCH_2Ar, CHCH$_2$CH$_2$CH_2N, OCH_3), 2.76-0.92 (12H, m, CHCH_2CH$_2$CH$_2$N, CHCH$_2$CH_2CH$_2$N).

^{13}C-NMR: (100 MHz, $CDCl_3$, mixture of rotamers) δ: 173.3, 173.2, 172.5, 171.9, 171.8, 171.6, 171.0, 169.8, 168.5, 168.3, 168.0, 167.3, 167.1, 166.9, 166.8, 165.6, 159.4, 159.2, 159.0, 158.7, 129.9, 129.5, 129.2, 129.0, 128.9, 128.7, 128.4, 128.3, 128.1, 127.9, 127.7, 114.4, 114.3, 114.2, 114.1, 113.9, 113.7, 58.7, 58.5, 58.2, 57.8, 57.6, 57.3, 57.0, 56.7, 56.2, 56.1, 55.7, 55.3, 55.1, 53.0, 52.6, 52.5, 52.3, 51.2, 50.8, 50.4, 50.3, 49.5, 49.2, 48.7, 48.4, 47.9, 47.7, 47.5, 47.4, 47.2, 46.7, 46.5, 46.4, 46.2, 37.4, 37.0, 36.8, 32.7, 32.0, 31.9, 31.6, 31.5, 31.4, 31.2, 30.2, 30.0, 29.6, 29.3, 29.2, 28.9, 28.2, 27.7, 27.5, 27.3, 27.0, 25.7, 25.4, 24.9, 24.8, 24.4, 22.9, 22.6, 22.1, 21.7, 21.3, 21.1, 20.5, 20.3, 19.7.

4.6.3 General procedure for the synthesis of complexed cyclopeptoids **107** *and* **108**

To a solution of cyclopeptoid **43** or **91** (0.034 mmol) in DCM:MeOH 9:1 (v/v) sodium hexafluorophosphate (5.6 mg, 0.034 mmol) was added. The mixture was stirred overnight and then concentrated *in vacuo*.

✓ *Compound* **107**

ES-MS: 713.7 *m/z* [M + Na^+].

^{1}H-NMR: (400 MHz, CD_3CN, mixture of rotamers) δ: 4.69 (6 H, d, J = 16.7 Hz,
NC*H*HCO), 3.84 (6H, d, J = 16.7 Hz, NCH*H*CO), 3.59–3.33 (24H, m, NCH_2CH_2O, NCH_2CH_2O), 3.34 (18 H, s, OCH_3).
^{13}C-NMR: (100 MHz, CD_3CN, mixture of rotamers) δ: 170.6, 71.0, 59.1, 50.5, 49.6.

✓ *Compound* **108**

ES-MS: 905.4 *m/z* [M + Na^+].
^{1}H-NMR: (400 MHz, CD_3CN, mixture of rotamers) δ: 7.37–7.26 (30 H, m, Ar*H*), 4.86 (6 H, d, J = 16.8 Hz, C*H*HAr), 4.72 (6 H, d, J = 16.3 Hz, NC*H*HCO), 4.41 (6 H, d, J = 16.8 Hz, CH*H*Ar), 3.72 (6 H, d, J = 16.3 Hz, NCH*H*CO).
^{13}C-NMR: (100 MHz, CD_3CN, mixture of rotamers) δ: 171.7, 136.8, 129.8 (×3), 128.9, 128.7, 53.2, 50.8.

4.6.4 Synthesis of 106

Synthesis of tosylate ester from 104

Alcohol **104** (9.61 g, 80 mmol) was mixed with DCM (200 mL) in a round-bottom flask, and *p*-toluenesulfonyl chloride (18.3 g, 96mmol) and 4-(*N*,*N*- dimethylamino)pyridine (80 mg, 655 mmol) were added to this solution. A reflux condenser was attached to the round-bottom flask, and the mixture was stirred for 10 min. Anhydrous triethylamine (10.5 g, 104 mmol) was added to the reaction mixture dropwise over 15 min, and as the stirring was continued, a white solid (triethylammonium chloride) precipitated out of the reaction mixture. This was accompanied by the liberation

of heat that caused visible evaporation and condensation of dichloromethane from the reaction mixture. The reaction mixture was stirred for 12 h, after which it was treated with 1M HCl (160 mL). The dichloromethane layer was separated from the aqueous layer, washed with water, dried over anhydrous magnesium sulfate, and evaporated under reduced pressure to yield the tosylate ester (21.9 g). This product was used in the next step without purification.

✔ *Tosylate ester from* **104**

^{1}H-NMR: (400 MHz, $CDCl_3$) δ: 7.80–7.32 (30 H, m, Ar*H*), 4.17 (2 H, t, *J* = 4.8 Hz, TsOC*H*$_2$), 3.69 (2 H, t, *J* = 4.8 Hz, TsOCH$_2$C*H*$_2$), 3.58-3.48 (4H, m, OC*H*$_2$C*H*$_2$O), 3.35 (3H, s, OC*H*$_3$), 2.44 (3 H, s, ArC*H*$_3$).

Synthesis of 105

A mixture of tosylate ester from **104**, finely powdered potassium phthalimide (17.7g, 96 mmol), and DMF (68 mL) were combined in a round-bottom flask. The reaction mixture was stirred at 80 °C under an air condenser for 12 h. Diethyl ether was added to the reaction mixture, which was then filtered to remove precipitated potassium tosylate. The salt was washed with diethyl ether and the washings were combined with the filtrate. To remove the solvents, diethyl ether was first evaporated under reduced pressure on a rotary evaporator. This was followed by vacuum distillation of DMF. The residue was purified by column chromatography

(petroleum ether/AcOEt, from: 85/25 to 45/55) to afford **105** (15.4 g, 77%).

✓ *Compound* **105**

^{1}H-NMR: (400 MHz, $CDCl_3$) δ: 7.86-7.70(4H, m, Ar*H*), 3.91 (2H, t, *J* = 6.0 Hz, NCH_2), 3.75 (2H, t, *J* = 6.0 Hz, NCH_2CH_2), 3.66-3.48 (4H, m, OCH_2CH_2O), 3.31 (3H, s, OCH_3).

Formation of amine 106

The phthalimide **105** (7.26 g, 29 mmol), hydrazine (1.81 mL, 58 mmol), and ethanol (147 mL) were combined in a round-bottom flask. The reaction mixture was stirred while being refluxed at 76 °C for 3 h, during which a white solid (phthalhydrazide) was formed in the reaction mixture. Ethanol was removed from the reaction mixture by rotary evaporation until the precipitate was nearly dry. Cold diethyl ether was added to the round-bottom flask, and the amine was extracted from the fluffy phthalhydrazide by stirring the mixture over a magnetic stir plate. The solution was filtered and the residual phthalhydrazide was washed using cold diethyl ether. The combined filtrate and washings were evaporated under reduced pressure to obtain **106**.

✓ *Compound* **106**

^{1}H-NMR: (400 MHz, $CDCl_3$) δ: 3.61-3.50 (6H, m, $CH_2OCH_2CH_2O$), 2.89 (2H, s, NCH_2).

4.6.5 General procedure for the substitution reaction

To a solution of *p*-nitrobenzyl bromide (21.5 mg, 0.10 mmol) in $CHCl_3$ (0.25 M, 0.200 mL), containing 5 mol% of the catalyst, a 0.75 M aqueous solution of thiocyanate salt (0.15 mmol) was added and the resulting mixture was stirred for up to 24 h in total. The reaction was monitored by TLC at intervals of 30 min. The mixture was filtered through a shortpath silica gel column and removal of the solvent *in vacuo* afforded a residue that was analyzed by ^{1}H-NMR to determine the % of conversion.

✔ *Compound* **115**

^{1}H-NMR: (400 MHz, $CDCl_3$) δ: 8.20 (2H, d, J = 8.0 Hz, Ar*H*), 7.56 (2H, d, J = 8.0 Hz, Ar*H*), 4.51 (2H, s, CH_2).

✔ *Compound* **116**

^{1}H-NMR: (400 MHz, $CDCl_3$) δ: 8.27 (2H, d, J = 8.0 Hz, Ar*H*), 7.56 (2H, d, J = 8.0 Hz, Ar*H*), 4.20 (2H, s, CH_2).

4.6.6 General procedure for the enantioselective epoxidation

To a mixture of *trans*-chalcone (**117**) (0.08 mmol) and catalyst (5% mol, 0.004 mmol) in toluene (0.8 mL) a 5.5 M solution of *t*-BuOOH in decane (0.096 mmol) and a 50% aqueous solution of NaOH (0.2 mL) were added subsequently. The mixture was stirred overnight at 0 °C. The reaction was stopped adding 3 mL of HCl 2 M. The aqueous phase was then extracted with DCM (2 x 4 mL). The

combined organic extracts were dried over Na_2SO_4. The solvent was evaporated and the residue was purified by column chromatography (petroleum ether/AcOEt, from: 95/5 to 90/10) to afford the epoxy ketone **118**. The enantiomeric eccess was determined by chiral HPLC analysis. The absolute configuration was determined by comparison of the HPLC retention time with the authentic sample reported in the literature.[101]

✔ *Compound* **118**

^{1}H-NMR: (400 MHz, $CDCl_3$) δ: 8.01 (m, 2H, *o*-COC_6H_4H), 7.63 (m, 1H, *p*- COC_6H_4H), 7.49 (m, 2H, *m*-COC_6H_4H), 7.45-7.33 (m, 5H, Ar*H*), 4.30 (d, 1H, J = 1.8 Hz, COC*H*), 4.08 (d, 1H, J = 1.8 Hz, PhC*H*).

HPLC: DAICEL CHIRALPAK AD-H, t_R: 21.3 min (α*R*β*S*) (minor), t_R: 27.8 min (α*S*β*R*) (major); conditions: hexane:ethanol = 9:1; flow: 1 mL min^{-1}, 260 nm.

4.6.7 General procedure for the enantioselective alkylation

Benzyl bromide (0.096 mmol) was added under a nitrogen atmosphere to a mixture of (diphenylmethylene)glycine *t*-buthyl ester (**78**) (23.0 mg, 0.08 mmol) and catalyst (5% mol, 0.004 mmol) in toluene (0.8 mL). The organic mixture was deoxygenated. Then, 50% aqueous NaOH (0.5 mL), previously deoxygenated, was added dropwise at 0°C and the

[101] M. S. Yoo, D. G. Kim, M. W. Ha, S. Jew, H. G. Park, B. G. Park *Tetrahedron Lett.*, **2010**, *51*, 5601-5603.

resulting mixture was stirred overnight at the same temperature. The mixture was then poured into water (2.5 mL) and extracted with DCM (2 x 4 mL). The organic extracts were dried over Na_2SO_4. The solvent was evaporated and the residue was purified by column chromatography (petroleum ether/AcOEt, from: 98/2 to 95/5) to give the benzylation product **79**. The enantiomeric eccess was determined by chiral HPLC analysis. The absolute configuration was determined by comparison of the HPLC retention time with the authentic sample reported in the literature.[102]

✔ *Compound* **79**

^{1}H-NMR: (400 MHz, $CDCl_3$) δ: 7.59 (m, 2H, Ar*H*), 7.43-7.24 (m, 6H, Ar*H*), 7.24-7.14 (m, 3H, Ar*H*), 7.12-7.02 (m, 2H, Ar*H*), 6.63 (bd, 2H, J = 6.8 Hz, Ar*H*), 4.14 (dd, 1H, J = 9.0, 4.5 Hz, NC*H*CO), 3.26 (dd, 1H, J = 13.3, 4.5 Hz, NCHC*H*H), 3.18 (dd, 1H, J = 13.3 Hz, 9.0 Hz, NCHC*H*H), 1.46 (s, 9H, C(CH_3)$_3$).

^{13}C-NMR: (75 MHz, $CDCl_3$) δ: 170.8, 170.3, 139.5, 138.3, 136.3, 130.0, 129.8 (x 2), 128.7 (x 2), 128.1 (x 3), 128.0 (x 2), 127.9 (x 2), 127.6 (x 2), 126.1, 81.0, 67.9, 39.6, 28.0 (x 3).

HPLC: DAICEL CHIRALCEL OD-H, t_R: 15.3 min (*R*) (major), t_R: 25.9 min (*S*) (minor); conditions: hexane:isopropanol = 9:1; flow: 0.5 mL min^{-1}, 260 nm.

[102] S. Shikarawa, Y. Tanaka, K. Maruoka *Org. Lett.*, **2004**, *6*, 1429-1431.

4.6.8 Determination of binding affinities for compounds 43, 47, 91, 92, 111

Association constants K_a were calculated from the equation $K_a = K_e/K_d$, according to methodology reported by Cram and coworkers.[51] K_d values, which represent the distribution constants of the picrate salts between water and $CHCl_3$, were previously determined by Cram,[51] while K_e values were calculated following the "ultraviolet method" reported by Cram and coworkers.[51] All ultraviolet (UV) measurements were made on a Varian Cary 50 UV-Vis Spectrophotometer at 380 nm at 24–26 °C, using spectrophotometric grade solvents. The picrate salts were prepared according to literature procedures,[103] and dried under high vacuum before use. Aqueous solutions 0.0150 M in the picrate of Li^+, Na^+, K^+ were prepared. Aliquots of these solutions (250 μL of Li^+, Na^+, K^+) were introduced in six Eppendorf vials, and to each of these, 250 μL of a 0.015 M solution of the host in $CHCl_3$ was added. The vials were capped (in order to prevent evaporation) and mixed thoroughly, using a Vortex "Maxi Mixer", for 5 minutes and then centrifuged (1000 rpm). Aliquots of 50 μL of each aqueous phase were diluted with CH_3CN up to 5.0 mL. Successively 200 μL of these solutions were diluted with CH_3CN up to 1.0 mL. Aliquots of 100 μL of each organic phase were also diluted with CH_3CN up to 5.0 mL. Successively 200 μL of the latter solutions were diluted

[103] M. Bhatnagar, A. Awasthy, U. Sharma, *Main Group Met. Chem.*, **2004,** *27*, 163–168.

with CH_3CN up to 1.0 mL. The absorbance of each sample was then measured against the appropriate blank solution at 372 nm at 25 °C. R, K_e, K_a and ΔG° were thus calculated in the proper way.[51]

4.6.9 Transport studies for compounds 43, 47, 91, 92

General procedures

L-α-phosphatidyl-DL-glycerol sodium salt (EYPG, 20 mg/mL chloroform solution) and 1,2-dipalmitoyl-sn-glycero-3-phosphocholine (DPPC, 20 mg/mL chloroform solution) were purchased from Avanti Polar Lipids; egg yolk phosphatidylcholine (EYPC, 100 mg/mL chloroform solution), and 8-hydroxypyrene-1,3,6-trisulfonic acid trisodium salt (HPTS) were from Sigma; Triton® X-100 and HEPES buffer were purchased from Fluka; all salts were of the best grade available from Aldrich and were used without further purification. Size exclusion chromatography (SEC) was performed using pre-packed columns Sephadex™ G-25 M (PD-10) from Amersham Biosciences. Liposomes were prepared by extrusion using a 10 mL Lipex™ Thermobarrel EXTRUDER (Northern Lipids Inc.) connected to a thermostatic bath (25°C). The 100 nm polycarbonate membranes are Nucleopore Track-Etch Membranes from Whatman. Fluorescence spectra were recorded on Perkin-Elmer LS-50B fluorimeter. Fluorimetric experiments were

conducted at 25°C. The ionophores concentration is given in percent with respect to the total concentration of lipids. Mother solutions of ionophores were prepared in methanol. Control experiments showed that the amount of methanol added to the vesicular suspension in the different experiments (maximum amount 1.0 % in volume) did not affect the permeability of the membrane.

HPTS assay[104]

A mixture of 225 µL of EYPC chloroform solution (100 mg/mL, 30 µmol) and 60 µL of EYPG chloroform solution (20 mg/mL, 1.5 µmol) was first evaporated with Ar-flux to form a thin film and then dried under high vacuum for 3 h. The lipid cake was hydrated in 1.5 mL of 0.1 mM HPTS solution (HEPES 25 mM, 100 mM NaCl, pH 7) for 30 min at 40°C. The lipid suspension was submitted to 5 freeze-thaw cycles (-196°C/40°C) using liquid nitrogen and a thermostatic bath, and then extruded under nitrogen pressure (15 bar) at room temperature (10 extrusions through a 0.1 µm polycarbonate membrane). The LUV suspension was separated from extravesicular dye by size exclusion chromatography (SEC) (stationary phase: pre-packed column Sephadex™ G-25, mobile phase: HEPES buffer) and diluted with HEPES buffer to give a stock solution with a lipid

[104] S. S. Moore, T. L. Tarnowski, M. Newcomb, D. J. Cram. *J. Am. Chem. Soc*. **1977**, *99*, 6398-6405.

concentration of 5 mM (assuming 100% of lipids were incorporated into liposomes). 104 µL of the lipid suspension were placed in a fluorimetric cell, diluted to 3040 µL with the same buffer solution used for the liposome preparation and kept under gently stirring. The total lipid concentration in the fluorimetric cell was 0.17 mM. An aliquot of methanolic solution of the ionophore (5-30 µL of the appropriate mother solution in order to obtain the desired $mol_{compound}/mol_{lipid}$ ratio) was then added to the lipid suspension and the cell was incubated at 25°C for 30 min. After incubation the time course of fluorescence was recorded for 200 s (λ_{ex} = 460 nm, λ_{em} = 510 nm) and then 50 µL of 0.5 M NaOH were rapidly added through an injector port and the fluorescence emission was recorded for 1200 s. Maximal changes in dye emission were obtained by final lysis of the liposomes with detergent (40 µL of 5% aqueous solution Triton® X-100). Fluorescence time courses were normalized using the following equation:

$$FI = \frac{(F^t - F^0)}{(F^\infty - F^0)} \cdot 100$$

where F^t is the fluorescence intensity measured at time t, F^0 is the fluorescence intensity at ionophore addition, F^∞ is the fluorescence intensity at saturation after lysis with Triton. The apparent first order rate constants for the transport process were obtained by non-linear regression analysis of the

fluorescence data vs. time. The fit error on the rate constant was always less than 1%.

Determination of sodium selectivity with the HPTS assay (Matile's protocol)[94]

The vesicle suspension (104 µL stock solution, prepared as described above) was placed in a fluorimetric cell and diluted to 3040 µL with the appropriate buffer solution (25 mM HEPES, 100 mM NaCl). The total lipid concentration in the fluorimetric cell was 0.17 mM. An aliquot of methanolic solution of the ionophore (5-30 µL of the appropriate mother solution in order to obtain the desired $mol_{compound}/mol_{lipid}$ ratio) was then added to the lipid suspension and the cell was incubated at 25°C for 30 min. After incubation the time course of fluorescence was recorded for 200 s (λ_{ex} = 460 nm, λ_{em} = 510 nm) and then 50 µL of 0.5 M NaOH were rapidly added through an injector port and the fluorescence emission was recorded for 1200 s. Maximal changes in dye emission were obtained by final lysis of the liposomes with detergent (40 µL of 5% aqueous solution Triton® X-100). Fluorescence time courses were normalized as previously described and corrected for the permeation of the sodium cation in the absence of ionophore by subtracting the relative fluorescence time course.

4 CYCLOPEPTOIDS AS PHASE-TRANSFER CATALYSTS

5 SYNTHETIC STRATEGIES FOR KALATA B1 CYCLOTIDE[105]

5.1 Introduction

The last part of doctorate research project has been devoted to novel synthetic strategies for kalata B1 cyclotide based on Fmoc/*t*-Bu solid-phase synthesis, and has been realized in the laboratories of the IRB institute in Barcelona (SPAIN) under the supervision of Prof. Fernando Albericio and Dr. Juan Baptista Blanco-Canosa.

Cyclotides are cysteine-rich cyclic peptides of vegetal origin, characterized by an enzymatic resistant secondary structure made up of a special arrangement of disulfide bridges, as illustrated in section 1.1.2.[13] This class of molecules represents a promising scaffold in drug design, infact it is possible to perform the grafting of small terapeutic peptide epitopes into the sequence of the cyclotide in order to stabilize them preventing the enzymatic degradation.[15]

Up to the date the cystine-knot peptides such as cyclotides are mainly synthesized with the Boc/Bn protection strategy on solid phase employing alkyl thioesther linkers located in the C-terminal position.[106] This strategy is hazardous and impracticable in many research laboratories

[105] B. Nardone, P. Dawson, F. Albericio, J. B. Blanco-Canosa *Chem. Eur. J.*, in preparation.
[106] J. A. Camarero, G. J. Cotton, A. Adeva, T. W. Muir *J. Pept. Res.*, **1998**, *51*, 303-316; N. L. Daly, S. Love, P. S. Alewood, D. J. Craik *Biochemistry*, **1999**, *38*, 10606-10614; J. A. Camarero, A. Adeva, T. W. Muir *Letters in peptide science* **2000**, *7*, 17-21.

because automated peptide synthesizers compatible with Boc chemistry are very expensive (corrosive HF is required for the cleavage). The thioester linkers are sensitive to the piperidine used in the Fmoc/*t*-Bu protection strategy and so are fully incompatible with this more convenient approach.

As a consequence recently many efforts have been devoted to find out an alternative route for obtaining these kinds of compounds. For example, recombinant DNA expression techniques have been applied to the biosynthesis of cyclotides.[107] Specifically, recombinant DNA which encodes for a certain cyclotide is transplantated in living bacterial cells. Indeed, recombinant DNA is expressed and a recombinant peptide is produced.

Moreover, an interesting chemical method makes use of the Fmoc/*t*-Bu strategy.[108] Particularly, the linear peptide is converted in the corresponding thioester with *p*-acetamidothiophenol, and finally it is performed the cyclization *via* native chemical ligation and the oxidative folding.

5.2 Fmoc/t-Bu solid-phase synthesis of kalata B1: General strategy

The retrosynthetic analysis of kalata B1 (figure 5.1) allows to identify as suitable initiation point for the synthesis

[107] J. A. Camarero, R. H. Kimura, Y. H. Yoo, A. Shekhtman, J. Cantor *Chem. Biochem.*, **2007**, *8*, 1363-1366.

[108] S. Park, S. Gunasekera, T. L. Aboye, U. Göransson *Int. J. Pept. Res. Ther.* **2010**, *16*, 167-176.

of the linear precursor **128** the valine, located in the very flexible loop 6, next to cysteine I.

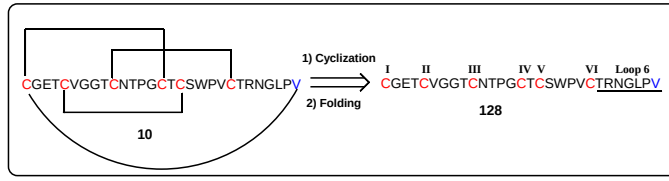

Figure 5.1: Retrosynthetic analysis of kalata B1 (**10**). The initiation point for the synthesis is the valine depicted in blue.

The choice of the specific initiation point is dictated by the possibility to perform the cyclization of the linear peptide precursor **128** containing a cysteine in the N-terminal position through a straightforward native chemical ligation reaction and afterwards to form the disulfide bonds. In addition, the flexibility of the loop 6 including the initiation point should reasonably favour the cyclization process.

At this point, in order to better understand the topic it is necessary to describe the general mechanism for a native chemical ligation (NCL) reaction (scheme 5.1).[109] The starting material for a native chemical ligation reaction is a peptide-thioester which can react with an other peptide containing an N-terminal cysteine in order to generate a longer peptide or a protein. Alternatively, as shown in scheme 5.1, a linear peptide reacts intramolecularly with an N-terminal cysteine forming a cyclopeptide according to a multistep proposed mechanism (scheme 5.1). Typically, NCL

[109] E. C. B. Johnson, S. B. H. Kent *J. Am. Chem. Soc.*, **2006**, *128*, 6640-6646.

is conducted in water at neutral pH and an exogenous aromatic thiol is added to promote the in situ formation of a more active thioesters (step 1 in scheme 5.1) and consequently to increase the kinetic of ligation. The added thiol also maintains the N-terminal cysteine in reduced form and reverses any nonproductive transthioesterification with the thiol moieties of side chains of internal cysteine residues. The most effective thiol catalysts used for NCL are (4-carboxymethyl)thiophenol and 4-mercaptophenol (**129** and **130**, figure 5.2).

The second step (scheme 5.1) consists in a transthioesterification with the thiol side chain of N-terminal cysteine so that a thioester-linked intermediate ligation product is formed. Finally, the thioester-linked intermediate undergoes spontaneous and irreversible acylation to form a native amide bond at the ligation site.

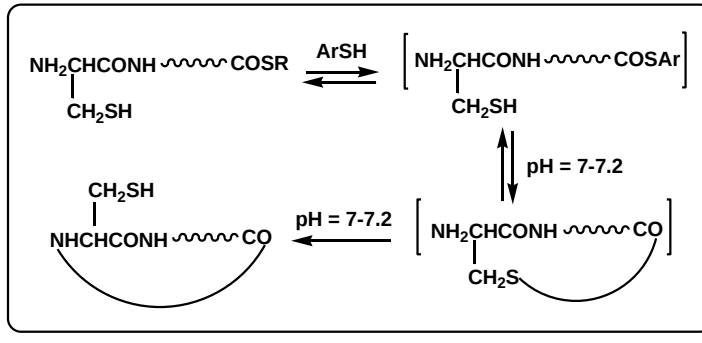

Scheme 5.1: Proposed mechanism for NCL.

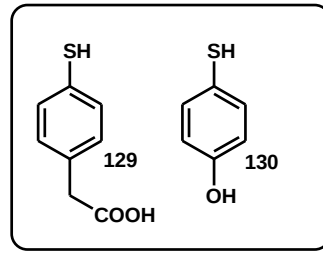

Figure 5.2: NCL thiol catalysts.

Returning to the synthesis of kalata B1, the key point is the generation of a peptide-thioester making use of the Fmoc/*t*-Bu solid-phase synthesis. In this regard, in 2008 Blanco and Dawson found an innovative approach for the Fmoc/*t*-Bu synthesis of a peptide-thioester precursor using 3-Fmoc-4-diaminobenzoic acid (Fmoc-Dbz) as special linker (**131**, figure 5.3), which is synthesized in a single step from 3,4-diaminobenzoic acid (scheme 5.2).[110]

This approach is described in scheme 5.3, in the case of a generic peptide containing a cysteine in the N-terminal position and cyclizable *via* NCL.

In detail, Fmoc-Dbz is coupled to the resin and the Fmoc group is deprotected with 20% piperidine. Subsequent amino acids were coupled by standard Fmoc/*t*-Bu approach with the N-terminal cysteine being introduced as Boc-Cys(Trt)-OH to protect the N-terminus of the peptide during subsequent acylation and to allow simultaneous deprotection. After the chain elongation, the linker is activated through acylation

[110] J. B. Blanco-Canosa, P. E. Dawson *Angew. Chem. Int. Ed.*, **2008**, *47*, 6855-6861.

with *p*-nitrophenylchloroformate followed by the addition of DIPEA to promote intramolecular attack of the anilide to form the resin-bound benzimidazolinone. The *N*-acyl-benzimidazolinone (Nbz) represents an aromatic *N*-acylurea moiety, precursor of a peptide-thioester. Indeed, following the cleavage of the peptide, in NCL reaction medium it is formed an aromatic thioester which converts in the cyclic molecule according to the above illustrated mechanism.

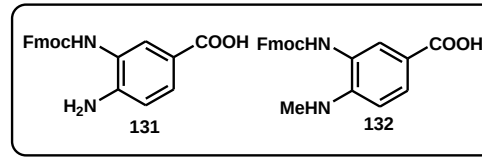

Figure 5.3: Fmoc-Dbz and Fmoc-Dbz(Me) linkers.

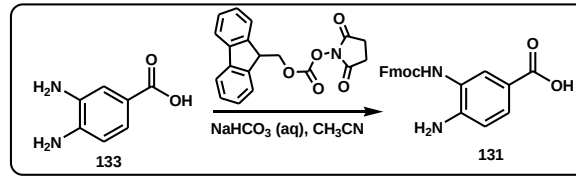

Scheme 5.2: Synthesis of linker **131**.

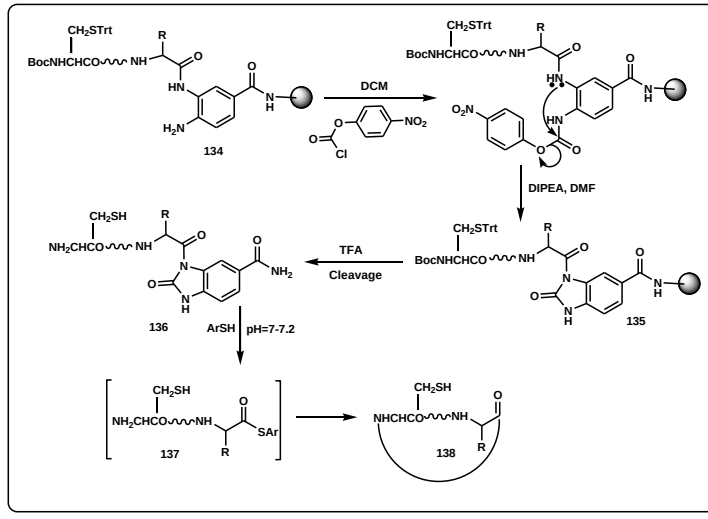

Scheme 5.3: Fmoc/*t*-Bu solid-phase synthesis (SPS) of peptide-thioesters with Fmoc-Dbz linker. Following SPS, aminoanilide **134** undergoes specific acylation and cyclization to yield the resin-bound acylurea peptide **135**. Following cleavage, peptide-Nbz **136** forms an aromatic thioester (**137**) in the NCL reaction medium and it converts in the cyclic peptide **138**.

The linker Fmoc-Dbz (**131**) was successfully used by Göransson *et al.* in the Fmoc/*t*-Bu synthesis of kalata B1.[111]

Recently, Blanco developed the new linker Fmoc-Dbz(Me) (**132**, figure 5.3)[112], an improved version of the linker Fmoc-Dbz, to eliminate acylated or branched byproducts arising from the second, free, amine of Dbz,

[111] S. Gunasekera, T. L. Aboye, W. A. Madian, H. R. El-Seedi, U. Göransson *Int. J. Pept. Res. Ther.*, **2013**, *19*, 43- 54.
[112] Unpublished results.

during the synthesis of long glycine-rich peptides, as reported by Ottesen and co-workers.[113]

The second generation linker Fmoc-Dbz(Me) has been tested in the Fmoc/*t*-Bu solid-phase synthesis of kalata B1-Nbz(Me) (**139**). Through a NCL step and a following folding step (formation of the disulfide bonds) the linear peptide **139** is converted in the final product kalata B1(**10**), as shown in scheme 5.4.

The use of an interposed glycine between the resin and the linker to increase its loading with respect to the direct linkage was also investigated.

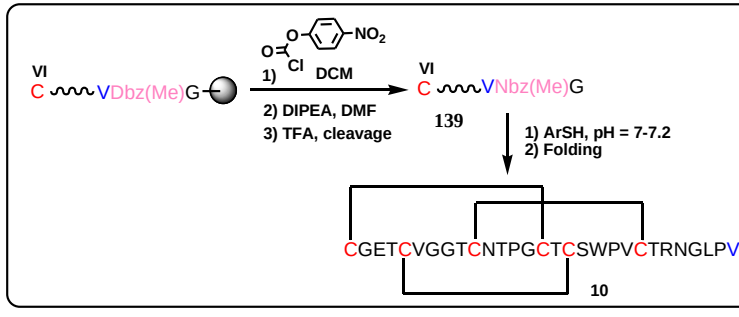

Scheme 5.4: General strategy for Fmoc/*t*-Bu solid-phase synthesis of kalata B1-Nbz(Me) (**139**). Kalata B1(**10**) is formed through the two following step of NCL and folding.

[113] S. K. Mahto, C. J. Howard, J. C. Shimko, J. J. Ottesen *Chem. Bio.Chem.*, **2011**, *12*, 2488-2494.

5.3 Aims of the work

Following the general Fmoc/*t*-Bu strategy, described in scheme 5.4, kalata B1 synthesis was investigated considering four different synthetic modifications:

a) Solid-phase synthesis with ChemMatrix rink amide resin (0.52 mmol/g);

b) Solid-phase synthesis making use of the *O*-acyl isodipeptide unit Boc-Thr(Fmoc-Gly)-OH (**140**, figure 5.4) in place of the TG dipeptide sequence, and with ChemMatrix rink amide resin (0.52 mmol/g);

c) Solid-phase synthesis with the commercial pseudo-proline dipeptide Fmoc-Gly-Thr(ψ(Me,Me)pro)-OH (**141**, figure 5.4) in place of the TG dipeptide sequence, and with a ChemMatrix rink amide resin (0.52 mmol/g);

d) Solid-phase synthesis with Boc-Thr(Fmoc-Gly)-OH (**141**, figure 5.4) and making use of a Tentagel SH resin (0.29 mmol/g).

The four different methodologies **a-d** were compared taking into account the purity of kalata B1-Nbz(Me) obtained (**139**) (section 5.4).

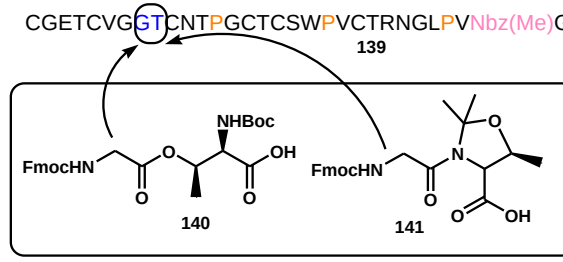

Figure 5.4: Building-block dipeptides incorporated in the backbone of kalata B1-Nbz(Me) (**139**) instead of the TG dipeptide sequence, in the synthetic modifications b-d.

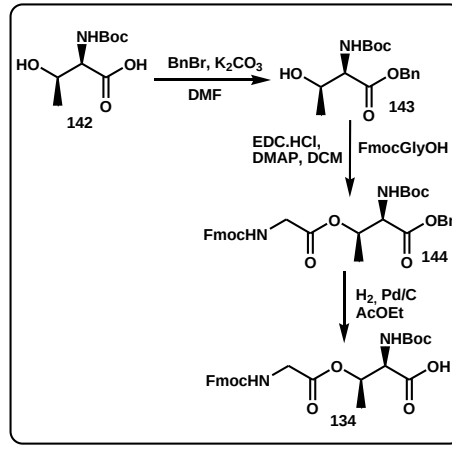

Scheme 5.5: Three-step synthesis of the *O*-acyl isodipeptide **140**.

Specifically, we employed two different resins: a ChemMatrix resin, made up of crosslinked PEG and characterized by a high chemical and thermal stability along with an excellent degree of swelling in DCM, DMF compared to polystyrene based resins; a tentagel resin which is a PEG hybrid polystyrene resin containing a core of polystyrene on

which are attached long chains of PEG. Both the resins are suitable for synthesizing long peptides such as kalata B1.

The use of the *O*-acyl isodipeptide unit **140**, synthesized according to a three step sequence (scheme 5.5) as described in literature[114], and of the pseudo-proline unit **141** is explained as follows.

The synthesis of long or difficult-sequence containing peptides is a challenging task because these kind of peptides are often obtained in a low synthetic yield and purity on solid-phase. This is usually due to aggregation phenomena in solvent during synthesis caused by inter-/intramolecular hydrophobic interactions and the hydrogen bond network among resin-bound peptide chains, resulting in the formation of extended secondary structures such as β-sheets. To solve this problem, it is possible to make use of the Boc/Bn approach in which the deprotection step in acidic conditions generates repulsing protonate chains. Alternatively, in the Fmoc/*t*-Bu approach pseudo-proline building blocks can be used, which are dipeptide derivatives containing Ser/Thr-derived oxazolidines or Cys-derived thiazolidines. These building blocks are able to disrupt the secondary structure of the peptide and are converted in the regular dipeptide sequence during the cleavage.

[114] T. Yoshiiya, A. Taniguchi, Y. Sohma, F. Fukao, S. Nakamura *Org. Biomol. Chem.* **2007**, *5*, 1720-1730.

Another building block recently discovered is the *O*-acyl isodipeptide, which allows to synthesize peptides with very difficult sequences. Specifically, the presence of an *O*-acyl instead of *N*-acyl residue within the peptide backbone significantly changes the secondary structure of the native peptide. Moreover, the target peptide is subsequently generated by an *O–N* intramolecular acyl migration reaction at neutral pH (scheme 5.6).[114]

In the case of the methodologies **b-d** the dipeptide building blocks as TG dipeptides of pseudo-proline (**141** in synthesis **c**) and *O*-acyl nature (**140** in synthesis **b, d**) only in the terminal region of the linear peptide **139** were incorporated due to the fact that in the first 20 aminoacid residues are contained prolines, which by theirself destroy the hydrogen-bond network.

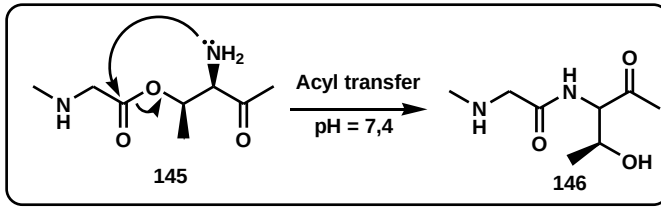

Scheme 5.6: *O–N* intramolecular acyl migration reaction of *O*-acyl isopeptides.

5.4 Comparation of the methodologies a-d

We compared the methodologies **a-d**, used for the Fmoc/*t*-Bu synthesis of kalata B1-Nbz(Me) (**139**) on the basis of its relative purity obtained. The relative purities were

calculated from integration of the HPLC trace at 220 nm, considering only peptidic peaks. Hereafter analytic HPLC chromatograms are illustrated.

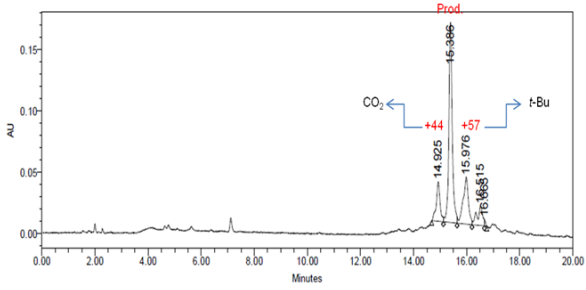

Figure 5.5: Analytic chromatogram of kalata B1-Nbz(Me) crude (**139**) in the case of the synthesis **a**. The relative purity is 56.99%. t_R = 15.39 min; conditions: 0 → 70% acetonitrile in 30 minutes (A: 0.1% TFA in water, B: 0.1% TFA in acetonitrile), flow: 1.0 ml/min, 220 nm, column: C_{18} XBridge, 4.6 x 150 mm, 5 µm.

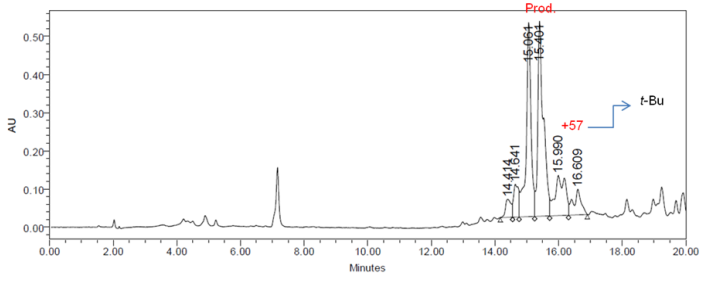

Figure 5.6: Analytic chromatogram of kalata B1-Nbz(Me) crude (**139**) in the case of the synthesis **b**. There are two peaks with the mass of **139** (ESI-MS determination) corresponding to the native sequence and to the sequence containing **140**. The relative purity calculated as sum of the two peaks is 62.87% (32.38% + 37.49%). t_R = 15.06 min, 15.40 min; conditions: 0 → 70% acetonitrile in 30 minutes (A: 0.1% TFA in water, B: 0.1% TFA in acetonitrile), flow: 1.0 ml/min, 220 nm, column: C_{18} Xbridge, 4.6 x 150 mm, 5 µm.

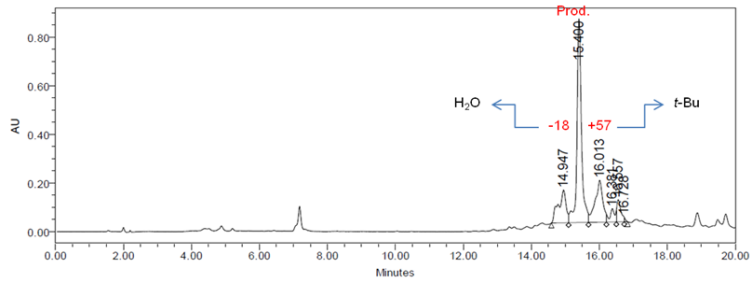

Figure 5.7: Analytic chromatogram of kalata B1-Nbz(Me) crude (**139**) in the case of the synthesis **c.** The relative purity is 55.56%. t_R = 15.40 min; conditions: 0 → 70% acetonitrile in 30 minutes (A: 0.1% TFA in water, B: 0.1% TFA in acetonitrile), flow: 1.0 ml/min, 220 nm, column: C_{18} Xbridge, 4.6 x 150 mm, 5 µm.

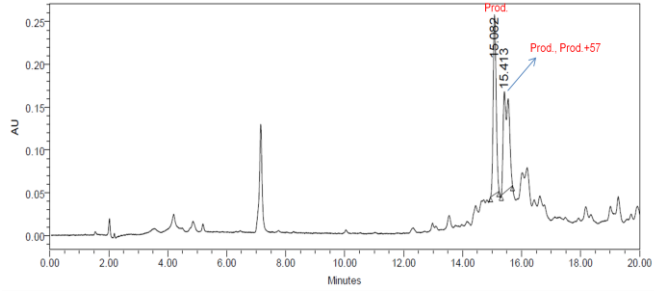

Figure 5.8: Analytic chromatogram of kalata B1-Nbz(Me) crude (**139**) in the case of the synthesis **d**. There are two peaks with the mass of **139** (ESI-MS determination) corresponding to the native sequence and to the sequence containing **140**. The relative purity calculated as sum of the two peaks is 56.40% (37.63% + 37.54%). t_R = 15.08 min, 15.41 min; conditions: 0 → 70% acetonitrile in 30 minutes (A: 0.1% TFA in water, B: 0.1% TFA in acetonitrile), flow: 1.0 ml/min, 220 nm, column: C_{18} Xbridge, 4.6 x 150 mm, 5 µm.

The above HPLC chromatograms are discussed as follows.

First of all, in addition to the peak of kalata B1-Nbz(Me) (**139**) are observed some secondary peaks corresponding in ESI-MS analysis to M+57 uma, M+44 uma, M-18 uma (M is the mass of **139**). The peak at mass M+57 uma derives from the addition of a *t*-Bu aminoacid protecting group on a cysteine or a tryptophan of the peptide backbone. Moreover, the peak at mass M+44 uma is attributed to the peptide containing an *N*-carboxylated indole originated from (Boc)Trp during the cleavage.[115] The conversion of the *N*-carboxylated indole in the free indole is slow so it is detected also the *N*-carboxylated compound (scheme 5.7).[115] The last peak at M-18 uma is ascribable to the aspartimide formation from an asparagine close to a glycine of the sequence (scheme 5.8). Aspartimide formation is a very common side reaction in peptide synthesis, and it is caused in Fmoc/*t*-Bu solid-phase synthesis by the repetitive piperidine treatments.[116] In addition, the deamidation reaction to aspartimide is more rapid if the susceptible amino acid (Asp, Asn) is followed by a small, flexible residue such as glycine.

Interestingly, in the case of the synthesis **b** and **d**, in the HPLC chromatogram are present two peaks with the mass of **139** (ESI-MS determination) corresponding respectively to the native sequence and to the sequence containing the *O*-acyl isopeptide **140**. This happens because the *O*–*N* intramolecular

[115] A. Isidro-Llobet, M. Alvarez, F. Albericio *Chem. Rev.*, **2009**, *109*, 2455-2504.
[116] M. Mergler, F. Dick, B. Sax, P. Weiler, T. Vorherr *J. Peptide Sci*, **2003**, *9*, 36-46.

acyl migration reaction of *O*-acyl isopeptides seems to be slow.

In table 5.1 are reported the relative purities of **139** obtained with the synthesis **a-d** performed. From these results it is possible to infer that the best purity (62.87%) is reached with the synthesis **b** in which ChemMatrix resin and the *O*-acyl isodipeptide **140** are used. In addition, comparing the purities obtained with the synthesis **b** and **d**, ChemMatrix resin resulted to be a better resin than tentagel.

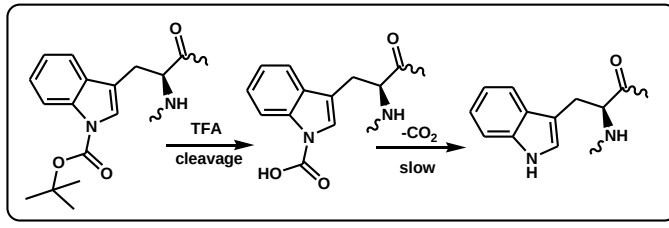

Scheme 5.7: Conversion of (Boc)Trp to the *N*-carboxylated species in acid conditions (cleavage) and following slow decarboxylation to Trp.

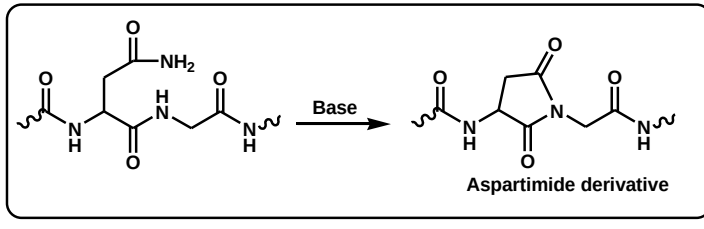

Scheme 5.8: Deammidation reaction of Asn-Gly to aspartimide.

Table 5.1: Purities of **139** obtained with the synthesis **a-d**.

Synthesis	Relative purity of **139**
a	56.99%
b	62.87%
c	55.56%
d	56.40%

5.5 Cyclization via NCL of kalata B1-Nbz(Me)

After the Fmoc/*t*-Bu synthesis of kalata B1-Nbz(Me) (**139**), the next step, according to the synthetic scheme 5.4, is the cyclization of **139** *via* a NCL reaction.

We tried to purify **139** with a C_{18} semipreparative column (C_{18} X Bridge, 5 µm × 19mm × 150 mm), but, due to the hydrophobic nature of the peptide, a purification yield of only 30% was experimented. So, we decided to perform the following cyclization reaction on **139** crude.

In scheme 5.9 it is reported the cyclization reaction carried out on compound **139**. It was conducted at pH 7-7.2 in high dilution conditions under nitrogen and making use of 4-mercaptophenol (**130**) as catalyst, which is less expensive than (4-carboxymethyl)thiophenol (**129**), tris(2-carboxyethyl)phosphine to prevent the oxidation of the thiole, and a phosphate buffer containing guanidinium hydrochloride. This last is a typic denaturing agent which is able to break a preferential conformation of the linear peptides

generating a mixture of rotamers, some of which are prone to the reaction. The pH must be neutral due to the fact that at basic pH the thiole oxidation is more favourite and at low pH the terminal amine could be protonated and the reaction could not occur.

The reaction mixture was purified making use of a C4 semipreparative column (C_{18} Symmetry 300, 5 µm × 10 mm × 150 mm) affording **147** with 35% yield as inferred by Maldi-TOF analysis.

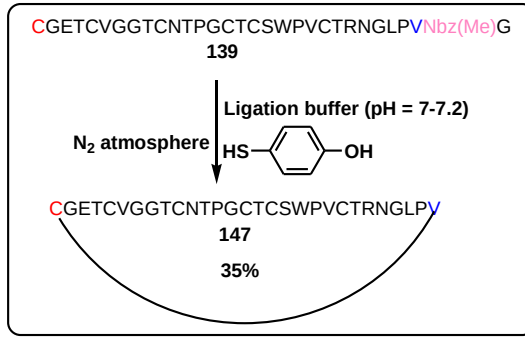

Scheme 5.9: Cyclization *via* NCL of the linear peptide **139**. The ligation buffer is a phosphate buffer containing guanidinium hydrochloride.

5.6 Folding of kalata B1

A folding reaction of kalata B1 in reduced form (**147**) was required to obtain kalata B1 (**10**). We successfully performed a test reaction on **147** but unfortunately there was not a sufficient quantity of **147** to scale up the reaction. As shown in scheme 5.10, the compound **147** was oxidized at pH 8.5 using a specific folding buffer (50% v/v isopropyl alcohol in ammonium bicarbonate solution) in presence of reduced

glutathione.[117]

The final molecule (**10**) was obtained with 100% relative purity (HPLC analysis) and was analyzed *via* Maldi-TOF confirming the formation of the three disulfide bonds. Due to the very small amount it was not possible to register the NMR spectrum. In absence of NMR data it is not possible to verify whether the connectivity of the three disulfide bonds in the synthesized cyclotide **10** is the same of the native kalata B1. Anyway, Craik reported that carrying out a reductive defolding of the native kalata B1 and subsequently an oxidative refolding in the conditions before reported, only the highly stable native structure was observed.[118] So, it is reasonable to affirm that the synthesis of kalata B1 with an innovative Fmoc/*t*-Bu strategy was accomplished.

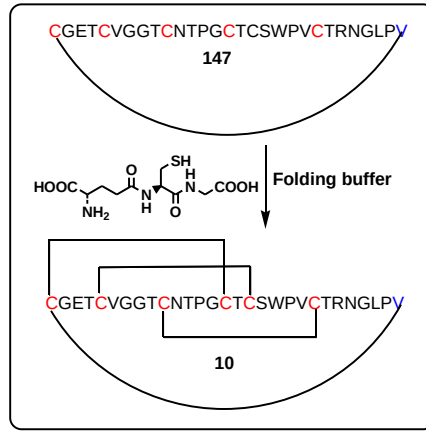

Scheme 5.10: Folding of kalata B1 in reduced form (**147**). The folding buffer is 50% v/v isopropyl alcohol in ammonium bicarbonate solution.

[117] N. L. Daly, R. J. Clark, D. J. Craik *J. Biol. Chem.*, **2003**, *278*, 6314-6322.
[118] N. L. Daly, S. Love, P. F. Alewood, D. J. Craik, *Biochemistry*, **1999**, *38*, 10606–10614.

5.7 Conclusions

In this chapter, the synthesis of kalata B1 linear precursor (**139**) with four different approaches (**a-d**), according to the innovative Fmoc/*t*-Bu strategy for the generation of peptide-thioesters, was reported. The best one revealed to be the synthesis **b** performed with the *O*-acyl isodipeptide unit (Boc-Thr(Fmoc-Gly)-OH) (**140**) on ChemMatrix rink amide resin.

In addition, the synthesis of kalata B1 in reduced form (**147**) was successfully performed using a NCL reaction.

Finally, a test folding reaction on 1mg of **147** produced kalata B1 (**10**) with 100% relative purity (HPLC analysis). The formation of the three disulfide bonds was confirmed *via* Maldi-TOF.

5.8 Experimental section

5.8.1 General procedures

Reagents purchased from commercial sources were used without further purification. All reactions involving air or moisture sensitive reagents were carried out under a dry argon atmosphere. CH_2Cl_2 was distilled from CaH_2. Glassware was flame-dried (0.05 Torr) prior to use. When necessary, compounds were dried in vacuo over P_2O_5 or by azeotropic removal of water with toluene under reduced pressure. Starting materials and reagents purchased from commercial

suppliers were generally used without purification. Reactions were monitored by TLC on silica gel plates (0.25 mm) and visualized by UV light or by spraying with ninhydrin solutions or drying with iodine. Flash chromatography was performed on Silica Gel 60 (particle size: 0.040–0.063 mm) and the solvents employed were of analytical grade. Analytical HPLC was performed on a Waters instrument comprising a Waters 2695 (Waters, MA, USA) separation module, an automatic injector, a photodiode array detector (Waters 996 or Waters 2998), and a Millenium^{32} login system controller. The columns used were a Sunfire^{TM} C_{18} reversed-phase analytical column (3.5 μm × 4.6 mm × 100 mm) with linear gradients of ACN (0.036% TFA) into H_2O (0.045% TFA) over 8 min or a Xbridge^{TM} C_{18} reversed-phase analytical column (5 μm × 4.6 mm × 150 mm) with linear gradients over 30 min. UV detection was at 220 and 254 nm and the system was run at a flow rate of 1.0 mL/min. Semi-preparative RP-HPLC was carried out on a Waters instrument comprising two solvent delivery pumps (Waters Delta 600), an automatic injector (Waters 2700 Sample Manager), a Waters 2487 dual wavelength absorbance detector, an automatic sample collector (Waters Fraction Collector II), a Masslynx v3.5 system controller and two different columns, obtained also from Waters: a Xbridge^{TM} BEH OBD C_{18} reversed-phase column (8.5 μm × 19 mm × 150 mm) and a Symmetry300^{TM} C_4 reversed-phase column (5 μm × 10 mm × 150 mm). Linear gradients of ACN (0.5% TFA) into H_2O (1%

TFA) with flow rates of 15 mL/min or 6 mL/min were used. HPLC-MS analysis was performed on a Waters instrument comprising a separation module (Waters 2695), an automatic injector, a photodiode array detector (Waters 2998), a Waters micromass ZQ spectrometer and a Masslynx v4.1 system controller. The column used was a Sunfire C18 reversed-phase analytical column (3.5 μm × 2.1 mm × 100 mm). Ultraviolet detection was at 220 and 254 nm, and linear gradients of ACN (0.07% formic acid) into H_2O (0.1% formic acid) were run at 0.8 mL/min over 8 min. Mass spectra were recorded on a MALDI-TOF Applied Biosystem 4700 with a N_2 laser of 337 nm using SA matrix [10 mg/mL of SA in ACN−H_2O−TFA (1:1:0.1)]. Sample preparation: a mixture of sample solution (1 μL) and matrix (1 μL) is prepared, placed on a MALDI-TOF plate and dried by air. Yields refer to chromatographically and spectroscopically (^1H and ^{13}C NMR) pure materials.

The NMR spectra were recorded on Bruker DRX 400, (^1H at 400.13 MHz, ^{13}C at 100.03 MHz), Bruker DRX 250 (^1H at 250.13 MHz, ^{13}C at 62.89 MHz), and Bruker DRX 300 (^1H at 300.1 MHz, ^{13}C at 75.5 MHz) spectrometers. Chemical shifts (δ) are reported in ppm relatively to the residual solvent peak ($CHCl_3$, δ = 7.26, $^{13}CDCl_3$, δ: = 77.0; CD_2HCN: δ = 1.98; $^{13}CD_3CN$: δ = 1.80, in the case of solvent mixtures, the considered residual peak was that of the most abundant deuterated solvent). The multiplicity of each signal is designated by the following abbreviations: s, singlet; d,

doublet; t, triplet; q, quartet; m, multiplet; b, broad. Coupling costants (J) are quoted in Hz.

5.8.2 *Synthesis of* 140

Synthesis of 143

Benzyl bromide (7.5 ml, 63 mmol) was added to a stirring solution of *N*-(*t*-butoxycarbonyl)-L-threonine (3.0 g, 14 mmol) and potassium carbonate (1.9 g, 14 mmol) in DMF (91 ml). The resulting mixture was stirred at room temperature overnight, concentrated *in vacuo*, diluted with AcOEt and washed successively with water (×2), brine. The organic layer was dried over Na_2SO_4 and the solvent was removed *in vacuo*. The resulting oil was purified by silica gel column chromatography (hexane/AcOEt, from: 98/2 to 7/3) to yield **143** (2.7 g, 57 %).

✔ *Compound **143***

HPLC: t_R: 6.8 min; conditions: 0 → 100% B in 8 min (A, 0.036% TFA in water, B, 0.045 % TFA in acetonitrile); Sunfire^{TM} C_{18} reversed-phase analytical column (3.5 μm × 4.6 mm × 100 mm); flow: 1 mL min^{-1}, 220 nm.

ES-MS: 310.0 *m/z* [$M+H^+$].

Synthesis of 144

EDC.HCl (1.15 g, 6.0 mmol) was added to a stirred solution of **143** (1.7 g, 5.0 mmol), Fmoc-L-glycine (1.8 g, 6.0 mmol), and DMAP (122 mg, 1.0 mmol) in DCM (50 ml) at 0 °C. The

mixture was slowly warmed to room temperature over 2h, stirred additionally overnight, diluted with EtOAc, and washed with water, 1 M HCl, water, saturated $NaHCO_3$ and brine. The organic layer was dried over Na_2SO_4 and the solvent was removed *in vacuo*. The resulting oil was purified by silica gel column chromatography (hexane/AcOEt, from 98/2 to 6/4) affording **144** (2.3 g, 80 %).

✔ *Compound **144***

HPLC: t_R: 9.1 min; conditions: 0 → 100% B in 8 min (A, 0.036% TFA in water, B, 0.045 % TFA in acetonitrile); Sunfire™ C_{18} reversed-phase analytical column (3.5 μm × 4.6 mm × 100 mm); flow: 1 mL min^{-1}, 220 nm.

ES-MS: 589.2 *m/z* $[M+H^+]$.

Hydrogenation step

Pd/C (210 mg) was added to a stirring solution of **144** (2.2 g, 3.7 mmol) in EtOAc (80 mL), and the reaction mixture was vigorously stirred under a hydrogen atmosphere overnight. The catalyst was filtered off through celite. The solvent was removed *in vacuo* and the crude product was purified by silica gel column cromatography, at first with hexane:AcOEt 2:1 and then the final product was washed out by methanol to give pure **140** (1.3 g, 70 %).

✔ *Compound **140***

^{1}H-NMR: (300 MHz, $CDCl_3$) δ: 7.76-7.30 (8H, m, Ar*H*), 5.56 (1H, m, C*H*OCO), 5.45 (1H, m, N*H*), 5.27 (1H, m, N*H*), 4.51 (1H, m, C*H*NHBoc), 4.39 (2H, d, J = 6.8 Hz,

CH_2Fmoc), 4.21 (2H, t, *J* = 6.8 Hz, C*H*Fmoc), 3.94 (2H, m, CH_2NHFmoc), 1.45 (9H, s, C(CH_3)$_3$), 1.34 (3H, d, *J* = 6.2 Hz, CH_3).

HPLC: t_R: 7.6 min; conditions: 0 → 100% B in 8 min (A, 0.036% TFA in water, B, 0.045 % TFA in acetonitrile); Sunfire^{TM} C_{18} reversed-phase analytical column (3.5 μm × 4.6 mm × 100 mm); flow: 1 mL min^{-1}, 220 nm.

ES-MS: 399.08 *m/z* [(M-Boc)+H$^+$].

5.8.3 Solid phase synthesis of kalata B1-Nbz(Me)

For the synthesis of kalata B1-Nbz(Me) (**139**) two different resins were used: PCAS H-Rink-amide ChemMatrix 0.52 mmol/g, Ernst- Simon Tentagel SNH_2 0.48 mmol/g. Fmoc aminoacids and the dipeptide Fmoc-Gly-Thr(ψ(Me,Me)pro)-OH (**141**) were purchased from Iris-Biotech. The linker Fmoc-Dbz(Me) (**132**) was previously synthesized in Albericio's laboratory. Fmoc aminoacids used were: Fmoc-Arg(Pbf)-OH, Fmoc-Asn(Trt)-OH, Fmoc-Cys(Trt)-OH, Fmoc-Glu(O*t*-Bu), Fmoc-Gly-OH, Fmoc-Leu-OH, Fmoc-Pro-OH, Fmoc-Ser(*t*-Bu)-OH, Fmoc-Thr(*t*-Bu)-OH, Fmoc-Trp(Boc)-OH, Fmoc-Val-OH. The valine next to cysteine in loop 6 was selected as the suitable initiation point for the synthesis.

General protocol. Synthesis were performed manually on a 0.05 mmol scale.

In the case of H-Rink-amide ChemMatrix resin washings with DCM 1% TFA, DMF 1% TFA, DMF were previously performed in order to remove residues of free amine. Aminoacids were coupled using a 10-fold excess (0.50 mmol). A solution of HBTU 0.5 M (0.50 mmol, 190 mg) in DMF (1mL) was added to the Fmoc protected aminoacid, then was added DIPEA (0.55 mmol, 95 µl) and the aminoacid was activated for 30 sec prior the coupling. The resin was bubbled with N_2. A single treatment of 1 h was used for the first three residues of the sequence (Gly, Dbz(Me), Val) and a double treatment of 1 h for the following residues. Dipeptides **141**, **142** were coupled using a 5-fold excess (0.25 mmol), a solution 0.5 M of HATU (0.25 mmol, 95 mg) in DMF (1mL) containing DIPEA (0.3 mmol, 52 µl) respectively for 1h and 2h. Boc-Cys(Trt)-OH was used in the final coupling step. The Fmoc group was deprotected with 20% piperidine/DMF (v/v, 1 mL) for 10 min. Couplings were checked using the ninhidrin test.

The resin was washed with DMF (6 × 1 mL) at the end of each coupling. After peptide elongation, the resin was washed with DCM and *p*-nitrochloroformate solution (101 mg, 0.5mmol, 0.5 M in DCM) was added. The resin was bubbled with N_2 for 2 h. Then, it was washed with DCM and treated with DIPEA 0.5 M (436 µl) in DMF (2.5 mL) for 1 h and, finally, washed with DMF and DCM. The peptidyl-resin was dried under vacuum and the peptide was cleaved from the resin in the case of methodologies **b-d** with the reagent

cocktail: 92.5% TFA, 2.5% H_2O, 2.5% EDT, 2.5% 1,2-dimethyl indole (2.5 mL) for 1.30 h. In the case of methodology **a**, the following reagent cocktail was used: 94% TFA, 2.5% H_2O, 2.5% EDT, 1% TIS (2.5 mL) for 1.30 h . The TFA solution containing the peptide was concentrated under vacuum to a minimal volume, added over cold Et_2O and precipitated by centrifugation. The supernatant was removed and the residue was dissolved in 20 mL of ACN/H_2O (1:1) 0.045% TFA (HPLC buffer) and lyophilized.

✓ *Compound **139***

Calculation of yield for methodology **a**

Resin substitution value: 0.52 mmol /g.

Synthesis scale: 0.05 mmol.

Peptide molecular weight = 3150 g/mol.

Peptide weight: 40 mg.

% yield : 25%.

Peptide weight for methodologies **b-d**

Crude peptide weight for methodology **b**: 147 mg.

Crude peptide weight for methodology **c**: 160 mg.

Crude peptide weight for methodology **d**: 150 mg.

Crude peptides contained 1,2-dimethyl indole.

Relative purity for methodologies **a-d**

HPLC purities were calculated from integration of the trace at 220 nm. Analytical HPLC chromatograms are illustrated in section 5.4.

Relative purity for methodology **a**: 57.0%.

Relative purity for methodology **b**: 62.9%.
Relative purity for methodology **c**: 55.6%.
Relative purity for methodology **d**: 56.4%.

Purification *via* RP-HPLC

The purification of the crude peptide *via* RP-HPLC on a C_{18} reversed-phase semi-preparative column (Xbridge™ BEH OBD C_{18} reversed-phase column (8.5 µm × 19 mm × 150 mm)) was performed with 10% yield. t_R: 37.4 min.; conditions: 5 → 70% B in 80 min (A: 0.05% TFA in water, B: 0.1% TFA in acetonitrile), degassing (helium): 30 mL/min, flow: 15 mL min^{-1}, 220 nm.

ES-MS: 1050.9 *m/3z* [M+3H$^+$].

HPLC: t_R: 15.4 min (methodology **a**), 15.1 min (methodology **b**), 15.4 min (methodology **c**), 15.1 min (methodology **d**); conditions: 0 → 70% B in 30 min (A, 0.036% TFA in water, B, 0.045 % TFA in acetonitrile); Xbridge™ C_{18} reversed-phase analytical column (5 µm × 4.6 mm × 150 mm); flow: 1 mL min^{-1}, 220 nm.

5.8.4 Cyclization by NCL of kalata B1-Nbz(Me)

A "one pot" buffer for peptide cyclization/ligation was prepared using 50 mM of 4-mercaptophenol, 20 mM of tris(2-carboxyethyl)phosphine hydrochloride (TCEP.HCl) and 6 M guanidinium hydrochloride in a 200 mM phosphate buffer. The pH was adjusted to be between pH 7.0-7.2. Buffer was degassed under N_2 for 15 min before the reaction. Kalata B1-

Nbz(Me) (0.8 µM, 13.5 mg) was incubated in 5 ml of the "one pot" buffer overnight. Later, the reaction mixture was purified *via* RP-HPLC to afford **147** (37%, 4.4 mg).

✔ *Compound **147***

The crude residue was purified by RP-HPLC on a C_4 reversed-phase semi-preparative column (Symmetry300™ C_4 reversed-phase column (5 µm × 10 mm × 150 mm)). t_R: 32.0 min.; conditions: 5 → 70% B in 80 min (A: 0.05% TFA in water, B: 0.1% TFA in acetonitrile), degassing (helium): 30 mL/min, flow: 6 mL min^{-1}, 220 nm.

MALDI-TOF: 2898.0 uma.

HPLC: t_R: 15.7 min; conditions: 0 → 70% B in 30 min (A, 0.036% TFA in water, B, 0.045 % TFA in acetonitrile); Xbridge™ C_{18} reversed-phase analytical column (5 µm × 4.6 mm × 150 mm); flow: 1 mL min^{-1}, 220 nm.

5.8.5 *Folding of kalata B1*

Oxidative folding reaction of **147** (1 mg) was performed at room temperature overnight in 50% isopropyl alcohol (v/v) in 0.1 M ammonium bicarbonate, pH 8.5 and 1 mM reduced glutathione.

✔ *Compound **10***

MALDI-TOF: 2892.0 uma.

HPLC: t_R: 18.9 min; conditions: 0 → 70% B in 30 min (A, 0.036% TFA in water, B, 0.045 % TFA in acetonitrile);

Xbridge^{TM} C_{18} reversed-phase analytical column (5 μm × 4.6 mm × 150 mm); flow: 1 mL min^{-1}, 220 nm.

Ringraziamenti

Ringrazio *in primis* la Prof. Irene Izzo per il continuo supporto umano e scientifico in questi tre anni. Ringrazio la dott.ssa Consiglia Tedesco per la passione che ha saputo trasmettermi. Rivolgo un grazie anche al Prof. De Riccardis per la sua disponibilità e al Dott. Giorgio Della Sala per avermi seguito in alcune occasioni. Per quanto concerne l'avventura spagnola, saluto affettuosamente il Prof. Albericio e il mio caro supervisor Juan.
Un grazie speciale a tutte le mie tesiste in ordine di apparizione (la mitica fata percoca, Serena, Laura, Caterina).
Un saluto affettuoso ai compagni di lab di questi tre anni (Mirko, Luca, Silvia, Tiziana).
Ringrazio la mia famiglia e Arianna per avermi sospinto sempre. Ringrazio il lab 63 attuale (Alessandra e Rosaria) per tutte le giornate divertenti che abbiamo trascorso insieme, mi mancherete un botto!!! Un ringraziamento speciale va anche ai miei maestri del vecchio lab 63 e 36 (Chiara, Gaetano, Graziella e Antonella) per avermi aiutato a muovere i primi passi in laboratorio. Ringrazio il caro "gruppo pranzo" di Fisciano e il Prof. Proto per tutte le pappatorie fantastiche (un bang a tutti voi), il gruppo Cafè de Paco di Barna (Salvo, Roby, Conzi, Catarina, Carolina, Belen, Jesus, Julia) e tutti i miei amici di Barna per aver reso quei sei mesi indimenticabili.